Thèse

Présentée à l'Université de Strasbourg
Ecole Doctorale des Sciences Chimiques

Pour obtenir le grade de
Docteur de l'Université de Strasbourg

Par
Lucia GRANIERI

Droplet-based microfluidics and engineering of tissue plasminogen activator for biomedical applications

Soutenue publiquement le 13 novembre 2009
Devant la commission d'examen:

Directeur de thèse: Prof. Andrew D. Griffiths
Institut de Science et d'Ingénierie Supramoléculaire, Strasbourg, France

Rapporteur: Prof. Christopher Abell
University of Cambridge, Department of Chemistry, Cambridge, United Kingdom

Rapporteur : Prof. Claude P. Müller
Laboratoire National de Santé, CRP Santé, Institut d'Immunologie, Luxembourg

Examinateur : Dr. Dino Moras
Institut de Génétique et de Biologie Moléculaire et Cellulaire, Strasbourg, France

Membre Invité: Prof. Jean-Marie Lehn
Institut de Science et d'Ingénierie Supramoléculaire, Strasbourg, France

Acknowledgements

First of all, I would like to thank Prof. Andrew GRIFFITHS for his help and advice during the time I have spend in his laboratory. You proved tremendously instructive scientifically and you also taught me valuable lessons on trust and generosity.

I owe the highest acknowledgement to the supervisor of my thesis- Dr. Christoph MERTEN. Thank you for your patience, your support, and your ideas and for kindly reading this manuscript.

It is a great honor for me that Prof. Christopher ABELL, Prof. Claude MULLER, Dr. Dino MORAS and Prof. Jean-Marie LEHN agreed to participate in the evaluation of my doctoral thesis. I am sincerely grateful for their time, patience and support.

I acknowledge the receipt of a studentship from the Fonds National de la Recherche (Luxembourg), which has enabled me to carry out the work described in this thesis.

Thanks to all the members of 'THE CHRISTOPH MERTEN group': Thanks Jenni for being my friend and for the nice time spent together talking about our chocolate addiction, Dianamann I will never forget our trip to Barcelona and Bacheee thank you for our nice conversations and for having many common interests. It's a miracle that 'THE CHRISTOPH MERTEN survived our group meetings.

Thanks 'office 205 people': Michaël, merci pour tes blagues (c'est 3 nains qui vont à la mine…), tes chansons, tes conseils scientifiques et pour ta bonne humeur, j'éspère que tu pourras bientôt jouer a guitar hero avec ton petit. Kerstin thanks for all the interesting 'political' conversations and for 'money for nothing'. Olli thank you for all the amazing things you told me about computers, for your patience and for your amazing knowledge of 'everything', I hope you will get your dream job. Dave thanks for your help in preparing figures, for our conversations and for your patience with a very talkative deskmate, I hope all your 'hopes and dreams' become reality.

Thanks ‘Barcelona people’: Lino I hope we will travel to Basilicata next year, thanks for being ‘THE BEST’. Yousr merci pour nos conversations. Lucas du bist ein Streber. Ali bonne chance pour tes tris (il va en falloir!). Good luck to all of you for your own defences!

Thanks ‘LBC group members’: Isa merci pour ton incroyable talent d’organisation, tu nous facilites la vie tous les jours. JC merci pour ton aide, c’est toujours pratique d’avoir un physicien sous la main. Abdes merci pour ton aide lors de la synthèse des surfactants. Antoine et François merci pour votre bonne humeur: allez Biloute! Val merci pour ton aide pour les demandes de financements.
Thanks: Estelle, Felix, Thomas M., Thomas B., Shigeyoshi, Christian, Deniz, Victoire, Yannick, Ashleigh, Gabrielle, Majdi, Faith, Alex.
Thanks ‘past LBC group members’: Gigia, Odile, Christoph, Josh, Kerstin, Sebastian, Philippe, Matthieu, Florian, Saya, Agnes.

During my 4 years in ISIS I have met many nice people, thank you for your help and advice: Fabienne, Fabien, Thierry, Pierre-Yves, Mehdi, Emilie, François, Zibi, Kasia, Mihail, Giusi.

Merci: Malou, Pascal, Olivier, Stéphanie, Zelda, Vincent, Naama, Sabrina, Maher, Elsa, Laura, Anouck.

Grazie mamma, papà, Anna, Pasqualino e Zaffiro.

Merci Joël.

Nel mezzo del cammin di nostra vita mi ritrovai per una selva oscura ché la diritta via era smarrita. Ahi quanto a dir qual era è cosa dura esta selva selvaggia e aspra e forte che nel pensier rinova la paura!

Inferno, La Divina Commedia, Dante

Per correr migliori acque alza le vele ormai la navicella del mio ingegno, che lascia dietro a sé mar sì crudele; e canterò di quel secondo regno dove l'umano spirito si purga e di salire al ciel diventa degno.

Purgatorio, La Divina Commedia, Dante

La gloria di colui che tutto move per l'universo penetra, e risplende in una parte più e meno altrove.

Paradiso, La Divina Commedia, Dante

Dedicato a Romeo.

Abstract

Phage display is a widely used method for directed evolution of proteins, allowing the generation of an enormous diversity of protein variants displayed on the viral particles (library diversity $<10^{12}$). These protein variants can then either be selected for binding affinity (e.g. antibodies) or for catalytic activity (e.g. enzymes). However, since selection for catalytic activity requires immobilized substrates and/or products, selection for multiple turnover or maximum rate acceleration remains challenging. To overcome these limitations a new method has been developed: Microfluidic-based compartmentalisation of viral particles displaying single protein variants on their surface. Encapsulation of these particles into picoliter drops allows the use of soluble substrates/products and therefore the selection for multiple turnover. The model system used here is based on retroviral particles displaying tPA (tissue plasminogen activator), a protein used in current emergency therapies of myocardial infarction and stroke, and a non-related control protein (neuraminidase, NA, inactive particles). Single particles displaying tPA and NA variants were encapsulated into aqueous droplets and the enzymatic activity was monitored using a fluorescence assay. Active variants could be sorted from a mixture of active and inactive variants.

List of Abbreviations

ALV	avian leukosis virus
ASLV	avian sarcoma leukosis virus
AMC	7-amino-4-methylcoumarin
ACMS	7-aminocoumarin-4-methane-sulfonic acid
α2-apl	α2-antiplasmin
BDE	bond dissociation energy
BSA	bovine serum albumin
CA	capsid
CGG	concentration gradient generator
CMC	critical micelle concentration
Da	average apparent diffusion coefficient
DBS	dichroic beam splitter
DLS	dynamic light scattering
DMP	dimorpholino phosphate
DMSO	dimethyl sulfoxide
EGF	epidermial growth factor
Env	envelope polyprotein
FACS	fluorescence-activated cell sorter
FADS	fluorescence-activated droplet sorter
FB	fibrin
FDA	the Food and Drug Administration
FRET	fluorescence resonance energy transfer
GFP	green fluorescent protein
HBS	hepes-buffered saline
HCS	high content screening
HEPG2	human liver carcinoma cells
HEK293T	human embryonic kidney 293 cells
HEK293tPA	human embryonic kidney 293 cells displaying tPA
HIV	human immunodeficiency virus

HIV-1 PR	human immunodeficiency virus type 1 aspartic protease
HLB	hydrophile-lipophile balance
HTS	high-throughput screening
IN	integrase
IVC	in vitro compartmentalisation
LTR	long terminal repeat
Mn	molecular mass of the whole molecule
MA	matrix proteins
Mh	molecular mass of the hydrophilic portion of a molecule
μFACS	miniaturised fluorescence-activated cell-sorting
MIC	minimum inhibitory concentration
MLV	murine leukemia virus
MoMLV	moloney murine leukemia virus
MMP	matrixmetalloprotease
MMP+	1-methyl-4-phenylpyridinium
MRSA	methicillin-resistant *Staphylococcus aureus*
NA	neuraminidase
NC	nucleocapsid
NMR	nuclear magnetic resonance
Np	number of tPA molecules per particle
PAI-1	plasminogen activator inhibitor
PCR	polymerase chain reaction
PD	Parkinson disease
PEG	polyethylene glycol
PEO	polyethylene oxide
PPO	polypropylene oxide
PDMS	polydimethylsiloxane
PDGFR-TM	platelet-derived growth factor receptor transmembrane domain
PG	plasminogen
PL	plasmin
PMT	photomultiplier tube
PR	protease
PrP^c	prion protein
ψ	psi-site

PTFE	polytetrafluoroethylene
Rh	hydrodynamic radius
RT	reverse transcriptase
rt-PCR	reverse transcriptase polymerase chain reaction
sc-tPA	single-chain tPA
SU	surface unit
tc-tPA	two-chain tPA
THF	tetrahydrofuran
TLC	thin layer chromatography
TM	transmembrane domain
tPA	tissue plasminogen activator
TSA	transition state analog
UV	ultraviolet
w/o	water-in-oil
w/o/w	water-in-oil-in-water

Table of Contents

Abstract		I
List of Abbreviations		II
Table of Contents		V
General Introduction		1
1	Tissue Plasminogen activator	1
1.1)	Function	1
1.2)	Structure	3
1.3)	Clinical Applications	5
2	Retroviruses	6
2.1)	Structure	6
2.2)	Incorporation of non-viral proteins	8
2.3)	Display Strategies	9
3	Directed Evolution of Enzymatic Activities	10
3.1)	Catalytic Antibodies	10
3.2)	Phage display	11
3.3)	In vitro Compartmentalisation	14
4	High-throughput Screening	17
4.1)	Microplate Systems	17
4.2)	Lab-on-a-chip System	18
	4.2.1) Non-fluidic systems: microarrays	18
	4.2.2) Fluidic systems: microfluidic chips	20
4.3)	Droplet-based Microfluidics	22

CHAPTER I: FLUORINATED SURFACTANTS FOR BIOLOGICAL APPLICATIONS IN DROPLET-BASED MICROFLUIDICS 25

1 INTRODUCTION 25

2 MATERIALS AND METHODS 28
2.1) CHEMICALS 28
2.2) SYNTHESIS OF LG SURFACTANTS 29
2.3) SOLUTION PREPARATION 30
2.4) DYNAMIC LIGHT SCATTERING (DLS) 30
2.5) HYDROPHILIC-LIPOPHILIC BALANCE (HLB) 31
2.6) MICROFLUIDIC DEVICES 32
2.7) BIOCOMPATIBILITY TESTS 32
2.8) LEAKAGE TESTS 32

3 RESULTS 33
3.1) SURFACTANT DESIGN 33
3.2) SURFACTANT SYNTHESIS 36
3.3) HYDROPHILIC-LIPOPHILIC BALANCE 36
3.4) DETERMINATION OF THE CRITICAL MICELLE CONCENTRATION 37
3.5) DROPLET STABILITY 38
3.6) BIOCOMPATIBILITY 40
3.7) MASS TRANSFER BETWEEN DROPLETS 41

4 DISCUSSION 47

CHAPTER II: ULTRA-HIGH-THROUGHPUT SCREENING OF ENZYMES BY RETROVIRAL DISPLAY USING DROPLET-BASED MICROFLUIDICS 49

1 INTRODUCTION 49

2 MATERIALS AND METHODS 51
2.1) PLASMIDS 51
2.2) CELLS 52

2.3) Freezing and thawing of cultured cells 52
2.4) Generation of competent bacteria and And transformation thereof 52
2.5) Generation of plasmid DNA for transfection 53
2.6) Generation of viral particles 54
2.7) Microplate tPA assays 54
2.8) Microfluidic devices 55
2.9) Optical setup 56
2.10) Synthesis of surfactants for the stabilisation of microdroplets 57
2.11) tPA Inhibition experiments 57
2.12) Droplet sorting experiments 58
2.13) Amplification of viral RNA by RT-PCR 58

3 Results 60
3.1) General setup of the assay 60
3.2) Coupling tPA activity with a fluorescence signal 61
3.3) Encapsulation of viral particles and inhibition experiments 63
3.4) Encapsulation of viral particles and sorting experiments 67
3.5) Average number of enzyme molecules per particle 70

4 Discussion 71

Chapter III: Using the new membrane-bound form of tPA for the selection of species-specific antibiotics 73

1 Introduction 73

2 Materials and methods 75
2.1) Cells 75
2.2) In vitro co-cultivation assay 75
2.3) Antibiotics 76

2.4) Determination of Z-Factors 76
2.5) Determination of the effect of bacterial metabolism on reporter cell survival 76

3 Results 77
3.1) General setup of the assay 77
3.2) Determinants for the viability of the human reporter cells within the co-cultures 79
3.3) Fluorescence signals using streptomycin and sodium azide as model compounds 81
3.4) Correlation between fluorescence signals and growth inhibition of S. aureus 83
3.5) Reliability of the assay 83

4 Discussion 86

General Conclusion 88

Résumé de these En Français 93

Introduction 94

1 Une approche microfluidique pour l'évolution dirigée du tPA exprimé sur des rétrovirus 94
1.1) Description du projet 94
1.2) Description des Méthodes utilisées 95
1.3) Résultats et Conclusions 96
2 Sélection d'anticorps spécifiques à une espèce grâce à l'utilisation de la nouvelle forme de tPA exprimée sur la membrane virale 97
2.1) Description du projet 97
2.2) Description des Méthodes utilisées 99
2.3) Résultats et Conclusions 100

Conclusions et Perspectives 101

Bibliography 102

GENERAL INTRODUCTION

1 Tissue Plasminogen Activator (tPA)

1.1) Function

The serine protease tPA was discovered in 1947 (Astrup and Permin, 1947) and is now considered to have at least two major physiological functions. Firstly it is involved in tissue histogenesis and remodelling and secondly it initiates fibrinolysis (Parekh et al., 1989) (Figure 1).

In response to clot formation, tPA is synthesised by the endothelium and released into circulation as single-chain tPA (sc-tPA). Plasmin (PL) converts sc-tPA to two-chain tPA (tc-tPA). tPA is unique in that the sc-tPA form exhibits considerable catalytic activity (1/5 to 1/10 of the two chain form) (Renatus et al., 1997). The relatively high enzymatic activity of the sc-tPA form (in particular when stimulated by fibrin) has been attributed to a lack of specific interactions stabilising the zymogen form (inactive or pro-form) and to additional interactions that stabilise the catalytically active form. Compared to other serine proteases, tPA has a low activity of processed protease/activity of zymogen (zymogenicity; values of 5-10 for tPA in contrast to 250 to 10^7 for other serine proteases) (Lamba et al., 1996; Madison et al., 1993).

tPA converts plasminogen (PG) to plasmin (PL) by specific cleavage of the Arg561-Val562 bond (Figure 1). The active serine proteinase PL in turn lyses and thereby dissolves the cross-linked fibrin (FB) network of blood clots leading to clot dissolution (Bennett et al., 1991). The whole process is stimulated by FB such that PG activation is mainly restricted to fibrin clots (Bode and Renatus, 1997).

The fibrinolytic system restricts its activity to FB clots by four different mechanisms. First, the catalytic activity of tPA is low and increases upon binding to FB clots. Second, the plasminogen activator inhibitor 1 (PAI-1) inhibits circulating tPA but does not affect tPA bound to fibrin. Third, PL is inhibited by α_2-antiplasmin (α_2-apl)

when it is not bound to fibrin. Finally, circulating tPA has a very short half-life (5-8 min) (Sheehan and Tsirka, 2005) (Figure 1).

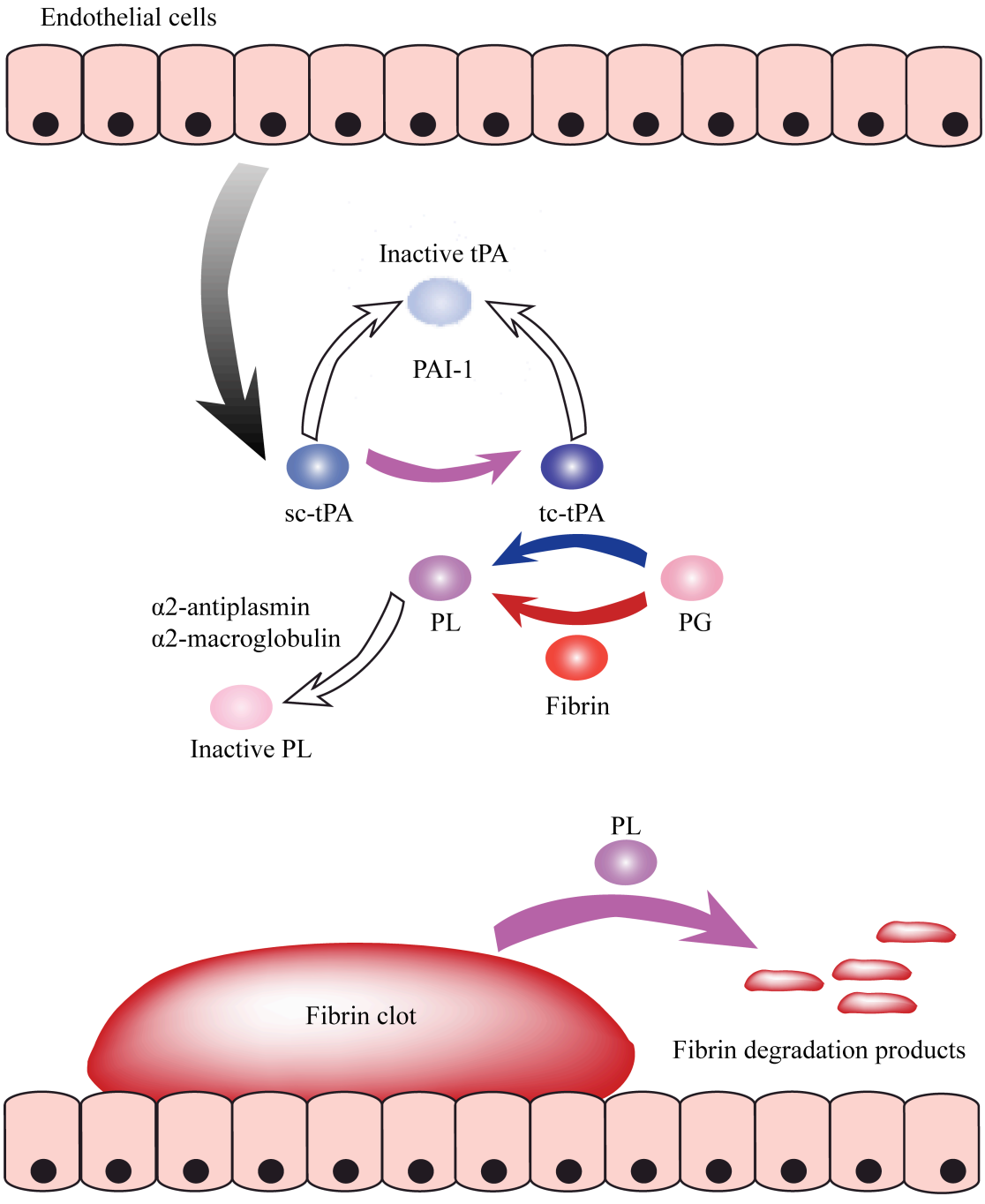

Figure 1. The fibrinolytic system. Endothelial cells release single-chain tPA (sc-tPA), which is cleaved into two-chain tPA (tc-tPA) by plasmin (PL). tc-tPA converts plasminogen (PG) into PL and is inhibited by plasminogen activator inhibitor 1 (PAI-1). PL degrades fibrin clots into fibrin degradation products and is inhibited by α2-antiplasmin and α2-macroglobulin.

1.2) STRUCTURE

tPA is a serine proteinase of the trypsin-family, it is mainly synthesised in endothelial cells and secreted as a 527 residue single-chain glycoprotein into the circulating blood. This mosaic protein is composed of five distinct domains: the finger domain (Ser1 to His44), an epidermial growth factor-like domain (Ser 50 to Asp87), two kringle domains (Cys92 to Cys173 and Cys180 to Cys261) and the carboxy-terminal catalytic domain (Ser262 to Pro527) (Pennica et al., 1983). Upon specific cleavage at the Arg275-Ile276 peptide bond, single-chain tPA (sc-tPA) is converted into the two-chain form (tc-tPA) consisting of the 275 residue heavy (A) chain and the 252 residue light (B) chain. The light and heavy chain are connected by a Cys264-Cys395 disulfide bond (Lamba et al., 1996). The catalytic residues forming the active-site triad of tc-tPA (Ser478, His322 and Asp371) are arranged as in (chymo)trypsin-like serine proteinases and are often numbered accordingly with chymotrypsinogen numbering denoted by the prefix 'C' (SerC195, HisC57 and AspC102) (Figure 2 and 3). The tPA molecule contains four potential glycosylation sites (Asn117, Asn184 and Asn448), Asn117 and Asn448 are invariably glycosylated, whereas variable site occupancy is observed at Asn184. This variation leads to the production of two tPA variants: type I (all three glycosylation sites occupied) and type II (two glycosylation sites occupied) (Walsh and Jefferis, 2006; Wittwer and Howard, 1990).

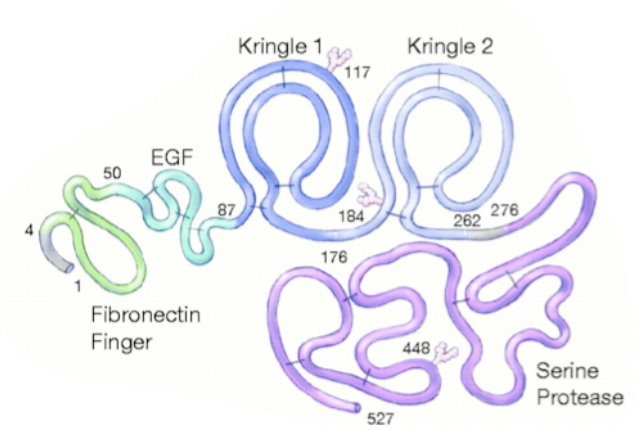

Figure 2. Primary structure of tPA. The structure-function relationships for the various domains are as follows: kringle 1, receptor binding (liver); kringle 2, fibrin binding (low affinity); fibronectin finger, fibrin binding (high affinity); epidermal growth factor, hepatic clearance; serine protease, catalytic activity and plasminogen activator inhibitor 1–binding; and glycosylation sites (indicated with a Y), clearance via hepatic endothelial cells. (Llevadot et al., 2001).

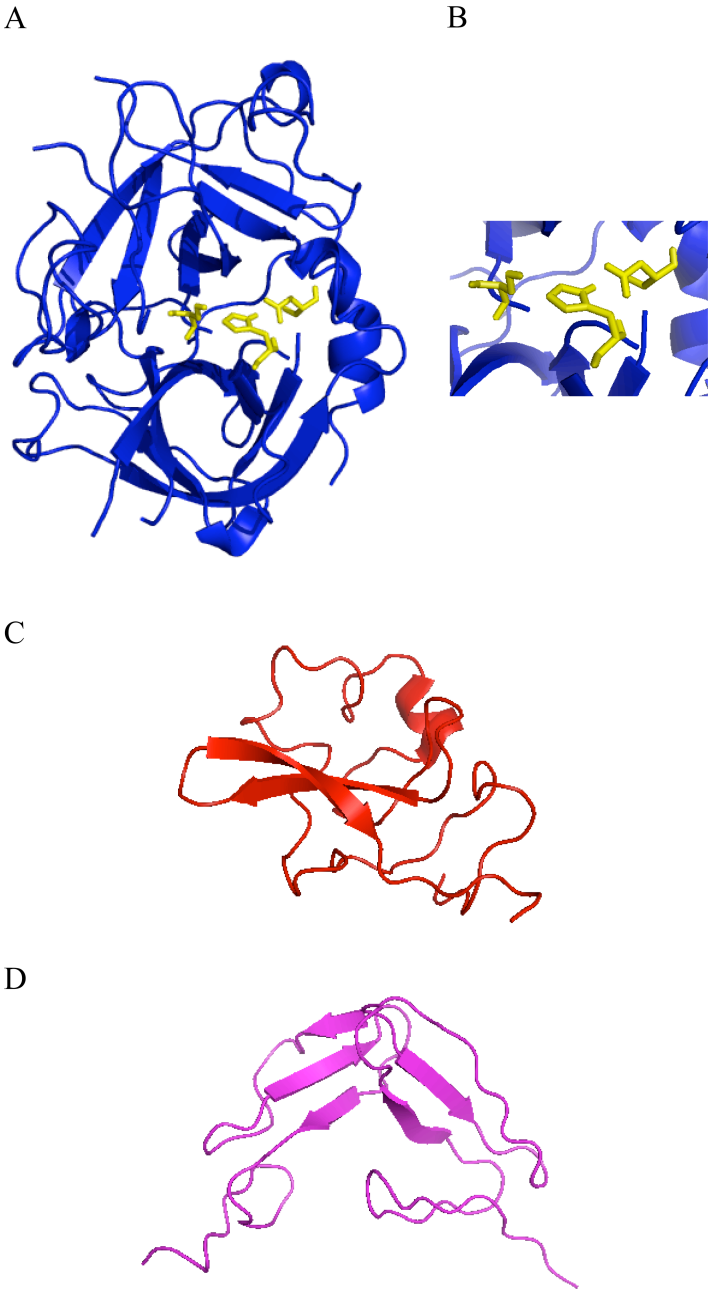

Figure 3. (A) Cartoon plot, generated with pymol, of the catalytic domain of human tc-tPA. The catalytic triad residues SerC195, HisC57 and AspC102 are given in yellow. (B) Closer view of the catalytic triad (Lamba et al., 1996). (C) Cartoon plot of the kringle 2 domain (de Vos et al., 1992). (D) Cartoon plot of the finger domain and epidermial growth factor-like domain (Smith et al., 1995).

1.3) Clinical applications

Recombinant tPA was evaluated during the 'national institute of neurological disorders and stroke recombinant tissue plasminogen activator stroke study' for the treatment of ischemic stroke (Qureshi, 1996). It is also used as a fibrinolytic agent in the treatment of acute myocardial infarction and pulmonary embolism (Collen and Lijnen, 1984; Parker et al., 1988). These conditions result from an obstruction of a blood vessel by a fibrin-containing thrombus. The biological function of tPA, which involves degrading clots, makes it a logical candidate for the treatment of ischemic stroke. The Food and Drug Administration (FDA) approved tPA because it improved patient outcomes after ischemic stroke (annual sales of 275 million US-$ in 2008; http://www.gene.com/gene/ir/financials/ historical/thrombolytic.html). Still, the use of tPA has a few disadvantages that if addressed could yield improved drug therapy. tPA has several major limitations: 1) increased risk of hemorrhagic transformation; 2) harmful extravascular functions (e.g. blood-brain barrier breakdown) ; 3) sensitivity to endogenous inhibitors ; and 4) short time window of opportunity for clinical use (Qureshi, 1996).

2 RETROVIRUSES

2.1) STRUCTURE

Retroviruses are enveloped viruses with a diploid, positive sense, single stranded RNA genome covering 7 to 13 kb per monomer, which is replicated through a DNA intermediate that becomes integrated into the host cell genome (Goff, 2007). The envelope, consisting of the host cell membrane and viral glycoproteins, surrounds a protein core harboring the viral replication enzymes and the RNA genome. The viral genome exhibits a CAP structure at the 5′-end and a polyadenylated 3′-end and therefore resembles eukaryotic mRNA (Varmus, 1982). Furthermore, the viral genes are flanked by so-called long terminal repeats (LTRs), which are required for their integration into the host cell genome and efficient transcription. In addition, a sequence termed psi-site (ψ) ensures efficient packaging of the viral RNA into the particles. The viral genome includes the structural genes gag/pro, pol and env, which are a common feature of all retroviruses (Figure 4).

All structural proteins like the core forming capsid (CA), the RNA-bound nucleocapsid (NC) and the membrane-associated matrix proteins (MA) are encoded within the gag gene. In addition, the pol gene provides all viral enzymes, namely the reverse transcriptase (RT), the protease (PR) and the integrase (IN). The env gene encodes the envelope polyprotein (Env), which mediates host cell entry and thereby determines the tropism. The Env protein consists of two non-covalently linked polypeptides, the surface unit (SU) and the transmembrane domain (TM). In some viruses, such as Avian Sarcoma Leukosis Virus (ASLV) and Moloney Murine Leukemia Virus (MoMLV or MLV), SU and TM are attached to each other by disulfide bonds (Coffin et al., 1997).

The retrovirus' lifecycle differs from that of other organisms: it includes transformation of genetic material from RNA to DNA, integration of DNA into the host genome to form a provirus, transcription of the provirus to obtain genomic and messenger RNA, translation and processing of virion proteins, and finally budding of virions from the cell surface (Coffin et al., 1997).

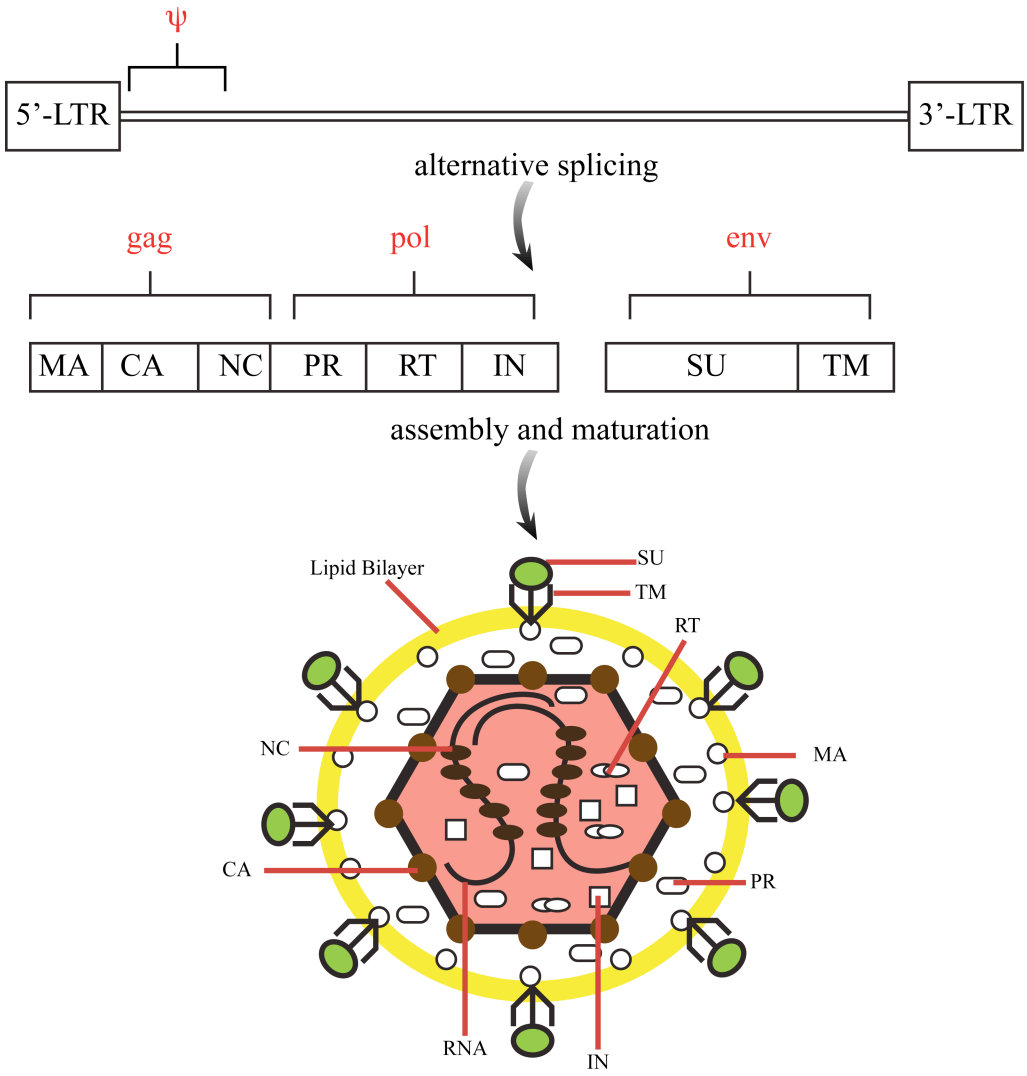

Figure 4. Schematic structure of a typical retroviral genome and the corresponding particle. All viral proteins are synthesised as precursor proteins, which are posttranslationally cleaved by viral and cellular proteases into single functional compounds. The core structure is formed by capsid proteins (CAs) and enveloped by a lipid membrane from the host cell. The Matrix protein (MA) is attached to the inside of the membrane. Furthermore, envelope proteins (Env) consisting of the surface unit (SU) and the transmembrane domain (TM) are embedded within the lipid bilayer and determine the tropism. The viral genome is complexed with nucleocapsid protein (NC) and packaged within the particle in form of RNA. In addition, all viral proteins required to initiate replication are incorporated. Among these there are integrase (IN), reverse transcriptase (RT) and protease (PR) molecules (Coffin et al., 1997).

2.2) Incorporation of non-viral proteins

During the processes of assembly and budding, host proteins are incorporated in the particle, either inside or on the surface of the virus (Ott, 2008). It is crucial to understand the mechanisms by which cellular proteins are brought into retroviruses. Some proteins are taken up as simple bystanders during budding, due to their close proximity to the budding site. These proteins are included non-specifically but they provide important information about the budding site and environment of retroviral assembly. Some proteins are incorporated because they interact with a retroviral protein, typically gag, they act like partners during the assembly and budding of the retrovirus. Other cellular proteins are 'captured' by retroviruses in order to obtain more biochemical functions. These cellular proteins are incorporated specifically into the particle during a post-assembly step and help the virus to evade the immune system or to replicate. Several studies have been conducted in this research area, mostly with eukaryotic cells infected with human immunodeficiency virus type 1 (HIV-1) (Table 1) (Cantin et al., 2005; Ott, 2008).

Table 1. List of molecules incorporated into HIV-1 and their functions (Cantin et al., 2005).

Host molecule	Function
CD45	Membrane phosphatase
CD46	Complement control protein
CD55	Complement control protein
CD59	Complement control protein
Actin	Cytoskeletal protein
Pin1	Peptidyl-prolyl isomerase
tRNA	synthetase Ligase
GAPDH	Aldehyde oxidoreductases
HSP27	HSPs, chaperone
HSP40	HSPs, chaperone
HSP60	HSPs, chaperone
HSP70	HSPs, chaperone
HSC70	HSPs, chaperone
HSP90	HSPs, chaperone
CypA	Immunophilin
CypB	Immunophilin
FKBP12	Protein degradation and sorting
Ubiquitin	Vesicular transport protein
Tsg101	Vesicular transport protein
Tal	Vesicular transport protein
VPS28	Vesicular transport protein
AIP1/ALIX	Vesicular transport protein
Staufen	RNA binding protein

2.3) DISPLAY STRATEGIES

The display of foreign proteins on the surface of retroviruses provides an important tool for the engineering of biomolecules and the analysis of their interaction with binding partners. For retroviral display, the protein of interest can be fused to the N-terminus of the Env protein, thus becoming incorporated into the particle membrane (Buchholz et al., 2008; Cosset et al., 1995; Russell et al., 1993). Different types of proteins have been displayed for various purposes on the surface of retroviral particles, the most important examples aim at: 1) redirecting particle binding and cell entry (Peng et al., 1999; Russell et al., 1993); 2) displaying of protease substrates (Peng et al., 1999); or 3) provoking an immune response (Nikles et al., 2005).

Single chain (sc) antibodies were the first polypeptides successfully displayed on retroviruses using the MLV Env protein as a scaffold. In particular, the sc antibody B1.8 was fused N-terminally to the MoMLV SU domain of Env and the resulting vector particles bound to the hapten recognised by B1.8, thus presenting the sc antibody in a functionally and accessible way (Russell et al., 1993).

The display of protease substrates was based on the phenomenon of growth factor receptor dependant sequestration. Engineering a protease substrate peptide between EGF and SU can restore the infectivity of particles bound to the EGF receptor. This strategy was used to display substrate peptides for disease-associated proteases such as matrixmetalloproteases (MMPs). Membrane-bound MMPs are expressed on the surface of many types of tumour cells or released into the extracellular matrix in order to allow invasion of metastasising cells. Thus, when added to EGF receptor positive cells expressing active MMPs, vector particles displaying EGF N-terminally of the MMP substrate peptide, bound the EGF recteptor, proteolytically cleaved it and finally entered the cell via the MLV receptor (Peng et al., 1999).

In another application the prion protein (PrP^c) was displayed on retroviruses to mediate a strong immune response in vaccination studies. Prions cause transmissible spongiform encephalopathies; they exist as the pathological conformer of the cellular protein PrP^c, which is essential for the replication of prions and disease development. An immune response against PrP^c can antagonise prion infection, but immunological tolerance against this self-protein must be broken if a vaccination strategy is envisaged. This was achieved successfully by displaying PrP^c on MLV-derived particles, which were subsequently injected into mice (Nikles et al., 2005).

3 Directed Evolution of Enzymatic Activities

3.1) Catalytic antibodies

The generation of protein variants that possess novel or improved catalytic activities by design or engineering has met with very little success, since it proved difficult to translate structural information into biological activity (Corey and Corey, 1996). However 'evolution' can be used as an alternative to 'design' or 'engineering'. Nature has generated tailored solutions for molecular recognition and catalysis by generating and selecting large libraries of proteins on an evolutionary time scale. The principles of evolution can be applied in the laboratory to generate enzymes with improved catalytic activities. These directed evolution systems must comprehend three features: 1) a method of generating genetic diversity; 2) a system to link genotype and phenotype and 3) a selection for biological activity.

The standard approach to prepare a catalytic antibody involves immunising animals with a stable transition-state analog for the reaction of interest. This approach relies on the assumption that a correlation exists between catalytic activity and transition-state analog affinity. Directed in vivo selection based on the complementarity to the transition-state analogue (TSA) for a given reaction has made it possible to efficiently produce catalytic antibodies. Phosphonate derivatives were the first and most successful haptens to elicit tailor-made esterolytic catalytic antibodies (Tramantano et al., 1986). Since then, a variety of catalytic antibodies have been generated based on haptenic TSAs (Blackburn et al., 1998). For example aldolase antibodies that catalyse the aldol and retro-aldol reaction have been generated, they exhibited an efficient turnover and rate accelerations above 10^8 (Zhong et al., 1999).

Catalytic antibodies are selected from an enormously diverse repertoire that evolves continuously, nevertheless, only a small portion of repertoire subsets that bind haptenic TSAs expresses catalytic activity. One of the most promising ways of expanding the structural space has turned out to be the selection of candidate antibodies in a phage-display system, in which heavy and light chain gene shuffling with subsequent randomised mutagenesis was performed (Fujii et al., 1998; Schultz

and Lerner, 1995). By generating a diverse repertoire of the appropriate complementarity-determining regions (CDRs) on a phage surface and screening for binding to an altered antigen (that was not used at the time of immunisation), substrate specificity and catalytic activity of catalytic antibodies were improved (Fujii et al., 1998).

3.2) PHAGE DISPLAY

Phages are viruses that infect bacterial cells; the majority of the vectors used in recombinant DNA research infect the bacterium *Escherichia coli*. The phage display vector incorporates 'foreign' DNA that is subsequently expressed as a protein and displayed on the outer surface of the phage particles (fused to the phage coat proteins, e.g. pIII or pV), thus allowing the coupling of genotype (a nucleic acid that can be replicated) to phenotype (a functional trait, such as a binding or catalytic or regulatory activity) (Smith and Petrenko, 1997).

The use of filamentous phage libraries has become a very powerful tool for the selection of peptides and protein ligands (Smith, 1985) . The five capsid proteins of the phage have been used for display purposes, the most common approach for protein display is the fusion of the foreign sequence to the amino terminus of pIII.

Huge libraries (10^{10}-10^{12} variants) have been generated and subjected to selection procedures. The most common selection procedure for binding requires the immobilisation of the target on a solid support. The phage mixture is passed over the target and the phages whose displayed proteins bind the target are captured allowing unbound phages to be washed away (Kehoe and Kay, 2005). The bound phages are eluted and subsequently propagated by simply infecting fresh bacterial host cells allowing multiple rounds of selection and directed evolution (Figure 5). Phage clones from the final selection step are propagated and the packaged DNA sequences are characterised individually.

Phage display has been successfully used for the selection of therapeutic antibodies that are now in clinical use (e.g. the anti-TNFα antibody Humira®). It has also been used to evolve properties different than binding. For example, it was employed to gain more insight into the substrate specificity of HIV-1 aspartic protease (HIV-1 PR). In this study a peptide phage display library was screened using HIV-1 PR to select for cleaved peptide sequences (Beck et al., 2000).

It is also possible to select proteins from phage-displayed libraries according to their catalytic activity. Many of these selections rely upon substrate analogues that bind the enzyme displayed on the phage covalently during or after catalysis. Nevertheless, this method has limitations, firstly it requires a detailed knowledge of the reaction mechanism, and secondly it imposes a considerable challenge in the design and synthesis of the substrate analogue. Finally the selection process might be directed to a single feature of the catalytic cycle such as a single transition state or to a reaction intermediate, whereas enzyme catalysis is likely to involve multiple transition states as well as product formation and release (Kehoe and Kay, 2005).

In general, phage display has some limitations: It is an *in vivo* method, as cells express the proteins, although selections take place under *in vitro* conditions. Thus proteins toxic to *Escherichia coli* and proteins whose export is suboptimal may be prevented from displaying on phage. Furthermore the maximum library size is restricted by the transformation efficiency ($>10^{12}$ independent clones). Moreover, it is challenging to display eukaryotic proteins requiring complex posttranslational modifications such as glycosylation or sulfation on phages. Hence, many proteins lack activity on the phage particles (Walsh and Jefferis, 2006).

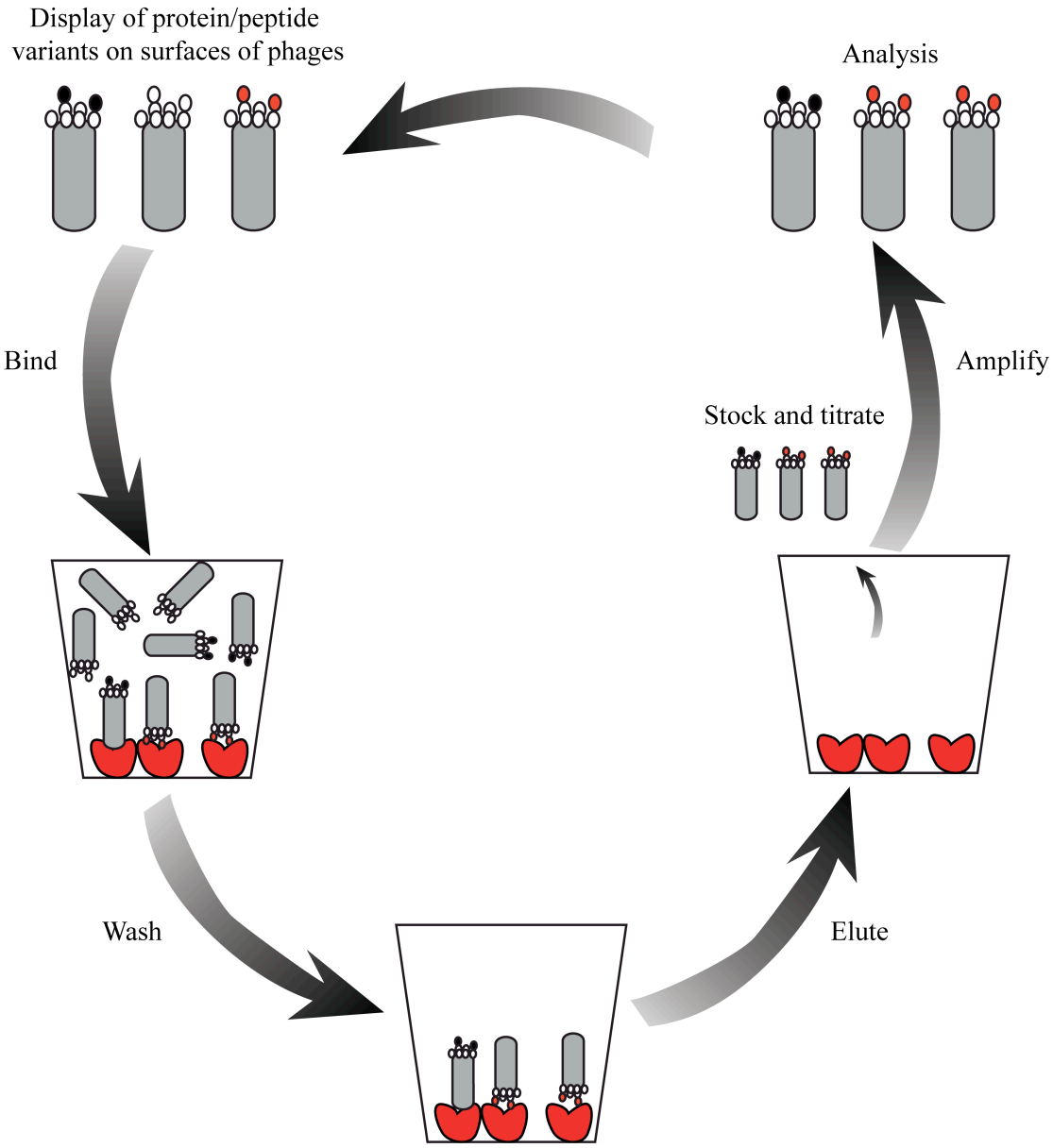

Figure 5. Selection of phages for the binding affinity of the displayed peptide/protein variants. Phages displaying different peptide and protein variants are added to the target (incubation and binding, top left). Subsequently, the unbound phages are washed away (bottom). The phages that bound the target are eluted (top right) and amplified (transformed into bacteria) for subsequent rounds of selection. After several selection rounds the eluted phages are transformed into bacteria and grown as single plaques for further analysis.

3.3) *IN VITRO* COMPARTMENTALISATION (IVC)

IVC is a directed evolution method in which all steps are performed *in vitro* (Tawfik and Griffiths, 1998). As mentioned before, evolutionary systems require a link between genotype and phenotype. In nature, this link is created by the compartmentalisation of genes in cells; in IVC the genes are compartmentalised in aqueous microdroplets of a water-in-oil (w/o) emulsion. IVC has several advantages over other *in vitro* selection techniques such as phage-display: first, it is possible to efficiently select for properties other than binding, such as catalytic or regulatory activities; second enzymes can be selected under multiple-turnover conditions by using fluorogenic assays and sorting droplets triggered on fluorescence using conventional FACS (Mastrobattista et al., 2005); and, third it allows selections without transformation steps.

In a typical IVC experiment, an aqueous solution of genes and an *in vitro* transcription/translation mixture is homogenised into oil to create a w/o emulsion. The emulsions are created at a ratio of genes to droplets such that most of the droplets contain no gene or a single gene. The most widely used IVC formulation provides droplets with a mean diameter of 1 μm and a mean volume of 5 femtolitres. Large libraries (10^8-10^{11} variants) of genes can be transcribed and translated in the microcompartments. Genes encoding enzyme variants are translated and the resulting proteins convert a non-fluorescent substrate into a fluorescent product, the emulsion is broken and all the microdroplets are combined. Genes linked to the product are amplified and then either characterised or linked to the substrate and compartmentalised for a further round of selection (Miller et al., 2006).

Although the first stage of all these laboratory evolution processes is generic (genes are transcribed and translated in discrete compartments), the second stage is not: different phenotypes dictate different means of selection. The different selection strategies comprise: selection for catalysis, selection for binding and selection for regulatory activities. IVC can be used to select for catalysis if the substrate and the subsequent product of the selected enzymatic activity are physically linked to the gene. Enzyme-encoding genes, with the product attached, can be separated (e.g. by affinity purification using a product-specific ligand) from genes that encode an inactive protein and carry the unmodified substrate. The simplest applications of this strategy lie in the selection of DNA-modifying enzymes, where the gene and substrate

comprise the same molecule; indeed, IVC was first applied for the selection of *M. HaeIII* DNA-methyltransferases. In the *M. HaeIII* selection procedure, a DNA encoding an active enzyme in a biotinylated DNA library was methylated in a compartment and rendered resistant to cleavage by restriction endonuclease HaeIII; thus, the biotin-label at the end of the DNA remained and could be used for affinity selection of uncleaved DNA encoding active methyltransferase with streptavidin beads (Tawfik and Griffiths, 1998). A similar strategy has been used to select restriction endonucleases (Doi et al., 2004) novel DNA polymerases (Ghadessy et al., 2001) and thiolactonases (Aharoni et al., 2005). Enzyme libraries have been selected by using fluorogenic substrates and subsequent sorting of emulsion droplets using fluorescence activated cell sorters (FACS) (Figure 6) (Mastrobattista et al., 2005). The water-in-oil emulsion was converted into a water-in-oil-in-water double emulsion, and the fluorescent droplets were sorted by FACS. As high-throughput screening (HTS) of double emulsions is a completely *in vitro* system, multiple cycles of mutation/recombination and selection can be performed quickly, and enzymatic activities which are toxic to a cell can be screened. Furthermore, the range of enzymes that can be selected is greatly expanded, as many fluorogenic substrates and coupled enzyme assays are available. IVC has also been used for the selection of proteins/peptides for binding, the expressed protein was coupled covalently or non-covalently to the gene that encodes it within the emulsion droplet. The emulsion was broken, the gene-protein complexes were recovered and those with desired activity were enriched by affinity purification using the target ligand (Bertschinger and Neri, 2004; Sepp and Choo, 2005; Yonezawa et al., 2003). IVC can also be used to select for regulatory functions. For example, highly potent protein inhibitors of DNA nucleases were selected, where selection was based on the ability to inhibit the DNase rather than binding it (as with phage-, or ribosome-display) and led to a $>10^5$ increase in affinity as well as selectivity (Bernath et al., 2005). Furthermore using a transcription-only system it has been used for the selection of ribozymes (catalytic RNAs) that catalyse Diels-Alder cycloadditions (Agresti et al., 2005).

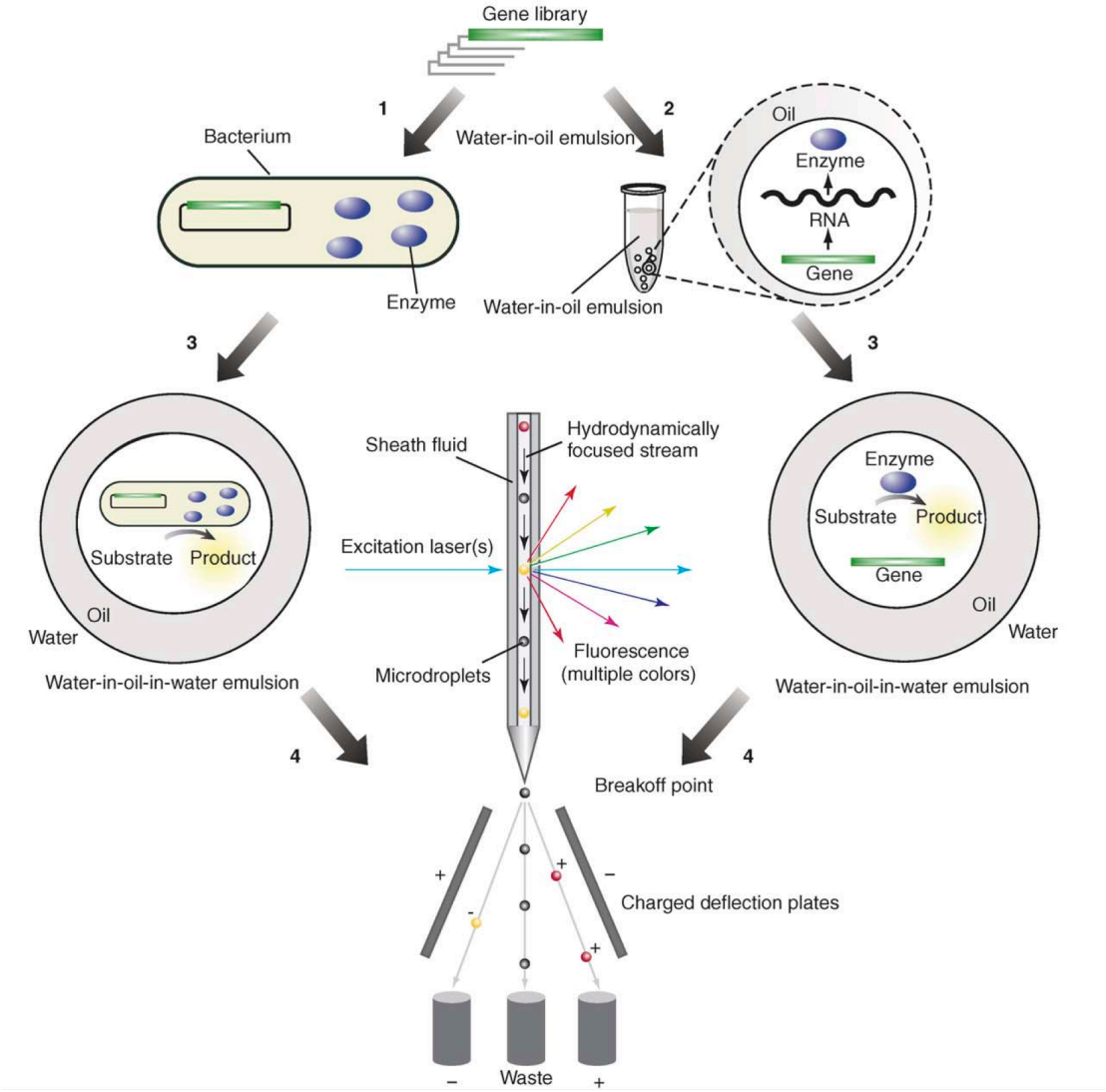

Figure 6. FACS selection of double emulsion droplets. (1) A library of gene variants is cloned and expressed in E. coli (in the cytoplasm, periplasm, or the surface of the cells). The bacteria are dispersed to form a water-in-oil (w/o) emulsion with typically one cell per aqueous microdroplet. (2) Alternatively, an in vitro transcription/translation reaction mixture containing a library of genes is dispersed to form a w/o emulsion with typically one gene per aqueous microdroplet and the genes are transcribed and translated within the microdroplets. (3) Proteins with enzymatic activity convert the non-fluorescent substrate into a fluorescent product and the w/o emulsion is converted into a water-in-oil-in-water (w/o/w) emulsion. (4) Fluorescent microdroplets are separated from non-fluorescent microdroplets using a fluorescence activated cell sorter (FACS).

4 High-throughput Screening (HTS)

4.1) Microplate systems

The number of new molecules available for screening has drastically increased during the last decade, because of new synthesis technologies such as combinatorial chemistry and automated synthesis. Moreover the advances in genomics and proteomics continue to produce new targets. As a result, pharmaceutical companies use HTS technologies as the primary tool for drug discovery. The goal of HTS is to accelerate drug discovery by screening large libraries (up to 100000 compounds per day) (Pereira and Williams, 2007). The development of assays for HTS requires high standards for reproducibility, robustness and compatibility with automation (Walters and Namchuk, 2003). Early in the HTS era (1980s), HTS assays were run in standard 96-well microplates. Twenty years later the industry has undergone a progression from 96-well plates to 1536-well plates in which reagent costs are typically 100 times lower and assay volumes have dropped from 100 µl to 1–5 µl. The 1536-well plate exhibits a good balance between low volume, high throughput and data quality, and several full screening campaigns have been performed (Maffia et al., 1999). Even further miniaturisation of microtiter plates is possible. A 3456-well plate with a volume of 1 µl per well has been introduced by Aurora (San Diego, CA, USA) (Mere et al., 1999). This system automatically screens >100 000 compounds per day in a miniaturised assay format. A tight fitting, specially designed lid controls evaporation. A plate reader measures the fluorescence from individual wells and a complete set of data can be obtained from the wells in <90 seconds, giving a potential throughput of >100 000 assay points per hour. 9600-well microplates with a volume of 0.2 µL have been molded from low fluorescence plastic, but evaporation at this volume becomes significant. These plates have been used for bead-based assays (Burbaum, 1998).
Current microplate systems involve robotics, liquid handling devices, sensitive detectors and software for data processing. However many issues burden the use of microplate systems: evaporation of liquids and inaccessibility to academic researchers due to high reagent, instrument and maintenance cost.

4.2) Lab-on-a-chip system

Alternatively to the use of microtiter plates, biological and chemical processes can be miniaturised on-chip. This technology includes non-fluidic systems such as microarrays as well as fluidic systems such as microfluidic chips.

4.2.1) Non-fluidic systems: microarrays

Microarray technology evolved from Southern blotting where fragmented DNA is attached to a solid support and then probed with a known gene. Microarray technologies include DNA microarrays, protein microarrays, cellular microarrays, antibody microarrays, tissue microarrays, and chemical compound microarrays (Khandurina and Guttman, 2002).

A microarray is any array (a large number of ordered objects) of biological material, printed on a solid substrate in a "micro" format, which allows many objects to share a relatively small area, on a microscope slide. The substrate material can be glass, plastic, or a silicon chip. The objects are placed on the substrate by a robot that can deposit very small volumes of material into discrete spots of the array. The material being deposited is in liquid form, and small pins dip down into wells of a microplate, pick up a small volume via capillary action, and then touch down on the substrate, leaving a tiny dot of liquid behind. This process is repeated by several pins operating in parallel, over many plates of material. Several categories of material can be spotted, typically DNA, RNA or proteins. More sophisticated techniques employ photolithography, electrochemical approaches, and even inkjet printing (Khandurina and Guttman, 2002). A typical screening experiment involves the incubation of the spotted material with a test substrate and an overnight hybridisation. After incubation all non-specific binders are washed off and a scanner performs the readout (Figure 7).

Microarrays can be used to understand basic cellular functions such as cell division, transcription, or photosynthesis. In the pharmaceutical industry microarrays are used to predict mechanisms of toxicity in drugs and to develop drugs that promote healthy living and enhance life span (Dhahbi et al., 2004). Winemakers have created a DNA chip containing the grape genome to help them develop strains that are better suited to certain climates (Waters et al., 2005).

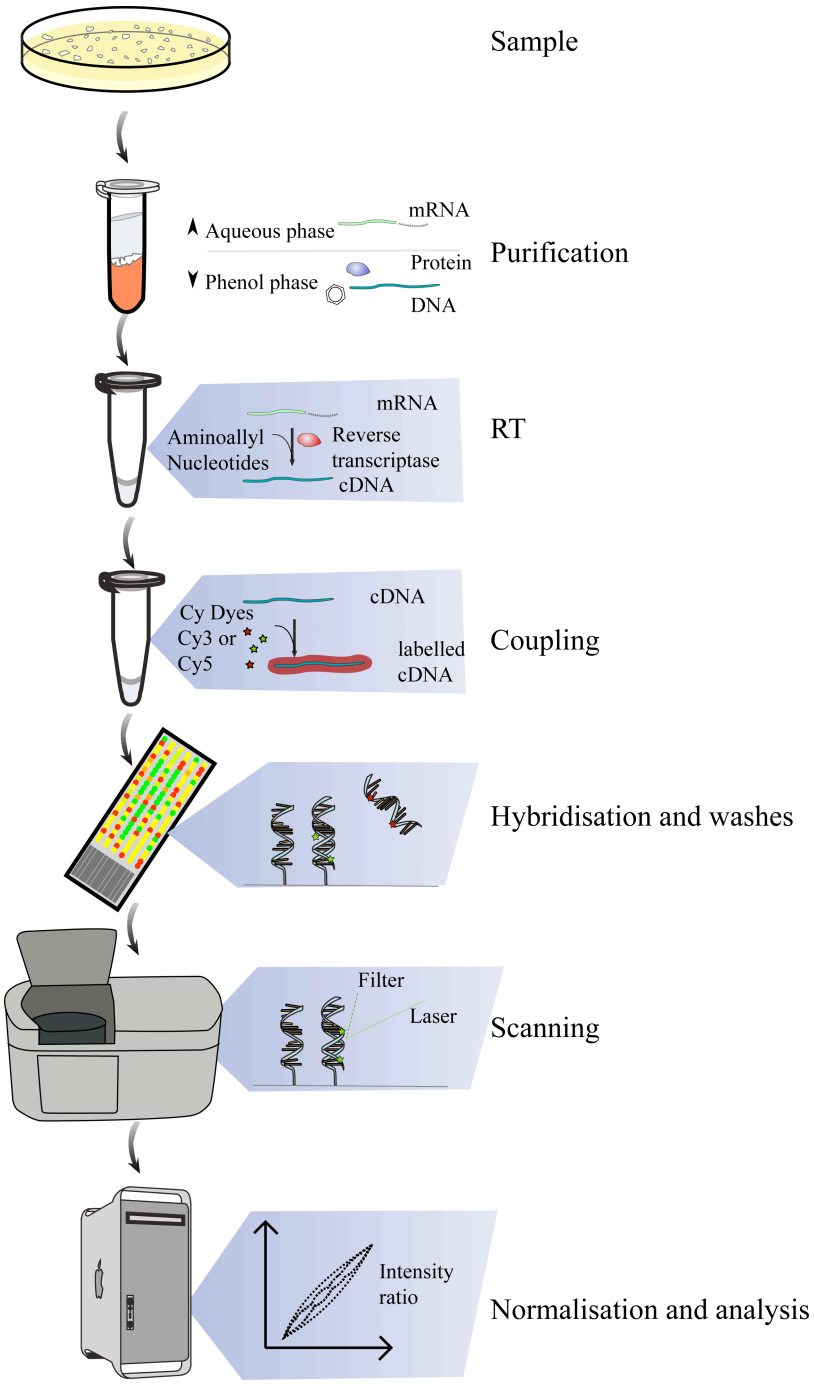

Figure 7. DNA Microarray. RNA is isolated by phenol-chloroform extraction. A Cy dye-labelled product is generated by reverse transcription of RNA into cDNA. Subsequently, the labelled samples are mixed with a hybridisation solution and the mix is denatured and added to the microarray. Following this, the microarray is hybridised overnight in a hybridisation oven and subsequently nonspecific binders are washed off. The microarray is dried and scanned by a device that excites the dye and measures its emission.

4.2.2) Fluidic systems: microfluidic chips

Currently available robotic systems are limited with regard to the speed of fluid dispensing that is achievable and the accurate handling of small liquid volumes that evaporate quickly (see 4.1). To overcome these limitations microfluidic technology has been developed; electrokinetic and hydrodynamic forces are used to move and mix reagents through the networks of microfluidic channels (Sundberg, 2000).

The advantages of miniaturisation comprise reduced reagent consumption and cost, reduced analysis time, accurate sample handling, easy automation and facile integration of functional components (Dittrich and Manz, 2006).

Several approaches have been developed, typically reagents are moved in channels or capillaries with diameters ranging from 10 μm to 500 μm. Initially, the channels were manufactured by deep etching processes on substrates such as glass or silicon or by hot embossing for polymeric substrates (Hong et al., 2009). Recently, the creation of integrated microfluidic devices has been accelerated by two developments in microfabrication techniques: Soft lithography using elastomeric polymers such as polydimethylsiloxane (PDMS) and multilayer soft lithography for the fabrication of valves, mixers and pumps.

Microfluidic devices have been used for a variety of applications. At Caliper Technologies Corporation (Mountain View, CA), microfluidic devices integrating direct compound sampling from microplate sources with continuous-flow enzyme inhibition assays have been developed (Sundberg, 2000). Furthermore, miniaturised devices for fluorescence-activated cell-sorting (μFACS) have been described and allowed a high-throughput of 12000 cells per second (Wolff et al., 2003). In another application, a microfluidic device consisting of multiple drug gradient generators and parallel cell culture chambers, in which the processes of liquid dilution and diffusion, micro-scale cell culture, cell stimulation and cell labeling were integrated was used to rapidly extract the maximum of information from human liver carcinoma (HepG2) cells in response to several drugs varying in concentration. The method called high content screening (HCS) allowed several independent cellular parameters to be measured in a single cell or populations of cells in a single assay (Figure 8) (Ye et al., 2007).

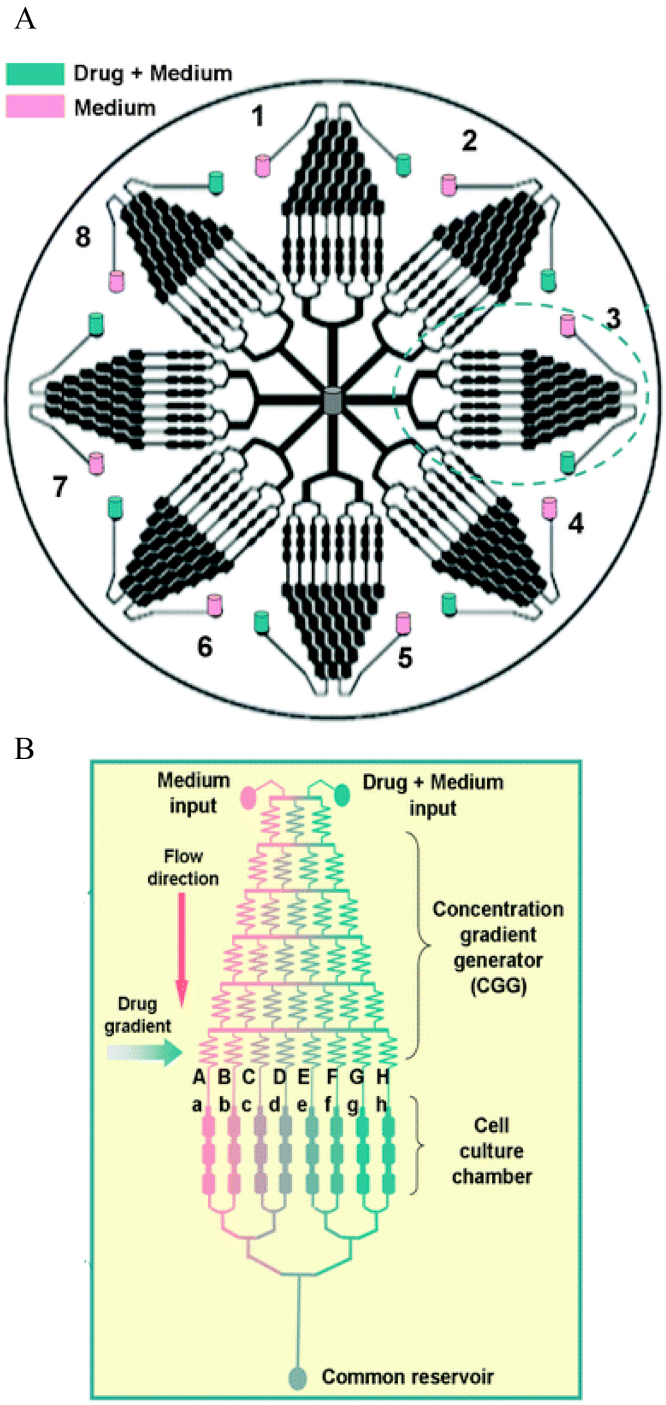

Figure 8. Integrated microfluidic device for cell-based high content screening (HCS). (A) The device consists of eight uniform structure units, which are connected by a common reservoir in the centre of the device. (B) Magnified section of a single structure unit containing an upstream concentration gradient generator (CGG) and downstream parallel cell culture chambers (Ye et al., 2007).

4.3) Droplet-based Microfluidics

The principle idea behind droplet based microfluidic systems is the use of single droplets as reaction compartments for biological assays or chemical reactions. Droplet-based microfluidics use a two-phase system, in which each assay is compartmentalised in an aqueous microdroplet surrounded by an immiscible carrier fluid (Figure 9).

The advantages of droplet-based microfluidics comprise the elimination of cross-contamination as a consequence of the isolation of the constituents in different droplets, the efficient mixing that occurs inside the droplets, the ability to incubate stable droplets off-chip and reinject them for analysis and the aptness to digitally manipulate droplets at very high-troughput. Droplets can be created at a rate of 10 kHz, they are generated either using fluid mixing in T junctions or flow-focusing in a microfluidic nozzle (Figure 9) (Song et al., 2006).

In the T-junction configuration, the inlet channel containing the dispersed phase perpendicularly intersects the main channel, which contains the continuous phase. The two phases form an interface at the junction and the head of the dispersed phase enters the main channel. Hence, the shear forces generated by the continuous phase and the subsequent pressure gradient cause the head of the dispersed phase to elongate into the main channel until the neck of the dispersed phase thins and breaks the stream into a droplet (due to the surface tension of the dispersed phase). In the flow-focusing configuration, the continuous phase and the dispersed phases are forced through a nozzle on the microfluidic device, in which the continuous phase symmetrically shears the dispersed phase into droplets (Teh et al., 2008).

Subsequent to their generation, the droplets can be manipulated in many ways on-chip. For example, they can be fused, subdivided, the reagents can be mixed, incubated in delay lines (Song et al., 2003) and sorted (Link et al., 2006) (Figure 9).

Droplet-based microfluidics have been used for a variety of applications such as: enzyme kinetics and DNA analysis (Zheng and Ismagilov, 2005), protein crystallisation (Zheng et al., 2004), synthesis of molecules (Hatakeyama et al., 2006), synthesis of nanoparticles (Frenz et al., 2008b; Shestopalov et al., 2004), microparticles and colloidal assemblies (Dendukuri et al., 2005) , synthesis of reaction networks (Gerdts et al., 2004) and cell-based assays (Clausell-Tormos et al., 2008).

Moreover, a living organism has also been encapsulated into a parallel series of nanoliter-volume droplets in a microfluidic device: *Caenorhabditis elegans* (*C. elegans*). The developed system was capable of accomplishing multiple functions including worm encapsulation, droplet generation, transportation and immobilisation on a single integrated device. *C. elegans* was co-encapsulated with a neurotoxin (1-methyl-4-phenylpyridinium, MMP+) which has been previously reported to cause Parkinson's disease (PD)-like symptoms in vertebrates. Subsequently, the mobility behavior and the phenotype features of individual worms in response to the neurotoxin were characterised (Shi et al., 2008).

In recent studies, fluorescence resonance energy transfer (FRET) measurements, in a segmented-flow microfluidic platform, have been used to analyse protein-protein interactions (Srisa-Art et al., 2009). In another study, fluorescence-activated droplet sorting (FADS) has been used to sort cells based on their fluorescence generated by an enzymatic activity (Baret et al., 2009b).

In general, droplet-based microfluidics offer significant advantages for directed evolution; aqueous droplets can be used as artificial cells containing genes, RNA, proteins and enzymatic products. Earlier studies have shown that droplets can serve as independent micovessels (Tawfik and Griffiths, 1998) enabling the selection for catalytic activities (Griffiths and Tawfik, 2006). Furthermore, the enzymes can be selected under multiple-turnover conditions by using fluorogenic assays and sorting droplets triggered on fluorescence (Baret et al., 2009b).

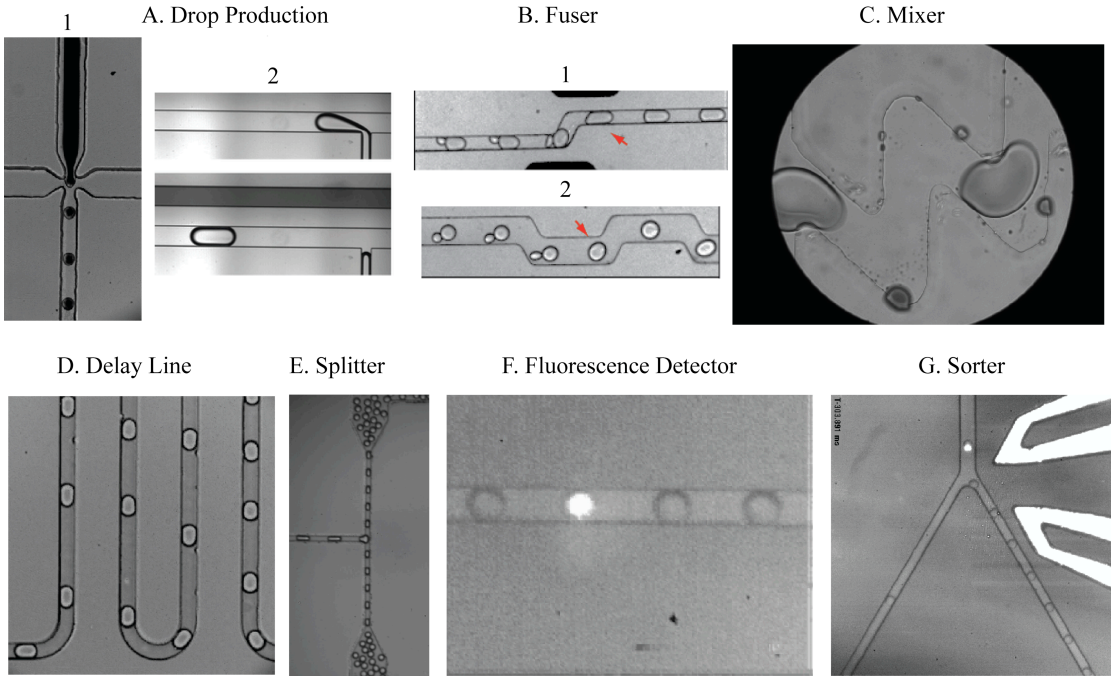

Figure 9. Microfluidic modules. (A) Formation of water-in-oil droplets by flow-focusing (1) or using a t-junction (2) (Thorsen et al., 2001; Vanapalli et al., 2009). (B) Fusion of droplets by electrocoalescence (1) or passive fusion (2) (Link et al., 2006; Mazutis et al., 2009; Song et al., 2003). (C) Mixing of droplets (Song et al., 2003). (D) Incubation of droplets in delay lines (Song et al., 2003). (E) Splitting of droplets (Link et al., 2004; Song et al., 2003). (F) Measurement of individual droplet fluorescence (Song and Ismagilov, 2003). (G) Sorting of droplets triggered on fluorescence (Ahn et al., 2006; Baret et al., 2009b; Griffiths and Tawfik, 2006; Link et al., 2006).

CHAPTER I

Fluorinated surfactants for Biological Applications in droplet-based microfluidics

1 Introduction

One of the major assets of microfluidic devices is the possibility of manipulating and analysing small samples of picoliter volumes in a high-throughput fashion. For applications that require compartmentalisation of the reagents (such as directed evolution) droplets of a water-in-oil emulsion can be used as independent reaction vessels. Drops can contain small numbers of molecules or cells, which due to the tiny volumes can still be analysed at biologically relevant concentrations. Furthermore, the small size of the drops greatly reduces the volume of reagents and thus the screening costs (Griffiths and Tawfik, 2006; Song et al., 2006).

The technological advancements of droplet manipulation have undergone considerable progress and high-throughput techniques have been developed (Baret et al., 2009b; Courtois et al., 2008; Frenz et al., 2009; Frenz et al., 2008a; Frenz et al., 2008b; Link et al., 2006). Droplets can be created at a rate of 10 kHz (Song et al., 2006), they can be fused, subdivided, the reagents can be mixed, incubated in delay lines (Song et al., 2003) and sorted (Link et al., 2006) (Figure 9). Furthermore, it has been shown that biological tests like enzymatic assays and single cell experiments can be performed in droplets (Baret et al., 2009b; Clausell-Tormos et al., 2008; Huebner et al., 2009; Koster et al., 2008; Song et al., 2006; Song and Ismagilov, 2003).

Many biological assays are based on an enzymatic activity generating a small fluorescent molecule for subsequent detection. In order to well distinguish the different biological activities within droplets these fluorophors must hence remain inside the compartment in which they were generated. Furthermore the long-term

storage of the emulsions is vital for the screening experiment. The basic requirement for successful screening is therefore reliable droplet stability and virtually no exchange of small molecules.

Since microfluidically generated emulsions are highly monodisperse, Ostwald ripening can be neglected and the lifetime of the droplets depends mostly on the stability of the thin film, or the magnitude of the disjoining pressure, between them.

The use of fluorocarbon oil as the continuous phase for the production of droplets is appealing because this oil is both hydrophobic and lipophobic (Studer et al., 1997). Thus, fluorocarbon oil has a very low solubility for biological reagents of the aqueous phase and inhibits molecular diffusion between drops. Furthermore, fluorocarbon oil causes less swelling of polydimethylsiloxane (PDMS), the material used to fabricate microfluidic devices (Lee et al., 2003). However, drops tend to coalesce for which reason they have to be stabilised by surfactants.

Fluorosurfactants are amphiphiles with fluorocarbon chains as the hydrophobic part. The strong hydrophobic interactions and low van der Waals interactions exhibited by fluorinated chains dramatically increase the tendency of fluorinated amphiphiles to self-assemble in water and to collect at interfaces, displaying strong surface activity compared to hydrocarbon surfactants. Fluorosurfactants can lower the surface tension of water down to a value half of what is attainable by using hydrocarbon surfactants (Kissa, 1994; Yoshimura et al., 2009), this ability is due to the lipophobic nature of fluorocarbons. The electronegativity of fluorine reduces the polarisability of the surfactants' fluorinated molecular surface; therefore they are not as susceptible to London dispersion force as hydrocarbon surfactants. Fluorosurfactants are more stable and fit for harsh conditions than hydrocarbon surfactants because of the very stable carbone-fluorine bond. This bond has a bond dissociation energy (BDE) of 130 kcal/mol, it is higher than any other carbon-halogen (carbon-chlorine 83.7 kcal/mol, carbon-bromine 70.1 kcal/mol, and carbon-iodine 57.6 kcal/mol) or carbon-hydrogen bond (104.9 kcal/mol).

Until now, only a few surfactants able to stabilise the interface between water and fluorocarbon oil have been described (Holtze et al., 2008). In addition to their role in emulsion stability, they can hinder the adsorption of biomolecules at the drop interface. Another requirement is the retention of small molecules in the droplets to avoid the mass transfer between droplets. Furthermore, during drop production, which is usually performed at rates of 1 to 10 kHz, surfactants must quickly reach the drop

interface in order to prevent coalescence upon contact between two drops. Hence surfactants must be mobile enough in the oil phase to reach the drop interface on the timescale of drop formation. This mobility depends on the surfactant size; therefore its molecular weight should not be too large.

An additional limitation is based on the critical micelle concentration (CMC), which determines the number of mobile surfactant molecules (Piirma, 1992; Tadros, 2005). Below CMC, all surfactant molecules are dissolved in the oil phase (unimers), but above CMC additional surfactant molecules assemble into micelles. Surfactant molecules can only diffuse to the interface in the form of unimers, but not in form of surfactant micelles. Hence the dissociation of surfactant micelles is the rate-limiting step for droplet stabilisation, when working above the CMC. Recent studies show that the CMC must be in the order of 10^{-4} mol/L or greater for a fast adsorption to the interface (Holtze et al., 2008).

Another important structural parameter of a surfactant is the hydrophile–lipophile balance (HLB; HLB = 20 x Mh/M with Mh: molecular mass of hydrophilic portion and M: molecular mass of the whole molecule). Surfactants with a low HLB (<8) are more lipophilic and thus tend to make a water in oil emulsion while those with a high HLB (>8) are more hydrophilic and tend to make an oil-in-water emulsion (Griffin, 1949).

Since fluorosurfactants are not commercially available, we synthesised them ourselves. There are several major challenges associated in synthesising a suitable surfactant that can be used for biological assays in droplets. The most obvious requirement is biocompatibility, i.e. all biological reactions should not be affected by the surfactant-decorated interface (Johnston et al., 1996). This limits especially the choice of charged surfactants since most proteins, cell walls and DNA are charged and could thus possibly interact strongly with an oppositely charged interface (Clausell-Tormos et al., 2008). The obvious solution for this problem is to use non-ionic surfactants. The second requirement is long-term stability of the resulting emulsions, since most biological assays require an incubation time of up to several hours.

2 Materials and methods

2.1) Chemicals

General Techniques. All reactions were carried out under a nitrogen atmosphere with dry, freshly distilled solvents under anhydrous conditions. Tetrahydrofuran (THF) was distilled from sodium-benzophenone. Anhydrous solvents were also obtained by passing them through commercially available alumina columns (Solv-Tek, Inc., VA). Reactions were monitored by thin layer chromatography (TLC) on 0.25 mm E. Merck silica gel plates (60F-254) using UV light for visualisation after vanillin treatment. E.Merck silica gel (60, particle size 0.040-0.063 mm) was used for flash column chromatography.

Oils. Perfluorinated oils FC-40 (Molecular formula: N-$(CF_2CF_2CF_2CF_3)_3$; MW: 650 g/mol; BP: 155°C), FC-3283 (Molecular formula: $(CF_2CF_2CF_3)_3N$ MW: 521 g/mol; BP: 128°C) and HFE-7100 (Molecular formula: $(C_5H_3F_9O)$ $(C_5H_3F_9O)$; MW: 250 g/mol; BP: 61°C) were purchased from 3M. 3M Fluorinert liquids are a family of clear, colorless, odorless, perfluorinated fluids having a viscosity equivalent to water but approximately 75% greater density. These products are thermally and chemically stable, compatible with sensitive materials, including metals, plastics and elastomers, non-flammable and practically non-toxic.

All low molecular weight chemicals, polyethylene oxide (PEO), polypropylene oxide (PPO) and Jeffamines were purchased from Sigma-Aldrich and used without further purification.

Educts for the synthesis of fluorosurfactants. Krytox FSH is a commercial lubricant from DuPont, its structure is $CF_3CF_2CF_2(\text{-O-}CF(CF_3)CF_2)_n\text{-O-}CF(CF_3)\text{-COOH}$ (Edmonds et al., 2007) and an endgroup analysis of the used batch, based on the CF_2-signal at -132.3 ppm yielded n = 37 and M_n = 6520 g/mol. ^{19}F NMR of 10 % (w/w) in FC40 (C6D6 insert for shimming): -81.4 (broad, -CF(C<u>F</u>$_3$)-COOH), -81.9 and -82.9 (broad, -O-CF(CF_3)C<u>F</u>$_2$-), -82.5 (d, J = 43 Hz, -O-CF(C<u>F</u>$_3$)CF_2-), -84.4 (CF_3CF_2C<u>F</u>$_2$-), -85.1 (s, C<u>F</u>$_3$$CF_2CF_2$-), -132.3 (s, CF_3C<u>F</u>$_2$

CF_2-), -134.6 (broad, -C<u>F</u>(CF_3)-COOH), -146.7 (t, J = 77 Hz, -O-C<u>F</u>(CF_3)CF_2-).

The molecular weight of the used polyethylene oxides, polypropylene oxides and their copolymers (Jeffamines®) were each determined by NMR end group analysis

(see Table 2). NMR spectra were recorded on Brucker Advance-400 instruments and calibrated using residual undeuterated solvent as an internal reference. The following abbreviations were used to characterise the multiplicities: s = singlet, d = doublet, t = triplet, m = multiplet, b = broad.

2.2) Synthesis of LG surfactants

Krytox-Chloride. Krytox FSH (1 equiv.) was dissolved in HFE7100, $SOCl_2$ (10 equiv.) dissolved in THF, was added slowly under nitrogen while stirring. The reaction mixture was stirred at r.t. for 4h and dried under vacuum for 24h.

LG8 and LG10. To 1 equiv. of Krytox-Chloride, dissolved in HFE7100, were added 1 equiv. (for LG8) or 0.5 equiv. (for LG10) of the respective Jeffamines (M-600 for LG8 and ED-600 for LG10) dissolved in THF. The reaction mixture was stirred for 4h at 75°C. The reaction mixture was concentrated, washed with FC3283 and filtered over celite. The excess solvent was removed and the crude oil was dried under vacuum for 12h to give clear, highly viscous liquid.
Yields: 97% (LG8), 87% (LG10)
^{1}H NMR of 10 % (w/w) in FC40 (C6D6 insert for shimming). LG8: 1.01 (d, J = 6.2 Hz, -CONH-CHC$\underline{H_3}$CH$_2$, endgroup), 1.14 (d, J = 6.2 Hz, -OCHC$\underline{H_3}$CH$_2$), 3.54 (broad, -OCHCH$_3$C$\underline{H_2}$-), 3.35 (s, H$_3$CO-, endgroup), 3.41 (broad, -OC$\underline{H_2}$C$\underline{H_2}$ and -OCHCH$_3$C$\underline{H_2}$), 3.07 (m, -CONH-C$\underline{H}$CH$_3$CH$_2$, endgroup). LG10: 1.013 and 1.221 (broad, -CONH-CHC$\underline{H_3}$CH$_2$), 3.637 (broad, -NH-C$\underline{H}$CH$_3$CH$_2$-), 3.700 (broad, PEO: OC$\underline{H_2}$C$\underline{H_2}$).

LG12. To a stirring solution of 1 equivalent 6-hydroxy-2-naphtalene sulfonic acid sodium salt (1 equiv.) in DMF was added K_2CO_3 (2 equiv.) and PEG750-Br (polyethylene glycol, 1 equiv.), the reaction mixture was stirred at 80°C for 12h. The reaction mixture was filtered through a 0.45 µm sterile filter and concentrated. The crude solid was purified by reverse phase C18 flash chromatography and eluted with MeOH-CH_3CN. The elute (1 equiv.) was dissolved in THF and $AlCl_3$ (1.3 equiv.) and Krytox-Chloride (1 equiv.) dissolved in HFE7100 was added dropwise. The reaction mixture was stirred at 80°C for 12h, concentrated, washed with FC3283, filtered over celite and concentrated. The crude oil was dried under vacuum for 12h.

Yield: 80%

^{1}H NMR of 10 wt.% in FC40 (C_6D_6 insert for shimming). LG12: 3.654 ppm (broad, PEO: OC$\underline{H_2}$C$\underline{H_2}$), 3.454 ppm (s, OC$\underline{H_3}$).

AEH17, AEH19 and AEH24 were kindly donated by Dr. Abdeslam El Harrak.

We analysed all surfactants by NMR and light scattering. Molecular weights of the polymer parts were determined by ^{1}H and ^{19}F NMR endgroup analysis and the purity of the low molecular weight hydrophilic head groups was confirmed by ^{1}H NMR.

2.3) Solution preparation

Stock solutions were prepared dissolving 10 % (w/w) of the surfactant in filtered FC40 (0.22 µm PTFE filter, Pall). The solutions were clear and no further purification was applied. Three solutions of 5, 2 and 1 % (w/w) were prepared from this stock solution and then further ten-fold dilutions (0.5 - 10^{-6} %) were set up. The solutions were transferred to dust free DLS cuvettes and sealed. The cuvettes were equilibrated for at least 24h at high concentrations above 0.5 % (w/w) and for 3 weeks for concentrations below. The equilibrium condition was checked by measuring the DLS of all solutions slightly above the CMC again after 2 months.

2.4) Dynamic light scattering (DLS)

DLS experiments were performed with a Malvern Zetasizer Nano S device, equipped with a 633 nm red laser (4 mW) at 25 °C. The autocorrelation function of the scattering intensity $\Gamma^{(2)}(t)$ and the mean scattering intensity were recorded from the backscattering intensity at 173°. The non-normalised autocorrelation functions, averaged over three consecutive measurements, were recorded for each concentration and fitted with a cumulant second order fit:

$$\Gamma^{(2)}(t) = b \exp(-2\Gamma t)\left(\frac{1 + \mu_2}{2t^2}\right)^2$$

where Γ is the decay rate with a pre-factor b, t the delay time and μ_2 the the second order polydispersity index. When the autocorrelation was very weak an offset was

applied to stabilise the fitting procedure. From this fit the apparent mean mutual diffusion coefficient D_a was calculated, by:

$$D_a = \frac{\Gamma}{q^2}$$

The scattering vector q was calculated, by:

$$q = \frac{4\Pi n}{\lambda}\sin(\frac{\theta}{2})$$

where λ is the incident laser wavelength (633 nm), n is the refractive index (1.396) of the sample and θ is the angle at which the detector is located with respect to the sample cell. Apparent hydrodynamic radii R_h were calculated using the Stokes-Einstein relation:

$$R_h = \frac{k_b T}{6\Pi\eta D_a}$$

With the Boltzmann constant k_b, the temperature T (in Kelvin) and the viscosity η (3.236 Pas), which was set equal to pure FC40 at 298 K.

2.5) Hydrophilic-lipophilic balance (HLB)

The hydrophilic-lipophilic balance was calculated by:

$$\mathrm{HLB} = 20 \times \frac{\mathrm{Mh}}{\mathrm{Mn}}$$

where Mh stands for the molecular mass of the hydrophilic portion and Mn is the molecular mass of the whole molecule.

2.6) Microfluidic devices

Microfluidic devices were prepared by standard soft-lithography techniques (see CHAPTER I for details) in polydimethylsiloxane (PDMS) with a channel depth of 21 µm. The PDMS was treated in an oxygen plasma oven (Gala Instrumente) and bound to a glass slide. A commercial surface coating agent (Aquapel, PPG Industries) was injected to decrease the wettability of the aqueous phase on the channel walls and subsequently dried with nitrogen prior to use. Volumetric flow rates were controlled using syringe pumps (PHD2000, Harvard Apparatus) and fixed throughout all the experiments in each of the inlet channels.

2.7) Biocompatibility tests

To assay the biocompatibility of the newly synthesised surfactants, we produced water-in-oil emulsions and determined the activity of encapsulated enzyme molecules. In particular we generated droplets containing viral particles displaying tissue plasminogen activator (tPA), HDVLK-AMC (Bachem) and Plasminogen (Roche) at a final concentration of 1 mM and 1.67 mM, respectively. Viruses and substrates were injected into the microfluidic device from separate 1 mL polyethylene syringes at a flow rate of 50 µL/h each. Droplets were generated by flow focusing (Anna et al., 2003) of the resulting stream with perfluorinated FC40 oil in presence of 2.5% (w/w) of the different surfactants (flow rate: 300 µL/h). For each sample, 200 µL of the resulting emulsion was collected in a 96-well plate, which was subsequently subjected to a fluorescence readout in a microplate reader (Spectramax M5 spectrophotometer, Molecular Devices). All measurements were performed with excitation and emission wavelengths of 370 nm and 450 nm, respectively.

2.8) Leakage tests

In order to assay the leakage of compounds out of the droplets, positive (high fluorescence) and negative droplets (low fluorescence) were mixed and the fluorescence was monitored over time. In case of leakage, the fluorescence intensity of the droplets should change over time, ultimately resulting in a single population of

medium fluorescence intensity. Three different leakage tests were conducted: First the tPA assay, second direct leakage of 7-amino-4-methylcoumarin and third leakage of Rhodamine 110.

A twin-dropmaker (see Chapter II, Figure 23A) was used to produce monodisperse droplets with a volume of 12 pL containing HDVLK-AMC (Bachem) and Plasminogen (Roche) at a final concentration of 1 mM and 1.67 mM, respectively, in presence (high fluorescence) and absence (low fluorescence) of MLV-tPA particles. The surfactant-stabilised droplets were collected in a reservoir and incubated for 1h at 37°C.

For direct product leakage tests we used the same twin-dropmaker to produce droplets containing 200 µM (positive droplets) or 20 µM (negative droplets) 7-amino-4-methylcoumarin. The surfactant-stabilised droplets were collected in a reservoir and incubated for 1h at 37°C.

To determine the leakage of Rhodamine 110, the twin-dropmaker was used to produce droplets containing 100 or 10 µM Rhodamine 110 (Interchim) and 10 mg/mL BSA (Sigma). The surfactant-stabilised droplets were collected in a reservoir and incubated for 6h at 37°C. (see Chapter II: In order to see a significant difference between the negative control (assay without MLV-tPA) and the positive control (assay with MLV-tPA) 6h of incubation were necessary in bulk assays).

Following incubation, the emulsions were reinjected into a microfluidic device (see Chapter I, Figure 23B) and the fluorescence of each drop was measured as described previously (Baret et al., 2009b). In brief, a 375 nm laser line (488 nm in the case of Rhodamine 110) was used to excite the fluorophores and the emitted light of each droplet was collected with a photomultiplier tube.

3 Results

3.1) Surfactant design

To be able to perform biological assays in droplets, we had to synthesise novel fluorosurfactants. These had to fulfil the following requirements: they must stabilise

the droplets (preventing coalescence), diffuse quickly to the droplet surface and show full biocompatibility.

Another important factor is the surfactant geometry, which is determined by the relative molecular weight of the surfactant moieties and its morphology. In general, low molecular weight surfactants with perfluorinated alkyl chains of six to eight carbon atoms do not stabilise the interface efficiently (Piirma, 1992; Tadros, 2005). Most likely this is due to a lack of steric repulsion between two neighbouring interfaces, which fuse quickly due to thermally induced fluctuations. In contrast, longer, polymeric perfluorinated chains stabilise the droplets efficiently (Clausell-Tormos et al., 2008; Holtze et al., 2008). Hence the perfluorinated tail seems to require a minimum chain length necessary to provide sufficient steric repulsion between the droplets. However, the surfactants have to be sufficiently small to be able to diffuse to the interface during the time scale of the droplet creation (~ms). Hence, there are many constraints concerning the fluorophilic part of the surfactant, but there are numerous possibilities for the hydrophilic head group. For example, variations on the head group can be performed on either the chain length of a hydrophilic polymer (e.g. of the ethylene oxide type) or by enhancing the hydrophilicity of a smaller head group. For our synthesis we used a commercially available perfluorinated polypropylene oxide carboxylic acid named Krytox FSH with a degree of polymerisation (DP) of 37 repeat units on average (Figure 10). We decided to keep this fluorophilic part for all surfactants and focus on the study of different headgroup morphologies. Three different surfactants based on an amide bonding between the perfluorinated polypropylene oxide (PPO) and the fully hydrogenated part were investigated, namely LG8, LG10 and AEH17 (Figure 10). LG8 is a copolymer of the A-B type where the hydrophilic part is a PPO with 950 g/mol. LG10 and AEH17 are copolymers of the A-B-A type with a $(PPO)_2$-$(PEO)_n$-$(PPO)_2$ hydrophilic part in between the two perfluorinated chains. The polyethylene oxide (PEO) part of AEH17 (n=18) is about 1/3 longer than that of LG10 (n=13). We also characterised two surfactants with more complex structures, based on a phosphoryl head group termed AEH 19 and AEH 24, and one ionic surfactant, LG 12, for general comparison. In order to circumvent possible problems that arise from a charged interface in combination with biological systems (protein adsorption etc.) the synthetic concept was to shield the charge in the naphtyl part with a PEO chain (Figure 10).

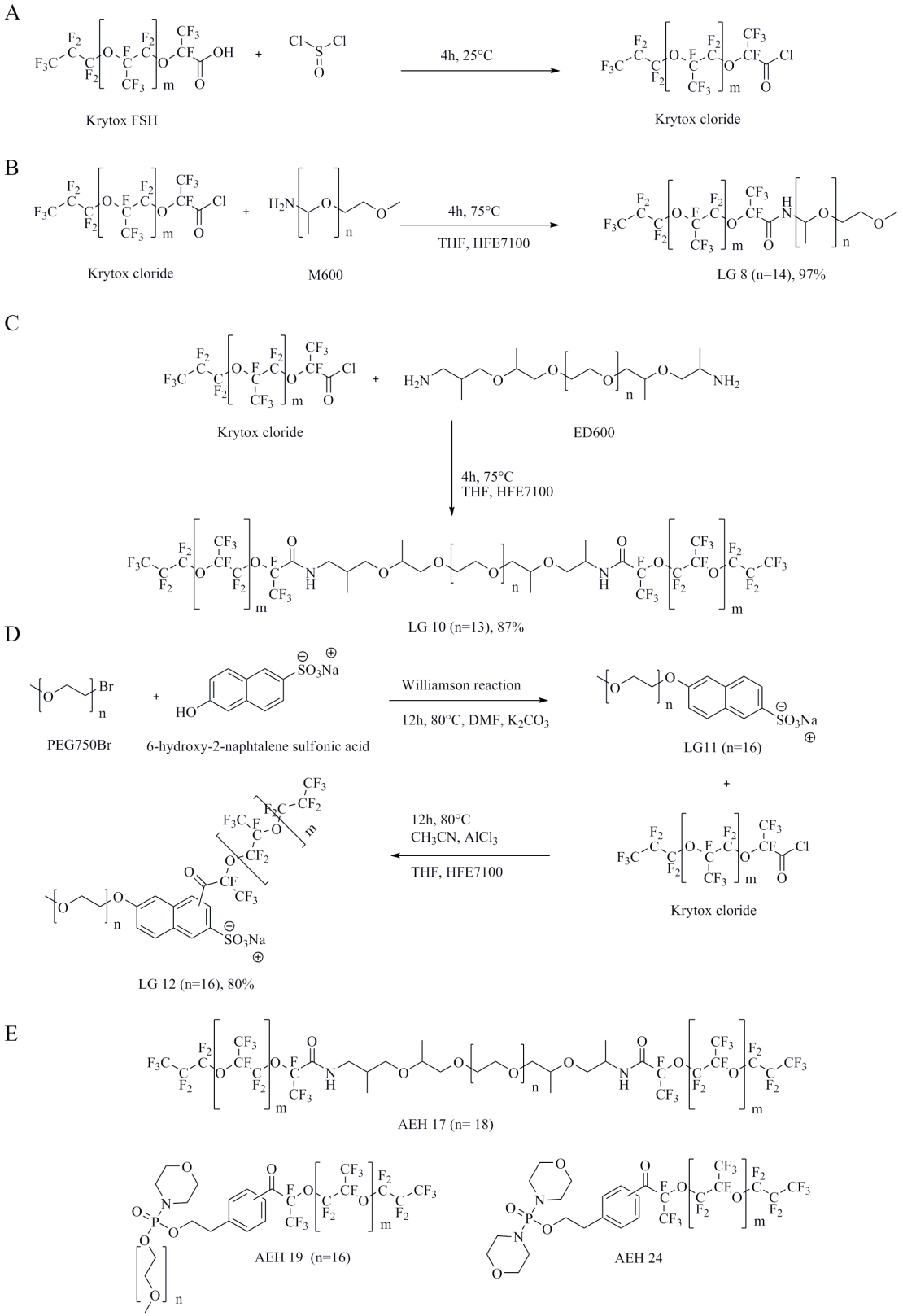

Figure 10. Surfactant synthesis. (A) Synthesis of Krytox-chloride. (B) Synthesis of A-B copolymer type surfactant LG8. (C) Synthesis of A-B-A block copolymer type surfactant LG10. (D) Synthesis of the ionic surfactant LG12. Williamson reaction yields LG11, which is subsequently reacted with Krytox chloride to yield LG12. (E) Surfactant structures. The perfluorinated polymer part has a chain length of m=37 units on average as determined by NMR end group analysis.

The structures of AEH19 and AEH24 are based on a phosphoryl head group and offer far more potential for varying the structure of both, the head group and the perfluorinated tail, for the desired properties. For example, it allows linking three chains in a simple way. Furthermore this group resembles the natural phospholipid bilayer and should therefore ensure complete biocompatibility (Figure 10).

3.2) Surfactant synthesis

Krytox chloride was prepared by addition of thionyl chloride (10 equiv. in THF) to Krytox FSH (1 equiv. in HFE7100). The carboxylic acid function of Krytox FSH was converted into the reactive derivative Krytox chloride (Figure 10).
Krytox chloride (1 equiv. in HFE7100) is a good electrophile and was converted into LG8 by nucleophilic substitution with the amine M-600 (1 equiv. in THF, Figure 10). Furthermore it was reacted with the diamine ED-600 (0.5 equiv. in THF, Figure 10) to yield LG10.
For the synthesis of LG12, 6-hydroxy-2-naphtalene sulfonic acid was used as a precursor. Williamson ether synthesis afforded LG11. LG12 was then prepared by reacting LG11 (1 equiv. in THF) with Krytox cloride (1 equiv. in HFE7100) (Figure 10).
The resulting surfactants showed entirely different characteristics: LG8 is an A-B copolymer type surfactant, LG10 is an A-B-A block copolymer surfactant and LG12 is an ionic surfactant.

3.3) Hydrophilic-lipophilic balance

To assure that the surfactants could be used for the formation of water-in-oil emulsions, we calculated their HLB number. The HLB number gives a useful indication of the solubility of the surfactants in the oil and water phases. A surfactant with a low HLB (<8) is predominantly hydrophobic, therefore it stabilises water-in-oil emulsions, and forms reverse micelles in oil. In contrast, a surfactant with high HLB (>8) is predominantly hydrophilic and stabilises oil-in-water emulsions, and forms micelles in water. We calculated the HLB number according to Griffin's method (Griffin, 1949) (for details see: Materials and Methods) (Table 2) .

Maximum stability for a water-in-oil emulsion is obtained for HLB numbers <8, because the surfactants are sufficiently surface active but do not lower the interfacial tension. In order to investigate the ability of the synthesised surfactant to stabilise droplets, a set of studies was performed.

3.4) Determination of the Critical Micelle Concentration

As a first step, we determined the CMC, which can be done by light scattering methods (Debye, 1949). We determined the CMC of the surfactants by plotting the averaged mean intensity of three consecutive DLS measurements as a function of the surfactant concentration in a double logarithmic plot. The mean intensity ($\bar{I}$) of the scattered light depends on the surfactant concentration (C). For C < CMC, the system contains only small surfactant monomers which scatter the light weakly; whereas for C > CMC the monomers associate to form large micellar aggregates, which scatter the light strongly. A discontinuity in the slope of $\bar{I}$ versus C thus defines the CMC. The apparent self-diffusion coefficient of the micelles was also determined and the corresponding apparent Stokes-Einstein radius calculated (Table 2). The hydrodynamic radius ($R_{h,app}$) is calculated from the diffusion coefficient using the Stokes-Einstein equation. By definition, the DLS measured radius is the radius of a hypothetical hard sphere that diffuses with the same speed as the particle under examination. This definition is somewhat problematic with regard to visualisation however, since hypothetical hard spheres are non-existent. In practice, macromolecules in solution are non-spherical, dynamic (tumbling), and solvated. As such, the radius calculated from the diffusional properties of the particle is indicative of the *apparent* size of the dynamic hydrated/solvated particle. Hence the terminology, 'hydrodynamic' radius.

The CMCs of all the surfactants were very low (Table 2), thus a high surface coverage of the interfaces at equilibrium at low surfactant concentration in the oil is obtained. Furthermore, the values of the apparent diffusion coefficients of all the surfactants were very similar. Consequently, we could not predict which surfactant was the best one, since the characterising parameters were very similar. Therefore a complementary method was applied to determine the drop stability.

Table 2. Average molecular weight M_n of the surfactants, their hydrophilic part M_h, average apparent diffusion coefficient D_a, apparent (Stokes-Einstein) hydrodynamic radii $R_{h,app}$, the hydrophilic-lipophilic balance (HLB) and critical micelle concentrations (CMC).

	M_n [1] g/moL	M_h g/moL	D_a [2] 10^{-12} m2/s	$R_{h,app}$ [2] nm	HLB	CMC w/w % (10^{-3} mol/L)
LG8	7500	870	0.73	92	2.32	0.01
LG10	13500	800	0.98	69	1.18	0.01
AEH17	14000	1020	0.71	82	1.45	0.033
LG12	7400	720 (+ionic)	0.12	512	1.95	0.12
AEH19	7500	720, (+MP) [3]	1.04	65	1.92	0.007
AEH24	6850	250 DMP [3]	0.94	72	0.73	0.006

[1] determined by NMR end group analysis
[2] average value slightly above the CMC, determined by DLS
[3] DMP: Dimorpholinophosphate, MP: Morpholinophosphate

3.5) Droplet stability

To determine the drop stability, we used a technique, based on a statistical video analysis of droplet coalescence as a function of the time after which the droplets get in contact with each other (after generation in the microfluidic device).

It was demonstrated, that in addition to the static effect of stabilisation by an increase of surfactant concentration, the dynamics of adsorption of surfactant at the water-oil interface is a key element for droplet stabilisation (Baret et al., 2009a). Therefore we measured the stabilisation capacity of different concentrations of surfactants, by gradually decreasing the time after which the droplets first come into contact following drop production (Baret et al., 2009a).

We used this technique, to calculate a stability parameter *S*:

$$S = \frac{n(1)}{\Sigma i\, n(i)}$$

where the number of non-coalesced droplets *n(1)* is divided by the total number of generated droplets, *i* corresponds to the number of fusions that one specific droplet was subjected to. The method yields stability curves that show a drop with a stability parameter *S* as function of a parameter t c^2, t being the time after which the droplets

get in contact and *c* the surfactant concentration (for details see (Baret et al., 2009a)) (Figure 11).

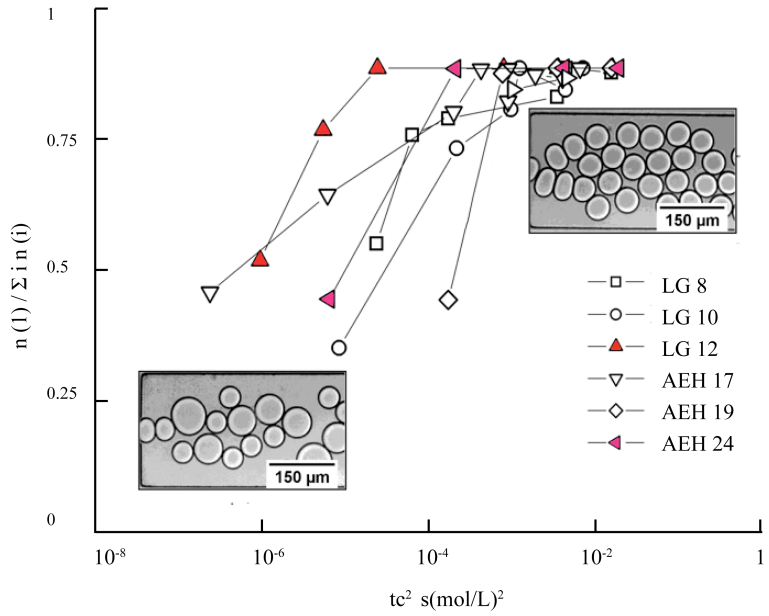

Figure 11. Stability curves of different surfactants in FC40, using Milli-Q water as the aqueous phase. The insets show a completely stable (upper right) and non-stable emulsion (lower left). The stability of the droplets (Y-axis) is represented as a function of the parameter tc^2 (X-axis).

Using our surfactants we obtained the highest stability for LG12 and AEH24. In fact, LG12 had the highest stability values for the lowest surfactant concentrations (Figure 11). This ionic surfactant stabilised the droplets more effectively than AEH19, the analogous non-ionic structure, thus the charge mediated a much lower minimal concentration to stabilise the droplets. AEH24 with its two morpholino moieties attached to the phosphoryl group showed a strongly increased short-term stability (e.g. increased mobility of the surfactant) compared to AEH19, which is probably due to the replacing of the large PEO part in AEH19 by a short and very hydrophilic part (DMP), as for AEH24. AEH 19 must not only reach the interface by diffusion, but swell its PEO chain in the aqueous environment in order to stay there. As there is a certain time necessary to swell the head group for rendering it more hydrophilic, the AEH19 molecules are probably detaching faster from the surface, before the PEO part is swollen. This kinetic effect drastically reduces the short-term stability, whereas the hydrophilic double morpholino headgroup of AEH 24 probably stays at the interface as soon as it has diffused to it. Its exchange rate with the bulk solution is much

slower. The highly dynamic effect of initial interface stabilisation is not only based on the ability to reach the interface but also on the exchange rate of adsorbed surfactants with the bulk solution. As it is known that micelles with copolymers are very stable (Tadros, 2005), the micelles of AEH 19 exchange slower than the ones of AEH 24 within the bulk solution. This leads to a depletion of free surfactant molecules in the vicinity of the interface.

Comparing the slopes of LG10 and AEH17, it was observed that the slope of LG10 shifted faster from the unstable regime ($S < 0.5$) to the stable regime ($S > 0.5$), thus the droplets were better stabilised at low surfactant concentrations by LG10 than by AEH17 (Figure 11). This difference in stability between LG10 and AEH17 is most likely based on the fact that the two fluorophilic chains are separated by different hydrophilic chain lengths, namely the PEO part (Table 2). LG10 has a shorter PEO part, therefore the two fluorophilic Krytox chain ends are closer to each other, resulting in a more prolate chain conformation that probably penetrates deeper into the oil phase. This results in a better steric repulsion of two neighbouring droplets due to a thicker repulsive oil layer (shell) and thus less coalescence. For AEH17, this proximity effect is lower. Consequently, AEH17 showed a very smooth transition from stable droplets at high surfactant concentrations to complete fusion at low concentrations. LG8 and LG10 showed similar stabilities, but LG10 produced stabler droplets due to its faster transition between the stability – instability regime.

3.6) Biocompatibility

After finishing the physical/chemical characterisation of the surfactants, we focused on their biocompatibility. It is well known that the surfactants may interact with biomolecules such as DNA, RNA and proteins, resulting in unfolding of their higher order structure at the drop interface. In many cases, this causes the encapsulated biomolecules to lose their activity (Roach et al., 2005). For this reason, we analysed the biocompatibility of the surfactants by performing the tPA fluorescence assay in the droplets and determining the enzymatic activity in presence and absence of the different surfactants. The reaction kinetics for the different surfactants were monitored by fluorescence readout and compared to the reaction in bulk (Figure 12A and B). None of the surfactants inhibited the reaction significantly, in fact for LG8, LG10 and LG12 the kinetics were even slightly accelerated compared to the bulk

experiment. Only AEH19 showed some inhibitory effects, resulting in a minor decrease of the enzymatic turnover (Figure 12B).

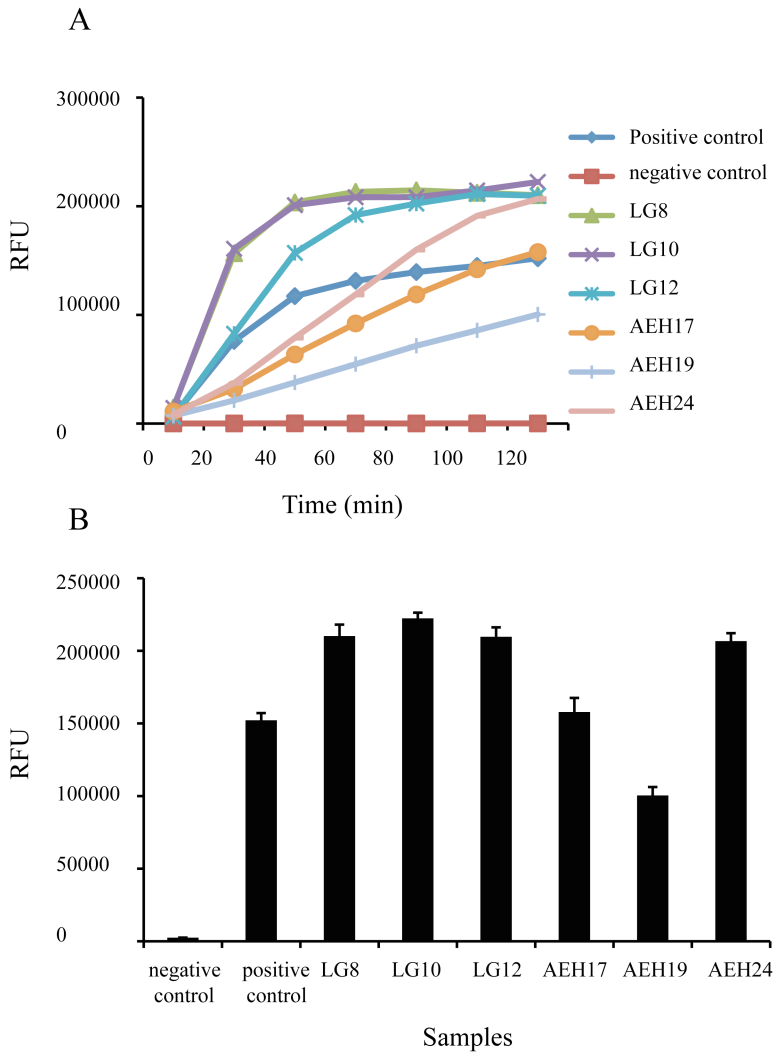

Figure 12. Biocompatibility tests. Droplets containing all components of a fluorescence-based assay for tPA activity were generated in presence of different surfactants (concentrations: 2.5% (w/w) in FC40). The resulting fluorescence was measured. For control purposes the reaction was also performed in bulk (positive control) or in absence of enzyme (negative control). The concentrations (enzymes and substrates) were the same for all assay conditions. (A) Kinetic data of the fluorescence assay for tPA. (B) Fluorescence after 2h (endpoint measurements).

3.7) Mass transfer between droplets

As a next step, we determined the mass transfer between droplets. Recent studies have shown that contents of microdroplets can leak into the oil phase, and mass transport of molecules from the continuous phase (oil) to the aqueous phase can occur too (Mary et al., 2008). Transport from or into droplets can occur on a time scale of milliseconds (ms) to hours, depending on the nature of the molecules being transported. Two main mechanisms have been established to explain this phenomena: 1) Diffusion of the droplet contents into the oil (Bibette et al., 1992; Hai et al., 2004; Hai and Magdassi, 2004; Pays et al., 2002) or; 2) formation of reverse micelles leading to the exchange of compounds between the droplets (Cheng et al., 2007; Hai and Magdassi, 2004; Koroleva and Yurtov, 2006).

Transport by diffusion is mainly dependant on the solubility of the droplet content into the aqueous phase and the oil phase. In contrast, transport mechanisms involving reverse micelles are mainly dependent on the surfactant concentration. In this case, an increase of the surfactant concentration in the oil phase leads to the formation of more reverse micelles, which serve as carriers of molecules from one droplet to another.

In order to assay the leakage of compounds out of the droplets, we generated and mixed positive (high fluorescence) and negative droplets (low fluorescence) and monitored their fluorescence over time. In case of leakage, the fluorescence intensity of the droplets should change over time, ultimately resulting in a single population of medium fluorescence intensity.

In a first experiment we used a twin-dropmaker to produce droplets containing 200 µM (positive drops) or 20 µM (negative drops) 7-amino-4-methylcoumarin (AMC). The surfactant-stabilised droplets were collected in a reservoir and incubated for 1h at 37°C.

In a second experiment we generated droplets in which the fluorescent product AMC was produced over time (Figure 13). We expected the product to leak slowly in this case as it is produced gradually. To do so, we generated droplets containing MLV-tPA particles, which convert plasminogen into plasmin. Subsequently the plasmin converts the substrate HDVLK-AMC into the fluorescent product AMC. We used the same twin-dropmaker to produce droplets containing all assay components in presence (positive drops) and absence of MLV-tPA particles (negative drops).

The surfactant-stabilised droplets were collected in a reservoir and incubated for 1h at 37°C. In bulk assays, 1h of incubation was sufficient to see a significant difference between the negative control (assay without MLV-tPA) and the positive control (assay with MLV-tPA).

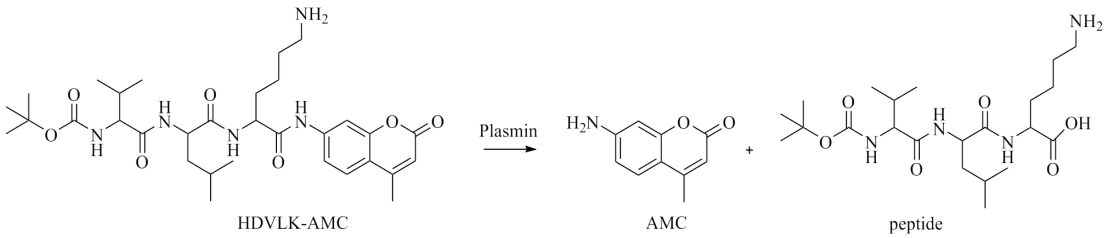

Figure 13. Assay for the activity of plasmin. This enzyme converts the substrate into the fluorescent product AMC.

In a third experiment we used the same twin-dropmaker to produce droplets containing 100 µM (positive drops) or 10 µM (negative drops) Rhodamine 110 and 10 mg/mL BSA. The surfactant-stabilised droplets were collected in a reservoir and incubated for 6h at 37°C. (see Chapter I: In bulk assays, 6h of incubation were necessary to see a significant difference between the negative control (assay without MLV-tPA) and the positive control (assay with MLV-tPA)).
Following incubation the emulsions were reinjected into a microfluidic device and the fluorescence of each drop was measured. A 375 nm laser line (488nm for Rhodamine 110) was used to excite the fluorophores and the emitted light of each droplet was collected with a photomultiplier tube.

For AMC (20µM or 200µM), we observed two distinct droplet populations directly after drop production (t_0). However, upon reinjection after 1h we observed only one resulting peak, clearly indicating massive leakage (Figure 14).

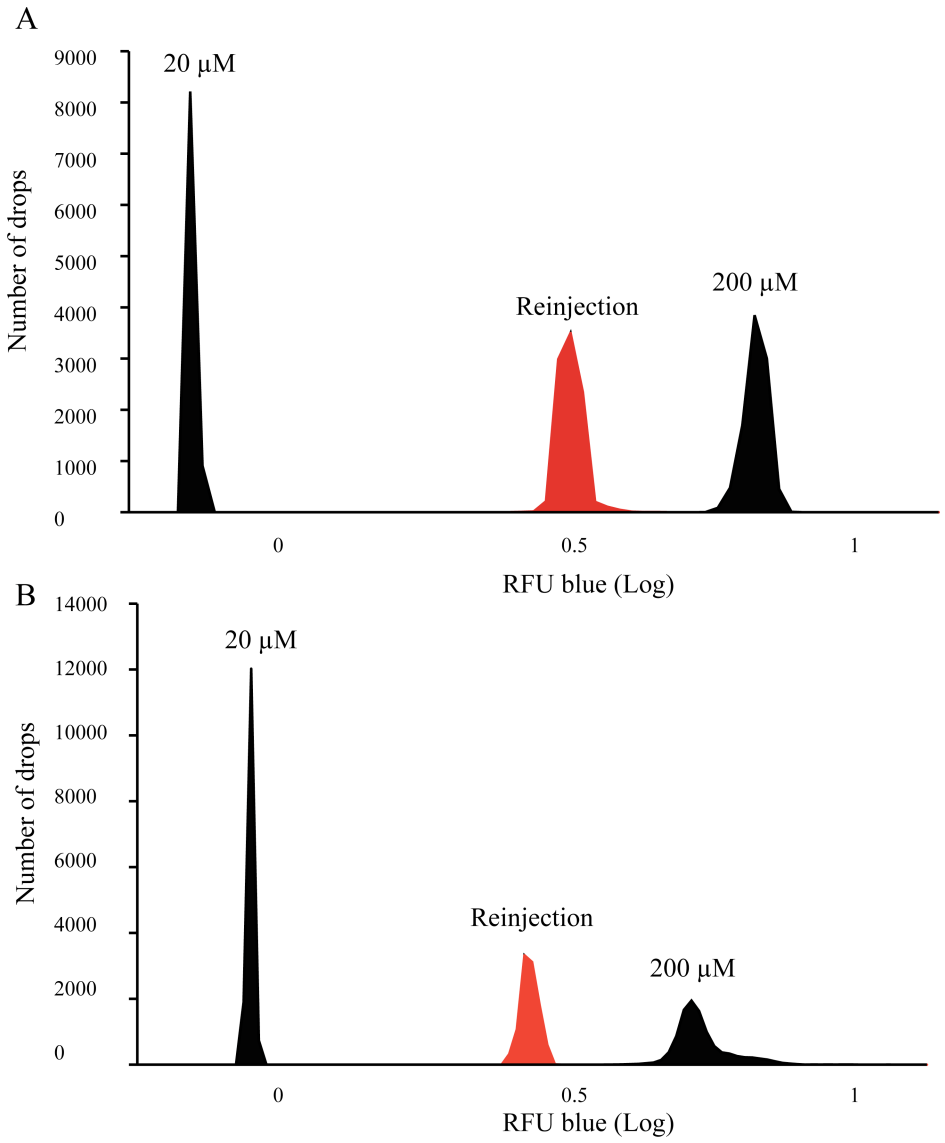

Figure 14. Leakage of 7-amino-4-methylcoumarin. Fluorescensce signals measured during drop production (black) and after 1h incubation off-chip (red). (A) Drops produced using 2.5% (w/w) LG12 in FC40. (B) Drops produced using 2.5% (w/w) AEH24 in FC40.

In a second experiment, we encapsulated the tPA assay components: in this assay the AMC is produced continuously. However after 1h incubation the product had leaked completely (Figure 15). We attributed the fast leakage of the coumarin to the hydrophobicity of the molecule (Figure 13). Recent studies have shown that substituent groups like methyl increase the diffusion of fluorophores into the oil phase (Courtois et al., 2009). In summary, we did not observe a significant difference in the transport properties for the two applied surfactants (LG12 and AEH24), which both showed significant leakage.

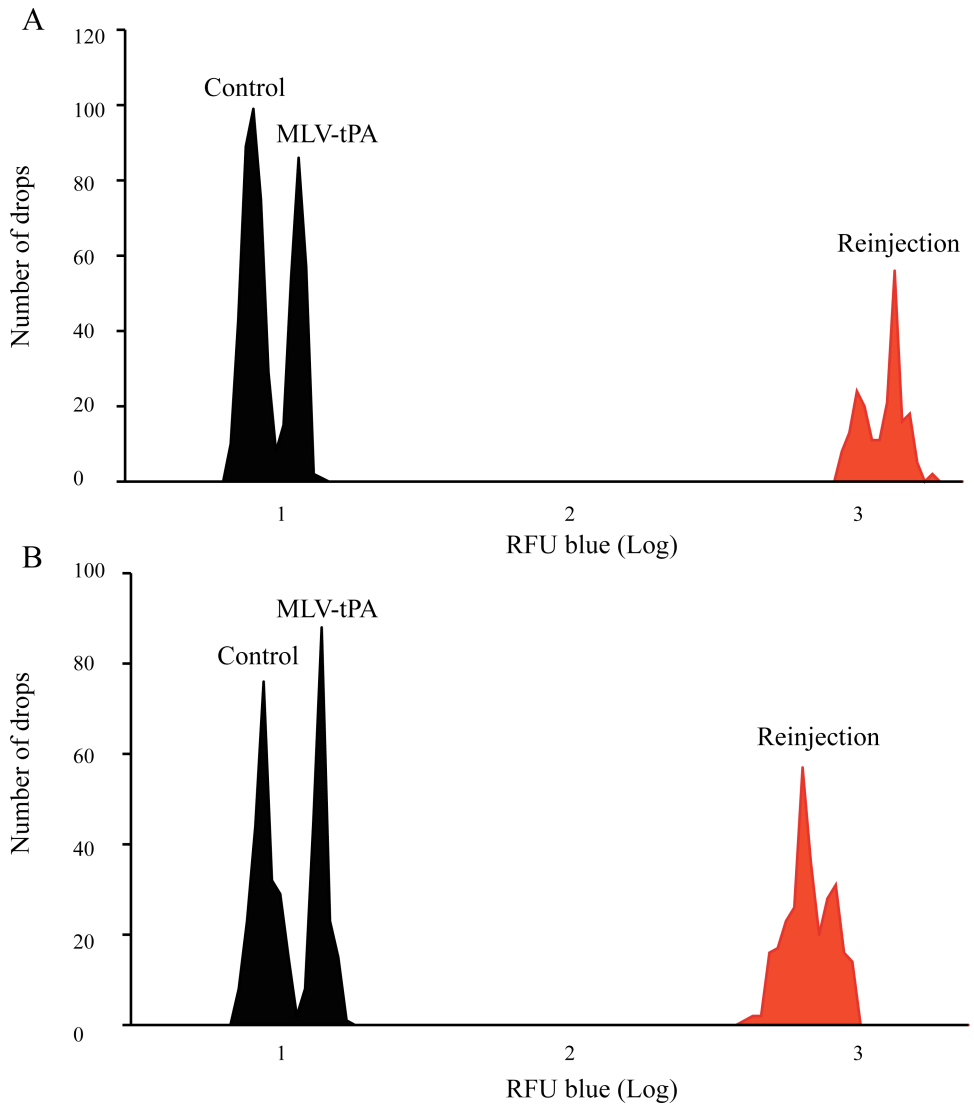

Figure 15. Leakage of 7-amino-4-methylcoumarin. Fluorescence signals measured during drop production (black) and after 1h incubation off-chip (red). (A) Drops produced using 2.5% (w/w) LG12 in FC40. (B) Drops produced using 2.5% (w/w) AEH24 in FC40.

In a third experiment we measured the fluorescence of the droplets containing Rhodamine 110 (10µM or 100µM), during drop production and obtained two clearly distinguishable peaks. Strikingly, even after 6h off-chip incubation and subsequent reinjection, we observed two distinct populations (Figure 16). This significant lower leakage of Rhodamine 110 in comparison to AMC is most likely due to its higher hydrophilicity, because of its zwitterionic properties (Figure 17). Furthermore we added BSA to the assay, since recent studies had shown that biopolymers such as BSA stabilise water-in-oil emulsions (Courtois et al., 2009). BSA molecules form a

complex at the oil-water interface, thus improving the stability of the drops. In this study, the effect of BSA was found to be independent of the surfactant concentration.

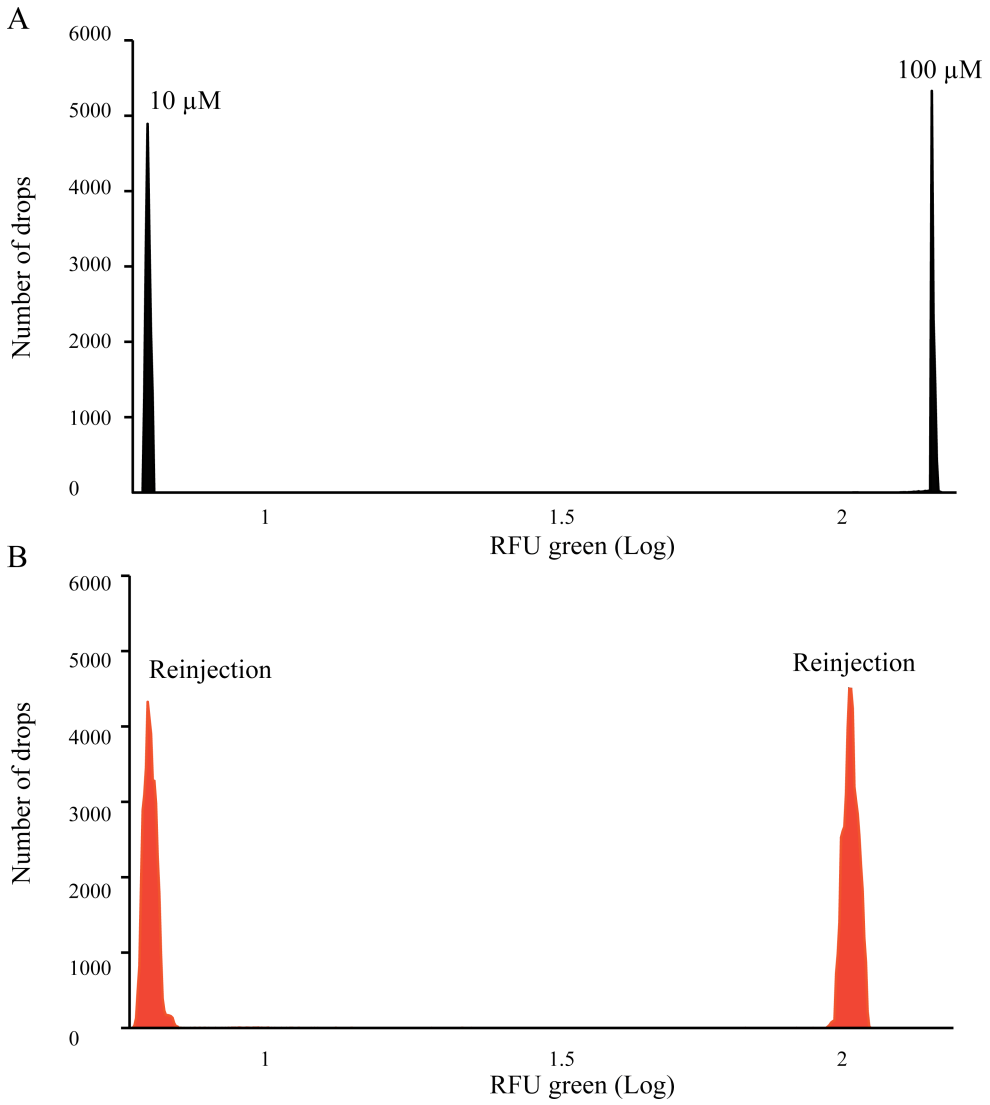

Figure 16. Leakage of Rhodamine 110. (A) Fluorescensce signals measured during drop production (black) (B) Fluorescensce signals after 6h incubation off-chip (red).

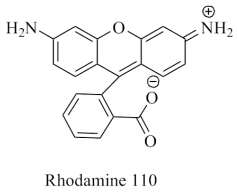

Rhodamine 110

Figure 17. Structure of Rhodamine 110.

In summary, LG12 showed the best surfactant properties: it efficiently stabilised the droplets and exhibited an excellent biocompatibility. Furthermore, it did not mediate significant mass transfer when using the highly hydrophilic Rhodamine 110 as the fluorophore. Rhodamine 110 is a valuable fluorophore for microfluidic droplet-based experiments, since its hydrophilicity decreases the transfer between droplets significantly.

4 Discussion

We synthesised a variety of novel perfluorinated surfactant molecules and tested the resulting droplet stability and biocompatibility using an enzymatic assay. All of the surfactants were biocompatible and produced stable droplets, although significant differences were obtained.

When looking at the CMC of the different surfactants under investigation, we observed no significant impact of the free surfactant concentration on the droplet stability. This was most clearly seen for LG12 with a CMC that is 20 times higher than that of AEH24, but with a relatively small difference in stability. The high concentration of free LG12 molecules did not at all improve the short-term stabilisation of the newly generated droplets. In fact, the CMCs of all surfactants are very low, which is desirable since it leads eventually to a high surface coverage of the interfaces at equilibrium at low surfactant concentration in the oil.

All the surfactants showed biocompatiblity and enzymatic reactions were even slightly accelerated in presence of some surfactants. Noteworthy we observed differences in the biocompatibility of different batches, most likely due to minor impurities in the final product that are already present in the unpurified educts.

Finding a surfactant that perfectly fulfils requirements for successful screening, like reliable drop stabilisation and biocompatibility, is challenging. Good biocompatibility as for LG8 was accompanied by less stable droplets. However, with LG12 we successfully synthesised a surfactant, which fulfils both requirements.

It was synthesised with the idea of using the stabilising properties of charged surfaces and preventing any negative effect (such as protein interaction) by shielding the charged group. To achieve this, a PEO chain was introduced in vicinity of the ionic

group. In agreement with this, LG12 indeed exhibited the best drop stability and the best biocompatibility. In general a high hydrophilicity of the headgroup seems to be preferable as it allows the generation of stable emulsions at low surfactant concentrations.

The transfer of small molecules between droplets is a consequence of diffusion into the oil phase as well as formation of reverse micelles. These inverse micelles are proportionally less likely to form on increasing headgroup charge, since hydrophilic sequestration would create highly unfavorable electrostatic interactions. We observed that diffusion was mainly dependant on the nature of the molecules being transported. The 7-amino-4-methylcoumarine diffused rapidly because of its hydrophobic properties. For Rhodamine 110 we observed almost no leakage, which is probably due to the presence of charges on the molecules resulting in lower solubility in the fluorous phase.

CHAPTER II

Ultra-High-Throughput screening of enzymes by retroviral display using droplet-based microfluidics

1 Introduction

Display technologies such as phage display are widely used techniques for protein engineering, allowing the selection and evolution of protein variants with desired properties (Levin and Weiss, 2006). In a typical phage display experiment, huge numbers (up to 10^{10} – 10^{12}) of protein variants are generated on the genetic level and subsequently displayed fused to the coat proteins of phage particles. Phage particles package the gene encoding the protein variant displayed on their surface, which allows coupling of genotype and phenotype to be achieved. Subsequently these particles are subjected to a selection procedure (most commonly the binding to an immobilised target molecule). The power of this approach results from the fact that the phage can be replicated to allow multiple rounds of selection and directed evolution (if mutations are introduced between the rounds of selection). Furthermore, the generation of the libraries, as well as the amplification/identification of selected variants can be performed using highly efficient genetic methods. This not only allows the rapid generation of billions of protein variants, but also their selection and identification at concentrations that are far below the detection level of conventional methods in protein chemistry. These conceptual advantages have also been exploited by further display methods such as the display of proteins on the surface of bacteria (Francisco et al., 1993) or yeast cells (Boder and Wittrup, 1997), or completely in vitro systems such as ribosome- (Hanes and Pluckthun, 1997) and mRNA display (Roberts and Szostak, 1997) where all steps of the selection procedure (including the

protein expression) can be performed without the need for any cell transformation, thus allowing the screening of even more diverse libraries.

Phage display has been effectively applied to the selection of therapeutic antibodies, which are now in clinical use (e.g. the anti-TNFα antibody Humira®).

Furthermore the method has proven to be extremely powerful for the selection of other target-binding molecules such as ankyrin repeat proteins (Binz et al., 2003) and for the characterisation of HIV protease cleavage sites (Beck et al., 2000). Phage display has also been used for the selection of proteins with catalytic activities. However, this application requires a technique coupling a catalytic property with an acquired binding activity. This can be achieved by displaying enzyme variants on the phage particles and subsequently selecting for binding to enzyme-inhibitors or transition state analogues (Soumillion et al., 1994), (Hansson et al., 1997). Alternatively, the enzyme and its substrate can be co-displayed on the phage particle before selecting for product-specific adsorption to a solid support (Demartis et al., 1999). However, these strategies, generally do not allow the selection for multiple turnover (Fernandez-Gacio et al., 2003). Therefore, enzyme variants that perform the desired chemical modification at very slow turnover rates (e.g. due to inefficient product release) are often selected (Vanwetswinkel et al., 2000). Consequently, the selection of efficient catalyts remains problematic. A further limitation of phage display is the fact that it does not allow the selection of eukaryotic proteins requiring complex posttranslational modifications such as glycosylation or membrane anchorage. Hence, many proteins lack activity on the phage particles or cannot be displayed at all (e.g. due to misfolding or aggregation in the periplasm) (Brinkmann et al., 1995; Deng et al., 1994; Jung and Pluckthun, 1997). In contrast, posttranslationally modified proteins can be efficiently displayed on viruses which infect eukaryotic cells such as baculovirus (Wang et al., 2005), avian leukosis virus (ALV) (Khare et al., 2003) or the murine leukemia virus (MLV) (Buchholz et al., 1998; Cosset et al., 1995; Russell et al., 1993). However, so far, none of these systems has been used successfully for the selection and directed evolution of surface-displayed enzymes.

We present here a novel approach allowing structurally complex mammalian enzymes to be screened under multiple turnover conditions. In this system, enzymes are displayed on the surface of the murine leukemia virus (MLV) and subsequently encapsulated into drops of a water-in-oil emulsion. Earlier studies have shown that

each droplet can serve as an independent microreactor (Tawfik and Griffiths, 1998), allowing the selection of RNAs and proteins for a range of binding, regulatory and catalytic activities (Griffiths and Tawfik, 2006). For example, enzymes can be selected under multiple-turnover conditions by using fluorogenic assays and sorting droplets triggered on fluorescence using either conventional fluorescence activated cell sorters (FACS) (Mastrobattista et al., 2005),(Aharoni et al., 2005) or microfluidic devices (Baret et al., 2009b). Here we show how the advantages of retroviral display can be combined with compartmentalisation strategies, thus allowing the screening of structurally complex mammalian enzymes at ultra-high-throughput. As a model system, we chose human tissue plasminogen activator (tPA), since this enzyme is of high therapeutic relevance (tPA is an emergency drug for deep vein strokes with annual sales of 275 million US-$ in 2008) and requires posttranslational modifications for enzymatic activity (Walsh and Jefferis, 2006).

2 Materials and methods

2.1) Plasmids

The plasmid pOGP3, encoding MLV gag/pol, and the MLV-packagable plasmid encoding tPA (pMSCV-puro-tPA) have been described elsewhere (Patent WO2006082385) (Randow and Sale, 2006). The neuraminidase (NA) gene was amplified, the PCR product was digested, ligated into the SfiI- and AccI-digested backbone and we obtained the MLV-packagable plasmid encoding NA (pMSCV-puro-NA). The following oligonucleotide sequences were used to amplify the NA gene from the plasmid pCMV-NA (Cosset and Verhoeyen, 2007):
NA-sfiI(+), 5'-AAAAGGCCCAGCCGGCCATGAATCCAAATCAGAAAATAATAACC-3'; NA-accI(-), 5'-AAAAAAAAAAAAAAAGTCGACTCTGCCCTCGATCTTGTCAATGG TGAATGGCAAC-3'.

2.2) Cells

HEK293T cells (a human embryonal kidney cell line expressing the large T antigen) were grown in DMEM medium (GIBCO-BRL) supplemented with 10% fetal bovine serum (GIBCO-BRL) and 1% penicillin/streptomycin (GIBCO-BRL). Cells were incubated at 37°C under a 5% CO_2 atmosphere saturated with water.
For passaging, cells were trypsinised (0.25% trypsin in PBS, GIBCO-BRL) and a fraction (1/10) of the resulting suspension was seeded into new culture flasks. Subsequently, fresh medium was added.

2.3) Freezing and thawing of cultured cells

Freezing. Cells were trypsinised and resuspended in DMEM. Subsequently a centrifugation step (340 g for 10min at 4°C in an Eppendorff 5810R tabletop centrifuge, was carried out to pellet the cells. These were then resuspended in freezing medium (90% FCS, 10% DMSO) and divided into cryotube aliquots of approximately 1.5 x 10^6 cells and frozen at -80°C.

Thawing. Cryotubes were incubated in a water bath at 37 °C until the samples thawed. Then the cell suspension was immediately transferred into a Falcon tube with 15 mL prewarmed medium. To remove the cytotoxic DMSO, cells were subsequently centrifuged (340 g for 10min at room temperature), resuspended in fresh medium (2.5 mL, 7.5 mL or 25 mL) and seeded into culture flasks of desired size (25 cm^2, 75 cm^2, or 175 cm^2).

2.4) Generation of competent bacteria and transformation thereof

2.5 ml of an over night (o.n.) culture were used to inoculate 100 mL of fresh LB-Media which was subsequently incubated at 37°C in a bacteria shaker. Cells were allowed to grow to an OD_{600} of about 0.3 – 0.4, hence reaching the logarithmic growth phase. Then the culture was incubated on ice for 5min, divided into two portions and pelleted at 3220 g for 10min at 4°C. Subsequently the cells were

resuspended in 1 mL 1M $CaCl_2$ (chilled) and water was added to a final volume of 20 mL (final concentration of $CaCl_2$ = 50 mM). After incubation on ice for 20min the cells were pelleted again (as above). Subsequently, the cells were resuspended in 3 mL, 50 mM $CaCl_2$, each, and incubated on ice for 2.5h. Afterwards 100 µL of the suspension was portioned into Eppendorf tubes and frozen at –80°C.

For standard plasmid amplification, transformation of chemically competent cells (generated as above) has been performed. For this purpose, the cells were thawed on ice and approximately 50 ng plasmid DNA (encoding the gene of interest and an additional antibiotic marker) were added. After further incubation on ice for 30min, a heat shock at 42°C for 60sec was performed in a thermoblock (Eppendorf). Then 500 µL of prewarmed (37°C) LB medium (Sigma) was added and the sample was incubated for 1h at 37°C to allow the expression of the antibiotic marker. Subsequently the bacteria suspension was plated onto LB-AMP-plates (1% (w/v) Bacto-Trypton, 0.5% (w/v) yeast extract, 1% NaCl, 50 µg/mL ampicilin 1.5% (w/v) agar agar) and grown over night (o.n.) at 37°C.

2.5) Generation of plasmid DNA for transfection

Preparation of plasmids from bacteria was performed using the Qiagen plasmid kits according to the manufacturers instructions. For purification of low amounts of DNA (Miniprep, purification of up to 20 µg plasmid DNA), 5 mL over night cultures were inoculated using LB-AMP-Medium (1% (w/v) Bacto-Trypton, 0.5% (w/v) yeast extract, 1% NaCl, 50 µg/mL ampicillin). The next day, bacteria were harvested and centrifuged at 1800 g for 15min (Eppendorf 5810R centrifuge). The concentrated cells were lysed using solutions delivered by the manufacturer (P1 & P2). Chromosomal DNA and cellular fragments were excluded by centrifugation (1800 g for 5min in a tabletop centrifuge, Eppendorff 5810R). Subsequently the supernatant was applied to anion exchange columns (Qiaprep-8-strips) to specifically purify nucleic acids.

For extraction of larger amounts of DNA (Maxiprep, purification of up to 1 mg plasmid DNA) 200 mL LB-AMP-Medium were inoculated and cultivated over night. Bacterial yield was performed at 1800 g for 15min (Eppendorf 5810R centrifuge). Afterwards cells were lysed and the remaining cell debris and chromosomal DNA

was removed by centifugation (3220 g for 20min). The resulting supernatant was subsequently purified over an anion exchange column and precipitated (isopropanol precipitation) according to the manufacturers instructions. Finally, concentration and purity of the DNA was determined photometrically.

2.6) Generation of viral particles

Retroviral particles were generated by calcium phosphate transfection of HEK293T cells (Gavrilescu and Van Etten, 2007). A hepes-buffered saline solution (HBS) containing phosphate ions was combined with a calcium chloride solution containing the DNA to be transfected. When the two were combined, a fine precipitate of the positively charged calcium and the negatively charged phosphate formed. The suspension of the precipitate was added to the cells to be transfected.
One day prior to transfection $1.1x10^7$ cells were seeded in 175 cm^2 culture flasks (Nunc). The next day, transfection was performed using 21 µg of pOGP (encoding MLV *gag/pol*) and 21 µg of the transfer vector encoding the displayed protein (pMSCV-puro-tPA or pMSCV-puro-NA). 24h post transfection, the medium was replaced by 12 mL of fresh DMEM media. 48h and 72h post transfection the supernatants were collected, centrifuged at 340 g and filtered through a 0.45 µm filter. The filtered supernatant was subsequently concentrated by ultracentrifugation (Optima L-100 XP, Beckman-Coulter) through a sucrose cushion (2 mL, 25%) for 2h at 77566 g.

2.7) Microplate tPA assays

For the measurement of tPA activity, two different assays have been performed. The first one is based on the fluorogenic plasmin substrate HDVLK-AMC (Bachem) which was added to 1.67 µM plasminogen (Roche) at a final concentration of 1 mM. All measurements were performed with excitation and emission wavelengths of 370 nm and 450 nm, respectively, using a Spectramax M5 microplate reader (Molecular Devices). In an alternative assay system, the tPA activity was measured using Z-FR-Rhodamine 110 (Interchim) which was added to 1.67 µM Plasminogen (Roche) at a

final concentration of 0.5 μM. All measurements were performed with excitation and emission wavelengths of 498 nm and 521 nm, respectively.

Inhibition experiments. Viral particles displaying tPA were incubated for 6h at 37°C with 1.6 μM plasminogen (Roche), 0.5 μM Z-FR-Rhodamine 110 (Interchim) and plasminogen activator inhibitor type 1 (PAI-1, Genentech) at the indicated concentrations (0.5 – 4 μg/mL). All measurements were performed with excitation and emission wavelengths of 498 nm and 521 nm, respectively.

2.8) Microfluidic devices

Each microfluidic device was designed to have a channel depth of 21 μm and nozzles (for drop formation) with a width of 21 μm. The devices were fabricated using polydimethylsiloxane (PDMS) and standard soft-lithography techniques (Squires and Quake, 2005.): A mould of SU-8 resist (MicroChem Corp.) was fabricated on a silicon wafer (Siltronix) by UV exposure (MJB3 contact mask aligner; SUSS MicroTec) through a photolithography mask (Selba SA) and subsequent development (SU-8 developer; MicroChem Corp.). Su-8 2015 was used to obtain a thickness of 21μm, the mould was pre-baked for 1min at 65°C and after UV exposure (Exposure Energy: 150 mJ/CM2, Exposure Time: 21sec), the mould was post-baked for 3min at 95°C. A curing agent (Sylgard 184 silicone elastomer kit; Dow Corning Corporation) was added to the PDMS base to a final concentration of 10% (w/w), mixed and poured over the mould to a depth of 5 mm. Following degassing for several minutes and cross-linking at 65 °C for several hours, the PDMS was peeled off the mould and the input and output ports were punched with a 0.75 mm-diameter Harris Uni-Core biopsy punch (Electron Microscopy Sciences). Particles of PDMS were cleared from the ports using pressurised nitrogen gas. The structured side of the PDMS slab was bonded to a 76 × 26 × 1 mm glass microscope slide (Paul Marienfeld GmbH & Co. KG) by exposing both parts to an oxygen plasma (PlasmaPrep 2 plasma oven; GaLa Instrumente GmbH, Power: 19.6%, exposure time: 90sec) and pressing them together. Finally, an additional hydrophobic surface coating was applied to the microfluidic channel walls by injecting Aquapel glass treatment (PPG Industries) into the completed device and then purging the liquid with nitrogen gas.

The geometry of the dielectrophoretic sorting module was as described previously (Baret et al., 2009b). Electrodes were included in the microfluidic device as additional

microfluidic channels, which were filled with metal: the device was heated to 85 °C and a 51In/32.5Bi/16.5Sn low-temperature solder (Indium Corporation) was melted inside the electrode channels (Siegel et al., 2007.). Electrical connections with the solder electrodes were made with short pieces of electrical wire (Radiospares) (Baret et al., 2009b).

The sorting module (21 µm depth) was used as follows: droplets were reloaded, spaced-out with fluorinated oil at a flow-focusing junction, and finally sorted at a Y-junction, triggering on droplet fluorescence (Baret et al., 2009b) (see also 2.12).

2.9) Optical setup

The optical setup consisted of an Axiovert 200 inverted microscope (Carl Zeiss SAS) mounted on a vibration-dampening platform (Thorlabs GmbH). A 20 mW, 488 nm solid-state laser (LAS; Newport-Spectraphysics) was mounted on the platform *via* a heatsink (Newport-Spectraphysics) (Figure 18). The laser beam was shaped into a ~10 × ~150 µm line by a combination of a 25 mm-diameter cylindrical lens (effective focal length: −50 mm; Thorlabs GmbH) and a 25 mm-diameter plano-convex lens (effective focal length: 25 mm; Thorlabs GmbH) with a 5 cm distance between them (LL). The shaped beam was guided to the side camera port of the microscope *via* a series of periscope assemblies (Thorlabs GmbH). Inside the microscope, the laser light was reflected up into a LD Plan Neofluar 40×/0.6 microscope objective (OBJ; Carl Zeiss SAS) and focused across a channel within the microfluidic device (CHIP). A Phantom v4.2 high-speed digital camera (CAM; Vision Research) was mounted on the top camera port of the microscope to capture digital images during droplet production and sorting. A 488 nm notch filter (F1; Semrock Inc.) positioned in front of the camera protected the camera sensor from reflected laser light. Light emitted from fluorescing droplets was captured by the objective and channeled back along the path of the laser into the system of periscope assemblies. The emitted light was separated from the laser beam by a 488/532/638 nm-wavelength transmitting dichroic beam splitter (DBS; Semrock Inc.), passed through a 510 nm bandpass filter (F2; 20 nm bandwidth; Semrock Inc.) and collected in an H5784-20 photomultiplier tube (PMT; Hamamatsu Photonics KK). Data acquisition (DAQ) and control was performed by a PCI-7831R Multifunction Intelligent DAQ card (National Instruments Corporation) executing a program written

in LabView 8.2 (National Instruments Corporation). The data acquisition rate for the system was 100 kHz. To sort a particular droplet, the DAQ card provided a signal to a Model 623B high-voltage amplifier (Trek Inc.), connected to the electrodes of the microfluidic device. Liquids were pumped into the microfluidic device using standard-pressure infusion-only PHD 22/2000 syringe pumps (Harvard Apparatus Inc.). Syringes were connected to the microfluidic device using 0.6 × 25 mm Neolus needles (Terumo Corporation) and PTFE tubing with an internal diameter of 0.56 mm and an external diameter of 1.07 mm (Fisher Bioblock Scientific) (Baret et al., 2009b).

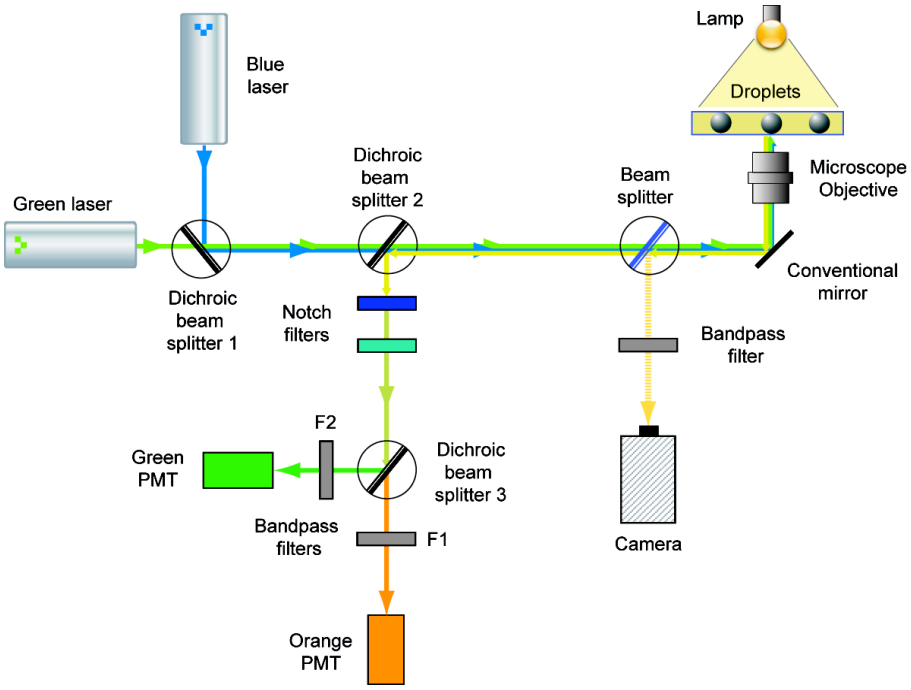

Figure 18. Optical setup (Baret et al., 2009b).

2.10) Synthesis of surfactants for the stabilisation of microdroplets

The synthesis of the surfactants is described in detail in Chapter I, 2.2.

2.11) TPA Inhibition experiments

A twin-dropmaker (Figure 23A) was used to produce monodisperse droplets with a volume of 12 picoliters containing active viruses displaying tPA, 1.6 x 10^{-6} M plasminogen (Roche), 10 mg/mL BSA (Sigma) and 5 x 10^{-5} M Z-FR-Rhodamine 110 (Interchim) and the same mixture including plasminogen activator inhibitor type 1 (PAI-1, Genentech) at either 0.5, 1.0, 2.0 or 4.0 µg/mL. The surfactant-stabilised droplets were collected in a reservoir and incubated for 6h at 37°C. Following incubation the emulsion was reinjected into a microfluidic device (Figure 23B) and the fluorescence of each drop was measured as described previously (Baret et al., 2009b). In brief, a 488 nm laser line was used to excite the fluorophores and the emitted light of each droplet was collected with a photomultiplier tube (using a 510 nm ± 10 nm Semrock filter).

2.12) Droplet sorting experiments

Monodisperse droplets with a volume of 12 picoliters containing a mixture of active viruses displaying tPA and inactive viruses displaying NA, 1.6 x 10^{-6} M plasminogen (Roche), 10 mg/mL BSA (Sigma) and 5 x 10^{-5} M Z-FR-Rhodamine110 (Interchim) were generated (Figure 23C). The surfactant-stabilised droplets were collected in a reservoir and incubated for 6h at 37°C. Following incubation the emulsion was reinjected into a microfluidic sorting device (Figure 23D) and sorted by dielectrophoresis at a Y-junction, triggering on droplet fluorescence (Baret et al., 2009b).

2.13) Amplification of viral RNA by RT-PCR

Recovery of viruses from sorted droplets. Subsequent to sorting, droplets were recovered from the collection loop by draining the liquid into a 1.5 mL microcentrifuge tube (Axygen Inc.). To dislodge any droplets remaining in the loop, it was flushed with 50 µL of fluorinated oil (FC40, 3M) and 10 µL Droplet Destabilizer (RainDance Technologies, Lexington, MA, USA). The emulsion was completely broken by vortexing the microcentrifuge tube in a vigorous manner for 30 s. The broken emulsion was then briefly centrifuged (3220 g for 5 s) and the supernatant, containing suspended viral particles, was transferred to a new microcentrifuge tube. The viral RNA was recovered from the viruses (RNeasy Mini Kit, Qiagen) and

subsequently subjected to RT-PCR (Two-step rtPCR & GO kit, MP Biomedicals) using the following primers:
tPA-NA(+), 5'-TCGACCCCGCCTCGATCCTCCCTTTATCCAGCCC-3'; tPA(-), 5'-
CAGGGCCTGCTGGCAGGTGCCCCCGTTAACGGGGGCACCTGCCAGCAGGC CCTG-3'; NA(-), 5'-ACCATTGGGTCAATCTGTATGGGGATCGGAATA-3'. While for the cDNA synthesis only the two reverse primers were used, the final amplification by PCR was performed additionally using a common forward primer (Table 3).

Table 3. PCR conditions

cDNA synthesis	**RTPCR (samples were kept on ice)**	**PCR**
1) 10 µL of RNA 1 µM + primer 1 µM – primer 5 µL water DEPC treated 2 µL DTT 100mM 2) 5 min at 70°C 3) 8 µL RTGO mix were added 4) 42°C for 1h 5) 70°C for 15min 6) 80 µL sterile H_2O were added	5 µL of the cDNA mixture 1 µM + primer 1 µM – primer 1 µM – primer 5 µL Taq and go mix H_20 was added up to 30 µL	1) 94°C for 2 min 2) 94°C for 30 sec 3) 50°C for 25 sec 4) 68°C for 30 sec 5) 35 cycles (2 to 4) 6) 68°C for 7 min

All PCR reactions were performed using an MJ Research Tetrad Thermal Cycler.

The amplified DNA was analysed on a 1% agarose gel stained with 50 µg/mL ethidium bromide. DNA samples were mixed with 0.2 volumes 5 x sample buffer (30 % glycerin and 1 % brome phenol blue in 5 x TAE buffer) and applied to the gel. A 100 bp ladder (Novagen) was used as marker. Electrophoresis was then performed at 80 V for approximately 1 hour, subsequently the intensity of the bands was measured at an excitation wavelength of 312 nm using a Kodak Gel Logic 200 Imaging System.

3 RESULTS

3.1) GENERAL SETUP OF THE ASSAY

The goal of this work was the establishment of a novel method suitable for the directed evolution of structurally complex mammalian enzymes under multiple turnover conditions. In general, multiple turnover conditions can be achieved using in vitro compartmentalisation (IVC), a technique in which proteins are translated within aqueous droplets of a water-in-oil emulsion (Tawfik and Griffiths, 1998). Each droplet then serves as an independent reaction vessel, thus allowing the use of soluble substrates and the selection for catalytic activity under multiple turnover conditions. However, as with phage display, this method is not suited for mammalian enzymes like tPA, requiring comprehensive posttranslational modifications. In fact, we observed that in vitro translated tPA is not active, unless translated under reducing conditions with simultaneous dialysis (Figure 19) (Merten et al., unpublished data).

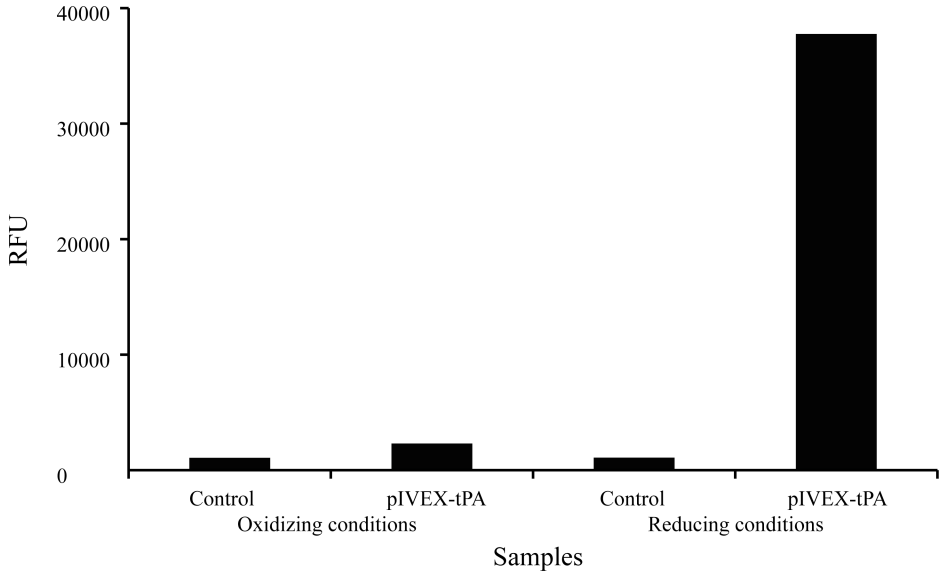

Figure 19. Activity of tPA translated *in vitro* either under oxidising conditions (Roche RTS 100 E. coli HY Kit) or under reducing conditions with simultaneous dialysis (Roche RTS 100 E. coli Disulfide Kit). The open reading frame of tPA was cloned into the *in vitro* translation vector pIVEX.

Subsequently 0.5 µg of the plasmid (pIVEX-tPA) was transcribed and translated for 20h according to the manufacturers instructions. The enzymatic activity was determined by applying 10 µl of each sample to the fluorogenic assay as described in material and methods. Fluorescence values after 45min of incubation are shown. Control = without plasmid.

Obviously, this procedure cannot be performed in aqueous microcompartments, for which reason we chose a different expression system. The murine leukemia virus (MLV) seemed to be perfectly suited since it allows protein expression in a eukaryotic context. To display the protein on the particle surface, we fused it N-terminally to the platelet-derived growth factor receptor transmembrane domain (PDGFR-TM). Earlier studies had shown that the resulting fusion proteins are incorporated highly efficiently into MLV particles (Nikles et al., 2005). Furthermore, displaying the enzyme of interest directly on a non-viral transmembrane domain instead of the viral envelope protein rendered it resistant to shedding during particle concentration (the viral envelope protein consists of two non-covalently linked subunits partially dissociating during ultracentrifugation, see General Introduction, 2.1) (Yu and Wong, 1992). To guarantee the coupling of genotype and phenotype, an MLV-packagable vector was used for the expression of the fusion protein. Consequently, MLV particles displaying tPA on their surface and having packaged the encoding vector were obtained (MLV-tPA) (Figure 20). For control purposes, we also generated particles displaying a non-related control enzyme (neuraminidase) and having packaged a distinguishable genetic marker (MLV-NA).

3.2) Coupling tPA activity with a fluorescence signal

In the next step, we focused on coupling a fluorescence signal with catalytic activity. The reaction catalysed by tPA is the cleavage of inactive plasminogen into active plasmin. Hence tPA activity can be monitored by either using a fluorescent tPA substrate, or by using a fluorescent substrate for plasmin (Figure 20). This latter approach seemed to be preferable, since it allows screening using the physiological tPA substrate.

Plasmin substrates belonging to two different fluorophore families were tested: Z-FR-Rhodamine 110 and HDVLK-Aminocoumarin (HDVLK-AMC). MLV-tPA particles generated a ten-fold stronger fluorescence signal when HDVLK-AMC was used (Figure 21). However, microfluidic experiments with this substrate proved to be very

challenging due to the leakage of the product out of the microdroplets (see CHAPTER I for details). Therefore we decided to use Z-FR-Rhodamine110 for all experiments in microdroplets.

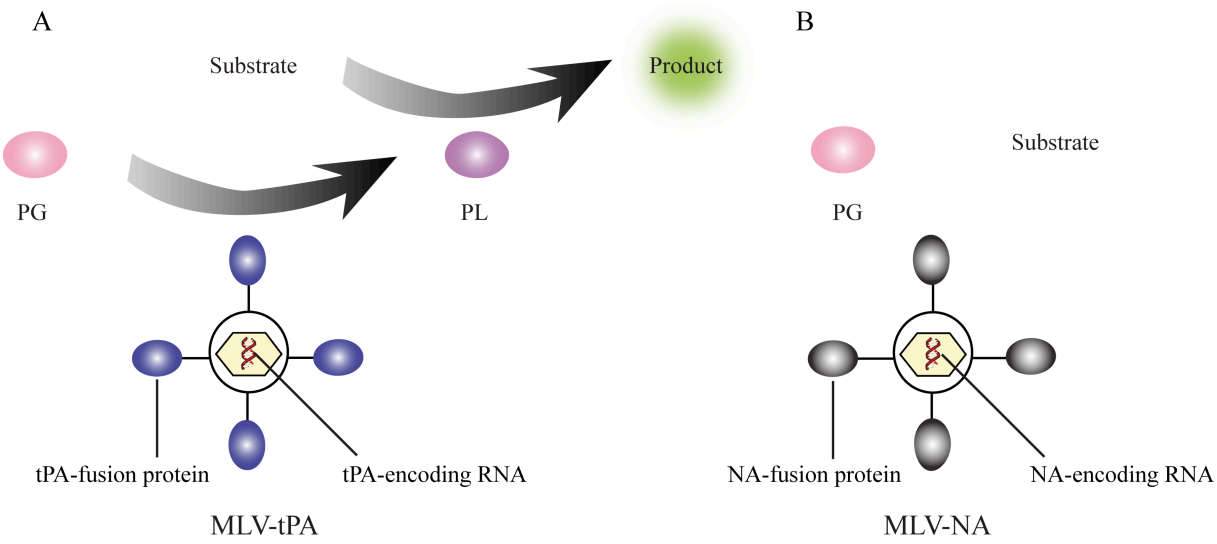

Figure 20. Assay for the enzymatic activity of tPA. The enzyme is displayed on the surface of MLV particles. (A) tPA cleaves plasminogen (PG) into active plasmin (PL), which in turn converts a non-fluorescent substrate into a fluorescent product. (B) Particles displaying NA do not generate a fluorescence signal since NA does not cleave plasminogen into plasmin.

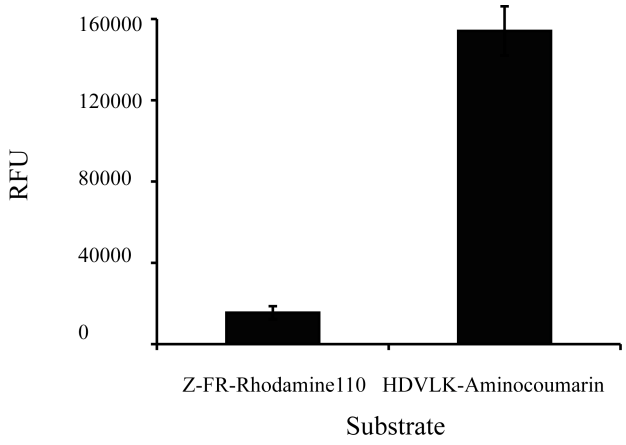

Figure 21. Comparison of two different plasmin substrates. Viral particles displaying tPA were incubated with plasminogen, and Z-FR-Rhodamine 110 (Interchim) or HDVLK-Aminocoumarin (HDVLK-AMC) (Bachem) for 6h at 37°C. Subsequently the fluorescence at 521 nm (Rodamine 110) or 450 nm (Aminocoumarin) was determined in a plate reader.

Bulk experiments (using a plate reader) confirmed that MLV-tPA particles generated a strong fluorescence signal using this assay. In contrast, the MLV-NA particles produced a very low background signal, thus confirming the specific monitoring of tPA activity (Figure 21). Noteworthy, when whole cells were used in the assay (instead of purified MLV particles), the generation of a significant fluorescence signal did not depend on the expression of tPA. Probably due to unspecific conversion of the substrate by other cellular enzymes, even wild-type HEK293T cells showed a significant fluorescence signal (Figure 22). This suggests that in vitro selection systems (such as phage- or retrovirus display) might be better suited for enzyme evolution than their in vivo counterparts based on cell-surface display.

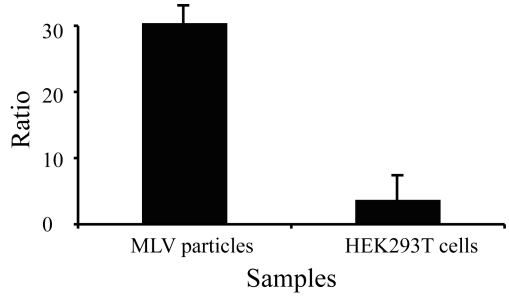

Figure 22. Signal to background ratios of retroviral particles and whole cells in the tPA fluorescence assay. HEK293T cells or MLV particles displaying either active tPA or an inactive control enzyme (NA) were mixed with the assay components. After an incubation time sufficient to generate a fluorescence signal of 5000 RFU in the active samples, the fluorescence of the inactive sample was determined and used to calculate the signal to background ratio.

3.3) Encapsulation of viral particles and inhibition experiments

As the next step, we used a microfluidic device (Figure 23A) to encapsulate the MLV-tPA particles together with all assay components into aqueous droplets (volume = 12 pL) of a water-in-oil emulsion.

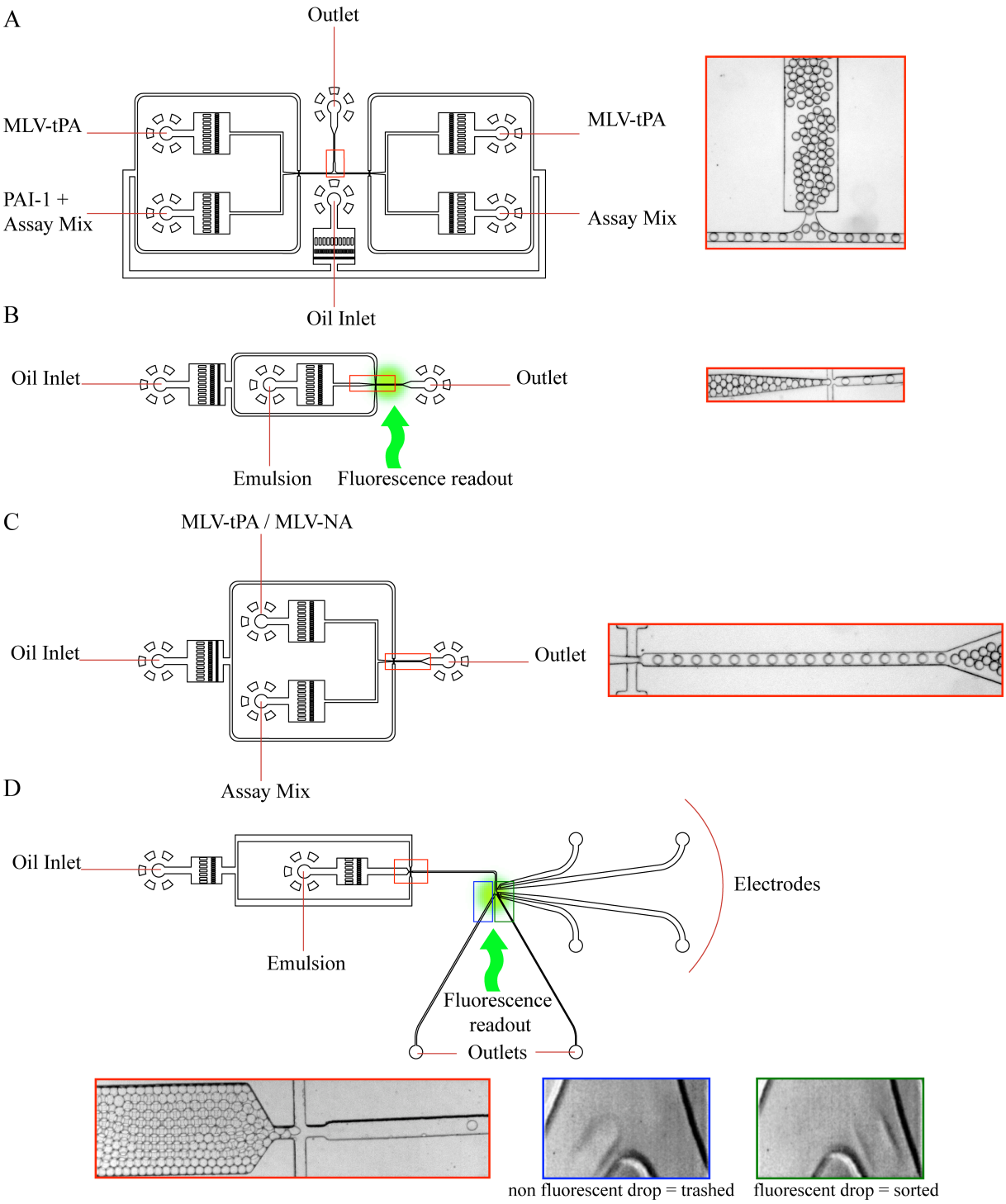

Figure 23. Microfluidic devices. (A) Twin drop maker for the generation of emulsions with two different droplet species (± inhibitors). (B) Reinjection device for fluorescence measurements. (C) Drop maker for the encapsulation of particle mixtures. (D) Sorting device. The geometry of the sorting module was as described previously (Baret et al., 2009b). Green spots indicate the focus of the laser beam for the fluorescence measurements. Colored rectangles indicate the sections shown in the microscopic images.

This step was performed in presence of different concentrations of the endogenous inhibitor PAI-1 (0.5 – 4 µg/mL). As an internal reference, we spiked each emulsion additionally with droplets containing no inhibitor (produced by the second drop maker on the device; Figure 23A). The resulting emulsions were collected off-chip and incubated for 6h at 37°C.

This incubation time turned out to be an optimal balance between signal intensity and product leakage. While shorter incubation times resulted in lower fluorescence intensities, longer incubation times mediated product leakage and thus lower signal to noise values (Figure 24).

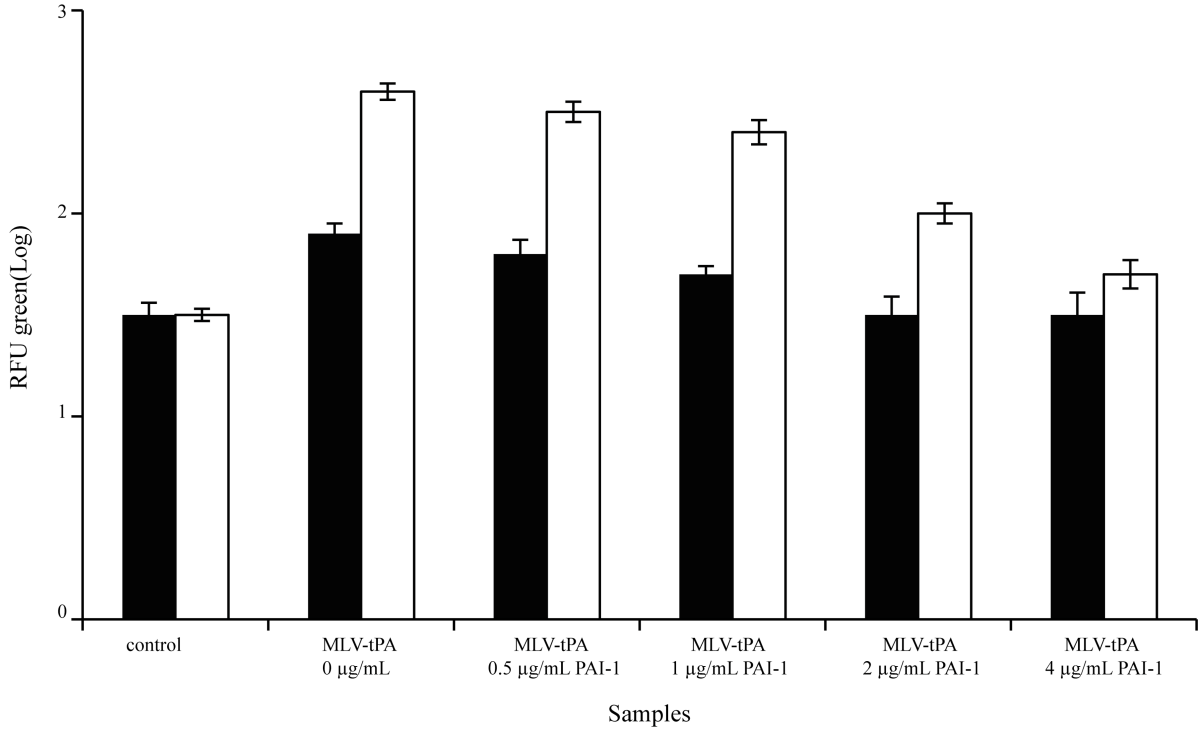

Figure 24. Fluorescence signals in presence and absence of different concentrations of PAI-1. The droplets contained MLV-tPA particles without the endogenous inhibitor PAI-1, MLV-tPA particles in the presence of PAI-1 at the indicated concentrations (µg/mL) and a control sample without MLV-tPA. The fluorescence of each sample was measured after 3h (black bars) and 6h (white bars) of incubation.

After incubation we reinjected the emulsions into a readout module (Figure 23B). A laser beam was focused onto the channels and the epifluorescence of each drop was recorded (processing 500 samples per second). As expected, after 6h of incubation we obtained three different populations in terms of the fluorescence intensity for each emulsion: The population with the lowest fluorescence intensity corresponding to

droplets that do not host any MLV-tPA particle (to avoid multiple particles per drop on average only 1 particle per 3 drops was encapsulated), the population with an intermediate intensity corresponding to drops hosting an MLV-tPA particle in presence of the inhibitor and the population with the strongest intensity corresponding to drops hosting an MLV-tPA particle in absence of any inhibitor (additional drops from the second drop maker). Having a defined positive and negative population for each emulsion allowed the fluorescence data of all samples to be normalised, thus enabling quantitative analysis of inhibition. As expected, increasing concentrations of PAI-1 resulted in decreasing fluorescence signals (Figure 25).

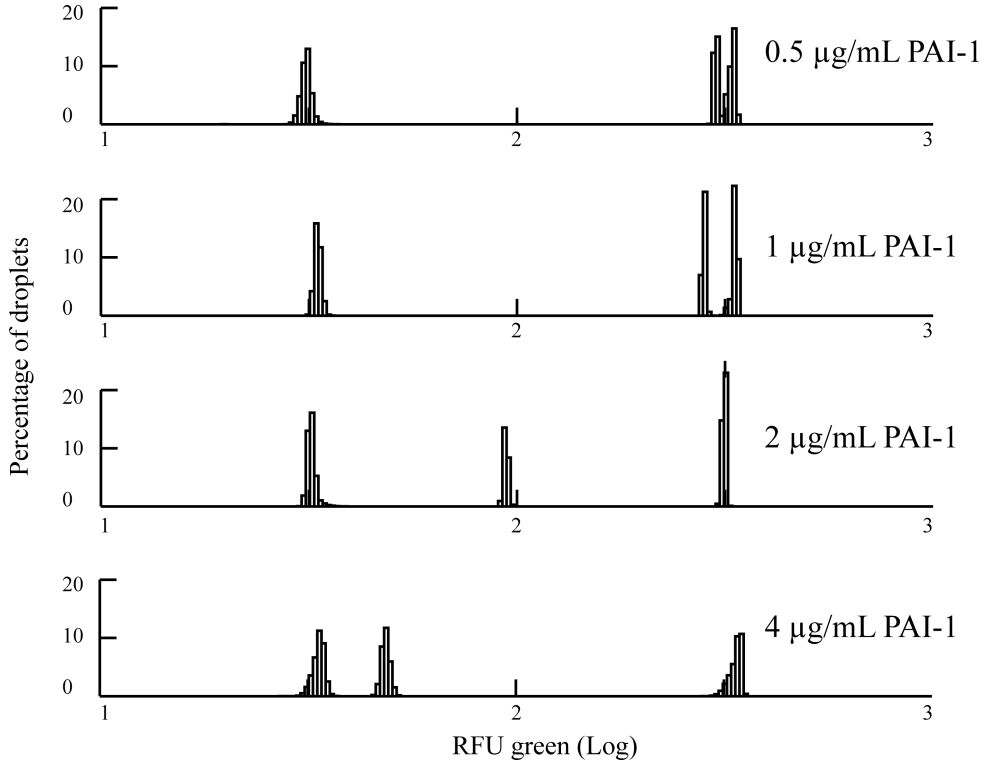

Figure 25. Fluorescence signals of droplets containing MLV-tPA particles in the presence of different concentrations of the endogenous inhibitor PAI-1 (µg/mL). For each inhibitor concentration, three different droplet species were generated: Empty droplets (lowest fluorescence), droplets containing MLV-tPA in presence of the indicated inhibitor concentration (intermediate fluorescence) and droplets containing MLV-tPA in absence of any inhibitor (highest fluorescence). All fluorescence signals were normalised in respect to the droplets containing MLV-tPA in the absence of any inhibitor (highest fluorescence). The fluorescence signal (X-axis, logarithmic scale) and the percentage of events (Y-axis) are shown for each inhibitor concentration.

Analysis of the kinetic data (using GraphPad Prism) revealed an IC_{50} of 1.1 µg/ mL which is in good agreement with bulk control experiments performed in a microplate reader revealing an IC_{50} of 2.7 µg/ mL (Figure 26). Furthermore, for all tested inhibitor concentrations, a peak well separated from the positive and negative population was obtained.

This clearly demonstrates that our system is capable of discriminating populations with only small differences in their enzymatic activity.

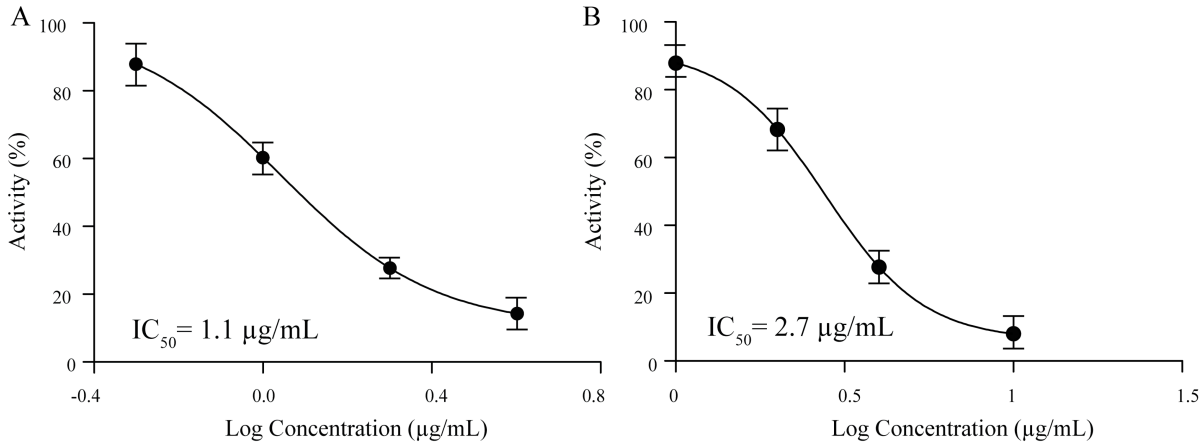

Figure 26. Mean tPA activity (Y-axis) from three independent experiments in dependence of the inhibitor concentration (X-axis) (calculated using the mean activity from each independent experiment). The error bars correspond to the standard deviation of the mean. The IC_{50} concentration was calculated using non-linear regression to fit the four parameter Hill Equation using GraphPad Prism. (A) IC_{50} determined in microfluidic assays. (B) IC_{50} determined in microplate reader assays.

3.4) Encapsulation of viral particles and sorting experiments

In a further experiment we demonstrated the possibility of specifically enriching particles displaying active enzyme variants. For this purpose we generated mixtures of MLV-tPA particles (active) and MLV-NA particles (inactive) in a ratio of 1:100 and 1:1000. Using a microfluidic device (Figure 23C) these particle mixtures were encapsulated together with all assay components at the single particle level (~1 particle per 3 drops). After 6h off-chip incubation at 37°C, the emulsions were reinjected into a microfluidic device designed for dielectrophoretic sorting of droplets (Baret et al., 2009b) (Figure 23D) and the fluorescence intensity of each drop was

determined. For both mixtures, two distinct populations were obtained corresponding to empty droplets or droplets hosting MLV-NA particles (negative population) and droplets hosting MLV-tPA particles (positive population; Figure 27). In both, the 1:100 and 1:1000 mixtures, the percentage of positive drops was very close to that expected (1.3% and 0.3% of all drops, respectively; on average less than 7.5% of the droplets had coalesced) (Figure 27B and C). The sorting gates (red rectangles in Figure 27B and C) were set to include solely high fluorescence, non-coalesced drops (coalesced drops show a higher peak width and can therefore be excluded). The definition of the peak width (the time a fluorescence signal is above a certain threshold) results in highly fluorescent (positive) drops appearing slightly bigger than low fluorescence (negative) drops. However, this phenomenon is well understood and does not interfere with the gating for non-coalesced positive drops (Clausell-Tormos et al., 2008) For both mixtures, approximately 3500 positive droplets were collected.
Based on the genetic markers of the two particle species (MLV-tPA and MLV-NA), we quantitatively determined the sorting efficiency. For this purpose, we took samples of our emulsified particle mixtures (MLV-tPA and MLV-NA in a ratio of 1:100 and 1:1000) before and after sorting, recovered the virally-packaged RNA, amplified it by RT-PCR and analysed it on a gel. While before the sorting step a very strong band corresponding to MLV-NA particles and only a very weak band corresponding to MLV-tPA particles was obtained, the MLV-NA band disappeared almost completely after the sorting step (Figure 27D). In contrast, the MLV-tPA band increased in intensity, thus proving significant enrichment. Quantitative analysis of the relative band intensities (using a Kodak Gel Logic 200 imaging system) revealed enrichment factors of 84-fold (1:100 mixture) and 260-fold (1:1000 mixture) during a single selection round. The higher enrichment observed with the 1:1000 mixture is consistent with the previous observation that the sorter has a very low false postive error rate (<1 in 10^4 droplets). The primary limit for enrichment is therefore the possible co-encapsulation (of different viral particles in this case) in droplets. Following a Poisson distribution, the encapsulation of more than one particle in a drop becomes more and more unlikely with higher dilutions of the particles (Baret et al., 2009b). Hence, higher enrichments are observed when the ratio of postive to negative particles is low. Furthermore, the reduction of the average number of particles per droplet to below 0.3 should allow higher enrichments at the expense of lower throughput (Baret et al., 2009b).

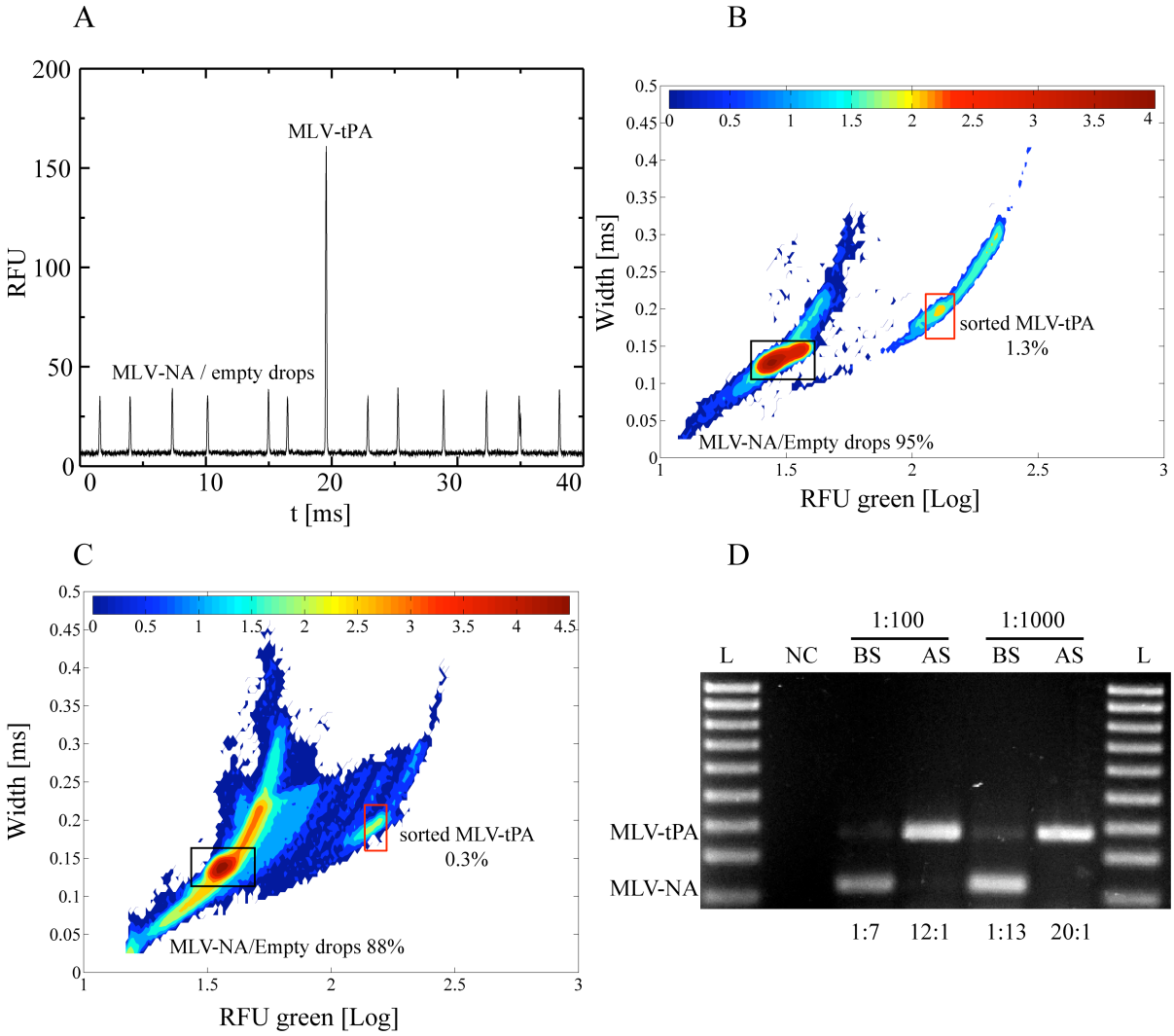

Figure 27. Specific sorting of particles displaying active enzyme variants. MLV-tPA and MLV-NA particles were mixed, encapsulated and subjected to fluorescence activated droplet sorting (FADS). (A) Time sequence (X-axis) and fluorescence (Y-axis) of droplets passing the laser beam (as shown in Figure 2D). Monitoring the droplet width (the time required for each droplet to pass the laser beam) allowed coalesced droplets (showing an increased width) to be excluded from the sort. (B) Sorting of the 1:100 (MLV-tPA:MLV-NA) mixture. The sorting gate (red rectangle) was set to include only droplets with high fluorescence (X-axis, logarithmic scale) and a width (Y-axis) indicating no coalescence. The black rectangle indicates the negative population. The percentage of total droplets in the gates are indicated. The color bar corresponds to the number of droplets on a logarithmic scale. (C) Sorting of the 1:1000 (MLV-tPA:MLV-NA) mixture. (D) Analysis of the sorting efficiency. Genetic markers recovered from the emulsions before (BS) and after the sort (AS) were amplified by RT-PCR and analysed on an agarose gel. The initial particle ratios (top) and the relative band intensities (bottom; as determined with a Kodak Gel Logic 200 imaging system) are indicated. L = size marker (100bp ladder; Novagen).

3.5) Average number of enzyme molecules per particle

The average number of tPA molecules per particle (N_P) was calculated according to the following equation:

$$Np = \frac{\text{number of tPA molecules in a given volume of the virus suspension}}{\text{number of MLV particles in a given volume of the virus suspension}}$$

To solve this equation we first determined the particle titer, based on the data from the microfluidic experiments: Using 12.5 µL of concentrated MLV-tPA particles we generated a total of 6.6×10^7 droplets of which 1/3 were fluorescent positive (hosting a particle). Hence the particle titer equalled:

$$\frac{2.2 \times 10^7 \text{ particles}}{12.5 \times 10^{-3} \text{ mL}} = 1.76 \times 10^9 \text{ particles/mL}$$

Next, we determined the concentration of soluble recombinant tPA (Roche) showing the same enzymatic activity (in bulk experiments) as the concentrated particles. This was the case for a concentration of 2.4×10^{-9} mol/L according to 1.44×10^{12} enzyme molecules per mL (2.4×10^{-6} mol/ mL x 6.022×10^{23} molecules/ mol = 1.44×10^{12} molecules/ mL).

Hence the average number of enzyme molecules per particle is:

$$Np = \frac{1.44 \times 10^{12} \text{ molecules} \times \text{mL}}{1.76 \times 10^9 \text{ particles} \times \text{mL}} = 818$$

Hence our display construct showed incorporation rates similar to that of homologous envelope proteins, of which normally several hundred are present on the particle surface (Bachrach et al., 2000). In contrast, usually no more than 1-5 copies of an enzyme can be displayed on phage particles (Fernandez-Gacio et al., 2003), for which reason the MLV system used here seems to be beneficial.

4 Discussion

We present here a novel approach for ultra-high-throughput screening of displayed enzymes. This method allows the selection of active variants under multiple turnover conditions, including eukaryotic enzymes that require complex posttranslational modifications.

Displaying the enzyme of interest, tPA, on MLV particles not only ensured its expression in a eukaryotic context, but also allowed highly efficient incorporation. Comparing the enzymatic activity of MLV-tPA at a defined particle titer (as determined during the encapsulation experiments) with that of soluble recombinant enzyme leads to the conclusion that on average 818 tPA molecules were displayed on the surface of each virion.

A strong advantage of the MLV system in comparison with cell-based eukaryotic display systems (e.g. yeast cell surface display (Shusta et al., 1999)) is the fact that the enzyme of interest can be screened in absence of cellular enzymes (potentially causing significant background activities). MLV consists of just 8 different proteins, thus minimising the chance for any undesired background activities. Indeed, tPA-negative particles (MLV-NA) mediated only a very low signal in the (bulk) fluorescence assay, whereas tPA-negative cells (HEK293T) generated significant fluorescence (Figure 22).

In contrast to conventional display techniques, the compartmentalisation approach allows screens to be performed under multiple turnover conditions and enables the use of soluble substrates and products. Especially when using microfluidic devices for the generation and sorting of droplets, this approach seems to be extremely powerful. First of all, the droplets generated using microfluidic devices are highly monodisperse, allowing quantitative measurements as demonstrated here (the IC_{50} of the tPA inhibitor PAI-1 measured in droplets and in microtitre plates was almost identical). Second, fluorescence activated droplet sorting (FADS) in microfluidic systems has a very low sorting error rate ($<10^{-4}$) and can be performed at rates of up to two kilohertz (Baret et al., 2009b).

Quantitative enzyme screens can also be performed under multiple turnover conditions in microtiter plates, however time and cost considerations generally limit the number of variants that can be screened to 10^3-10^5: even using sophisticated

robots, it is only possible to process 100,000 assays a day, or ~1 per second, and it is difficult to reduce the assay volume below 1 µL due to problems related to evaporation and capillary forces (Dove, 1999). By contrast, the droplet-based system allows the quantitative analysis of up to 500 samples per second (corresponding to 4.3 x 10^7 samples per day); a throughput over 100-times higher than with microtitre plates.

Chapter III

Using the new membrane-bound form of tPA for the selection of species-specific antibiotics

1 Introduction

Infectious and parasitic diseases are the second most frequent cause of death in the world after cardiovascular diseases. Respiratory infections alone account for 6.5% of all deaths worldwide (The World Health Organisation, 2004). Even in countries with well-developed health systems, the emergence of multiresistant bacterial strains, such as methicillin-resistant *Staphylococcus aureus* (MRSA), is causing major problems. Some reports suggest that in 2005 more people in the USA died from an MRSA infection (18000 victims) than from AIDS (16500 victims) (Bancroft, 2007). Hence, there is a huge demand for novel antibiotics and assay systems allowing the screening of large compound libraries for antimicrobial properties.

Assays for the screening of potential antibiotics can be divided into two main classes: biochemical assays and whole-cell assays. Biochemical assays make use of isolated and purified proteins from the pathogen. However, this strategy requires well-characterised drug targets and may lead to the selection of compounds that do not show any significant activity towards the whole pathogen (rather than the purified target). For example, the selection of compounds that do not penetrate or persist in cells is a significant problem especially since many bacterial strains express so-called drug efflux pumps whose activities on small molecules are difficult to predict (Brown and Wright, 2005).

These limitations can be circumvented using whole-cell assays. In these systems phenotypic changes of the pathogen (e.g. growth arrest) are monitored in response to a drug candidate. In the simplest case, bacterial growth directly results in an easily-

detectable signal. Such signals include changes in absorption, fluorescence, bioluminescence (Bio-Siv) or the release of radioactively-labelled CO_2 (BACTEC) (Arain et al., 1996; De La Fuente et al., 2006; Srivastava et al., 1998; Tarrand and Groschel, 1985). More complex systems that allow conclusions to be drawn about the drug targets involved have also been established. For example, arrays of bacterial strains, each one hypersusceptible to the inhibition of one particular gene, have been generated (DeVito et al., 2002). In addition, assays based on the mass spectrometric analysis of cell lysates have been used to screen compounds for their ability to specifically inhibit a given drug target (Greis et al., 2005). However, these kinds of assays require detailed knowledge of the pathogen and its potential drug targets as well as genetic modifications of the corresponding microorganisms.

One common limitation of both biochemical and whole-cell assays is the potential selection of compounds that harm human cells as well as the pathogens. Even when using purified pathogen-specific drug targets, potential cytotoxic side effects for human cells cannot be ruled out completely. Therefore, a primary screen for hits is usually followed by a secondary screen, which determines the degree of cytotoxicity towards human cells.

We describe here a novel assay system based on the co-cultivation of human cells with the pathogen of interest. In this way, cytotoxic side effects can be directly monitored during the primary screen. Furthermore, the readout signal for the assay is generated by the human cells (rather than the microorganisms), meaning that no genetic modification of the pathogen is necessary. In theory, the assay does not require any detailed knowledge of the pathogen employed, nor its potential drug targets.

2 Materials and methods

2.1) Cells

Reporter cells expressing a membrane-bound and HA-tagged form of tissue plasminogen activator (HEK293T-tPA) were obtained by retroviral transduction of HEK293T cells with MLV (VSV-G) pseudotype particles packaging the encoding vector (Patent WO2006082385). High-expression cells were selected with a fluorescence-activated cell sorter (MoFlo, BD) using goat polyclonal antibodies raised against tissue plasminogen activator (tPA, Abcam).

HEK293T-tPA cells were grown in Dulbecco's modified Eagle's medium (DMEM; GIBCO-BRL) supplemented with 10% (v/v) fetal bovine serum (GIBCO-BRL) and penicillin/streptomycin (10^5 U/L and 100 mg/L, respectively; GIBCO-BRL). Cells were incubated at 37°C in a 5% CO_2 atmosphere saturated with water. *Staphylococcus aureus* (*S. aureus*) was obtained from the American Tissue Culture Collection (ATCC 52156) and grown in DMEM (GIBCO-BRL) supplemented with 10% (v/v) fetal bovine serum (GIBCO-BRL). Bacteria were incubated at 37°C with 230 rpm shaking, except when growing co-cultures.

2.2) In vitro co-cultivation assay

To set up the co-cultures**,** *S. aureus* was grown in DMEM (GIBCO-BRL) supplemented with 10% (v/v) fetal bovine serum (GIBCO-BRL) to an OD_{670} of 0.4 (corresponding to 3×10^7cfu/mL, as determined by plating on agar). Subsequently, the samples were diluted 10^5-fold and 100 µL (~30 bacterial cells) were added to each well of a 96-well plate. In parallel, HEK293T-tPA cells were washed twice with DMEM supplemented with 10% (v/v) fetal bovine serum and seeded into the same wells at a density of 2×10^4 cells/well (determined with a Neubauer counting chamber). Antibiotics were added to the wells to the indicated concentrations. All samples were prepared in triplicate and incubated for 3 days at 37°C under a 5% CO_2 atmosphere saturated with water. For the fluorescence readout HDVLK-AMC (Bachem) and Plasminogen (Roche) were added to a final concentration of 1 mM and 1.67 µM, respectively. All measurements were performed with excitation and

emission wavelengths of 370 nm and 450 nm, respectively, using a Spectramax M5 microplate reader (Molecular Devices).
For control purposes, supernatants of the co-cultures were plated on agar and incubated overnight at 37°C. The next day, surviving colonies were counted manually.

2.3) Antibiotics

Penicillin (Sigma) and streptomycin (Sigma) were diluted with sterile 1× PBS (Euromedex) to a concentration of 10^3 mg/L. For control purposes, sodium azide (Sigma) was diluted with sterile 1× PBS

2.4) Determination of Z-Factors

Z-Factors were calculated using the following equation (Zhang et al., 1999):

$$Z - factor = 1 - \frac{3 \times (\sigma_p - \sigma_n)}{(\mu_p - \mu_n)}$$

where σ is the standard deviation, μ the mean signal, x_p the parameter of the positive control and x_n the parameter of the negative control.

2.5) Determination of the effect of bacterial metabolism on reporter cell survival

One day before starting an assay, HEK293TPA cells were seeded at a density of 2 × 10^4 cells/well into 6-well plates (VWR). In parallel, *S. aureus* was grown at 37°C in DMEM medium (GIBCO-BRL) supplemented with 10% (v/v) fetal bovine serum to high density (72 h of incubation to mimic the conditions on the day of the assay readout). The bacterially-conditioned DMEM was recovered by filtration through a 0.22 μm sterile filter (Millipore) and its sterility was confirmed by plating samples on agar plates. Subsequently, 1 mL was added to each well hosting HEK293T-tPA cells (after removing the primary media from those wells). For control purposes, the pH of the bacterially-conditioned medium was adjusted to 7.7 (by adding 1 M HCl) and/or

glucose was added to a final concentration of 4 x 10^3 mg/L. Fresh DMEM lacking glucose (pH 7.7 and 8) and fresh DMEM supplemented with glucose (pH 8) served as additional controls. Each sample was incubated with HEK293T-tPA cells for 3 days at 37°C under a 5% CO_2 atmosphere and bright-field micrographs were taken daily (using a LEICA DMIRB microscope and a Guppy camera, Allied Vision Technologies). On the third day of incubation the media was removed from the cells and 1 mL of 0.25% (w/v) trypsin (GIBCO-BRL) was added. After detachment the cells were centrifuged at 217 g for 5 min and resuspended in a live/dead staining solution (LIVE/DEAD Viability/Cytotoxicity Kit for animal cells, Invitrogen Kit L-3224). After 1 hour of staining the cells were manually counted using a microscope (Leica DM IRB) with a mercury-vapor lamp. For each sample 1000 cells were counted to determine the fraction of living (green-stained) and dead (red-stained) cells.

3 Results

3.1) General setup of the assay

The first requirement for establishing the novel assay system was the use of human reporter cells continuously generating a fluorescence signal. For this purpose, we chose HEK293T-derived cells constitutively expressing a membrane-bound and HA-tagged form of tissue plasminogen activator (HEK293T-tPA). These cells were originally developed for viral inhibition assays (Patent WO2006082385) and generate a strong fluorescence signal upon the addition of plasminogen and the fluorogenic substrate HDVLK-7-amino-4-methylcoumarin (HDVLK-AMC, Bachem). During this reaction, the membrane-bound tPA converts plasminogen into plasmin, which subsequently releases the 7-amino-4-methylcoumarin group of HDVLK-AMC, resulting in fluorescence (Figure 28A).

The next step was to find a way of competitively co-cultivating these cells with a metabolically-active pathogen. In particular, we wanted to set up a system in which the absence of an antibiotic would result in the reporter cells being outgrown by the pathogen and dying, while remaining alive and generating a strong fluorescence

signal in the presence of an antibiotic (Figure 28B). Using *S. aureus* (ATCC strain 52156) as a model organism, we determined whether reporter cells seeded into the wells of 96-well plates indeed died due to the growth of the pathogen. We inoculated the samples with different amounts of *S. aureus* in the presence and absence of streptomycin (at concentrations of 10^{-3}–10^{4} mg/L) or penicillin (at concentrations of 10–10^{3} mg/L) and performed microscopic analyses during the following days. The biggest difference between the two samples (+/- antibiotics) and the lowest standard deviations were obtained when inoculating each well with ~30 bacterial cells: within 3 days, the absence of an antibiotic resulted in the detachment and fragmentation of the reporter cells and the formation of large bacterial aggregates. In contrast, the addition of the antibiotics inhibited bacterial growth and resulted in viable, proliferating reporter cells.

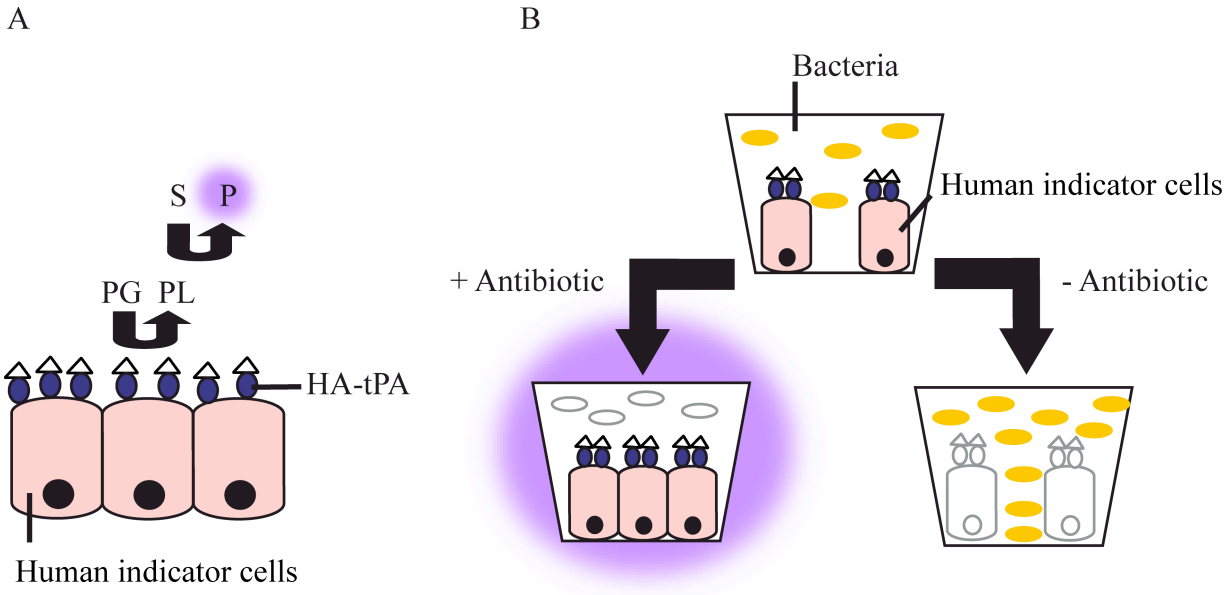

Figure 28. Assay for the selection of species-specific antibiotics. (A) Human reporter cells displaying an HA-tagged and membrane-bound form of tissue plasminogen activator (HA-tPA) on their surface. This enzyme converts plasminogen (PG) into plasmin (PL), which in turn converts a substrate (S) into a fluorescent product (P). (B) Competitive co-cultivation of a metabolically-active pathogen with the human reporter cells. In the absence of an effective antibiotic (-antibiotic), the pathogen outgrows the indicator cells, which finally die due to the lack of nutrition and the accumulation of cytotoxic waste products. Hence, no fluorescence signal is generated. In contrast, the presence of an effective antibiotic (+antibiotic) results in the death of the pathogen and the proliferation of the reporter cells. Consequently, the addition of the assay components yields a strong fluorescence signal.

3.2) Determinants for the viability of the human reporter cells within the co-cultures

To elucidate the mechanism by which the reporter cells were ultimately killed, we performed experiments using sterile, filtered supernatants of *S. aureus* cultures grown in DMEM medium for 72 h (as it is the case for the co-cultivation assay). We incubated human reporter cells with this bacterially-conditioned medium and determined the survival rate by microscopic analysis and a commercially-available live/dead stain (Figure 29A and B). We observed that the death of the reporter cells was not dependent on the presence of viable bacteria. In fact, the reporter cells appeared to have died due to the presence of toxic metabolic products or the lack of nutrition. To test this, we repeated the experiments with additional samples. In particular, we included bacterially-conditioned medium whose pH was adjusted to 7.7 (instead of pH 8 without any treatment), bacterially-conditioned medium supplemented with 4 x 10^3 mg/L glucose and bacterially-conditioned medium with glucose and a pH of 7.7. Adjustment of the pH as well as the addition of glucose to the bacterially-conditioned medium significantly increased the survival rates of the reporter cells (with the addition of glucose having the stronger effect). Performing both modifications at the same time resulted in survival rates almost identical to the control samples with fresh DMEM (>97% viable cells). This indicated that within the co-cultures the reporter cells ultimately died due to the lack of nutrition and changes in the pH.

As further proof for this hypothesis we also performed experiments using fresh (non-bacterially-conditioned) DMEM lacking glucose (pH 7.7 and pH 8) and fresh DMEM supplemented with glucose (pH 8). In agreement with our earlier experiments the lack of glucose and the increase in pH significantly decreased the survival of the reporter cells after 3 days. It is noteworthy that the survival rates matched almost exactly the values obtained for the bacterially-conditioned counterparts (e.g. when comparing the survival rates of glucose-free samples with bacterially-conditioned samples at the same pH). Hence there is clear evidence that the availability of nutrition and the resulting pH are the main determinants for cell survival within the co-cultures.

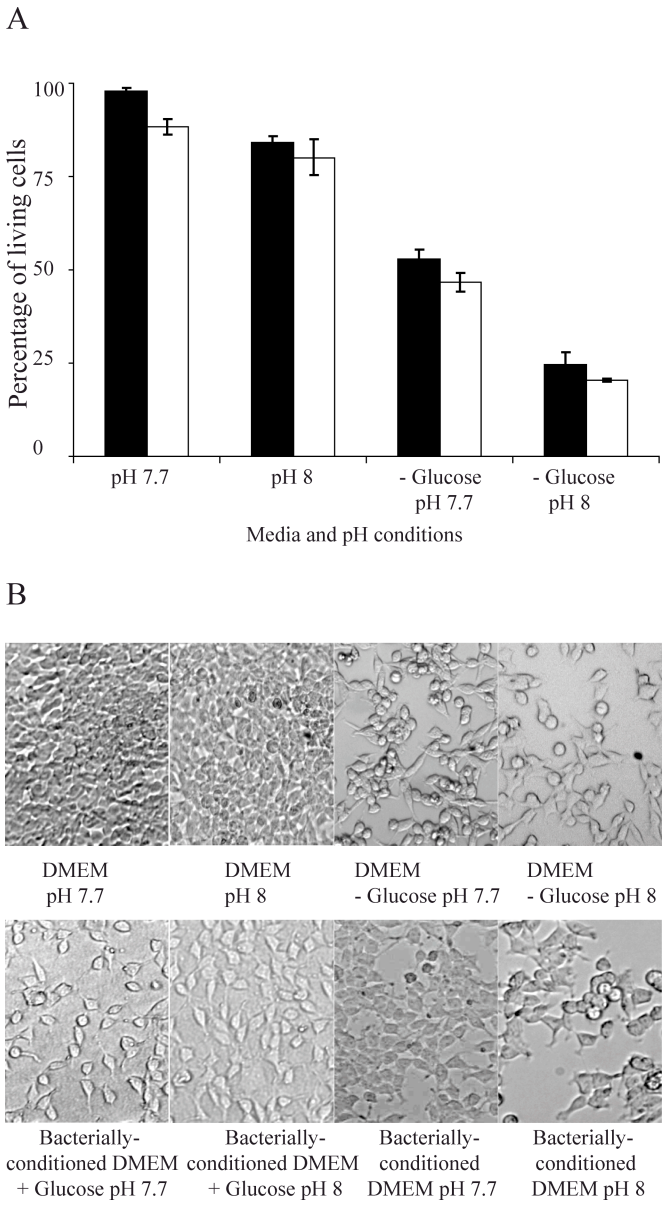

Figure 29. Survival of human reporter cells exposed to bacterially-conditioned DMEM. (A) HEK293T-tPA cells were grown either in fresh DMEM (black bars) or in sterile, bacterially-conditioned DMEM (white bars). For control purposes the pH was modified (by the addition of 1M HCl or 1M NaOH) and/or the glucose concentration was changed (with and without 4 x 10^3 mg/L). Survival rates were determined after 3 days of incubation using a live/dead stain. (B) Microscopic images of the HEK293T-tPA cells after 3 days of incubation.

3.3) Fluorescence signals using streptomycin and sodium azide as model compounds

Next, we focussed on the fluorescence readout of the assay and characterised its suitability for high-throughput screening of drug candidates. In 96-well plates we seeded reporter cells, cultures of *S. aureus* and co-cultures of both species in the presence and absence of streptomycin (an antibiotic active against bacteria) and sodium azide (a compound which kills both species). After 3 days of incubation, we added the components of the fluorescence readout (plasminogen and HDVLK-AMC) and determined the fluorescence signal (Figure 30). While the samples with the reporter cells alone generated a strong fluorescence signal, the *S. aureus* cultures and the co-cultures of both species showed very low background fluorescence (Figure 30A). This changed when adding different concentrations of streptomycin (10^{-3}–10^{4} mg/L): for all concentrations ≥1 mg/L, a significant increase in fluorescence was observed (Figure 30B). A concentration of exactly 1 mg/L resulted in the strongest signal, with an intensity corresponding to that of the positive control (reporter cells without *S. aureus*). Higher concentrations of streptomycin yielded continuously decreasing fluorescence intensities, most likely due to the increasing cytotoxicity. In fact, when incubating the reporter cells with streptomycin in the absence of bacteria we observed decreasing fluorescence intensities for concentrations of the antibiotic $>10^{-1}$ mg/L (Figure 30B). As a further demonstration that our assay system takes cytotoxic effects into account, we analysed the results for the samples containing the highly toxic compound sodium azide (killing both bacterial and human cells). As expected, even very low concentrations (10^{-2}–1 mg/L) of the compound abolished the fluorescence signals of the reporter cells when they were alone as well as when they were co-cultured (Figure 30C). The sodium azide was effective at killing the *S. aureus* (as determined by plating the supernatants on agar; Figure 30C), but its toxicity towards human cells prevented a fluorescence signal being generated.

In summary, these results show that the assay can be used to identify compounds that specifically kill a given pathogen without harming human reporter cells.

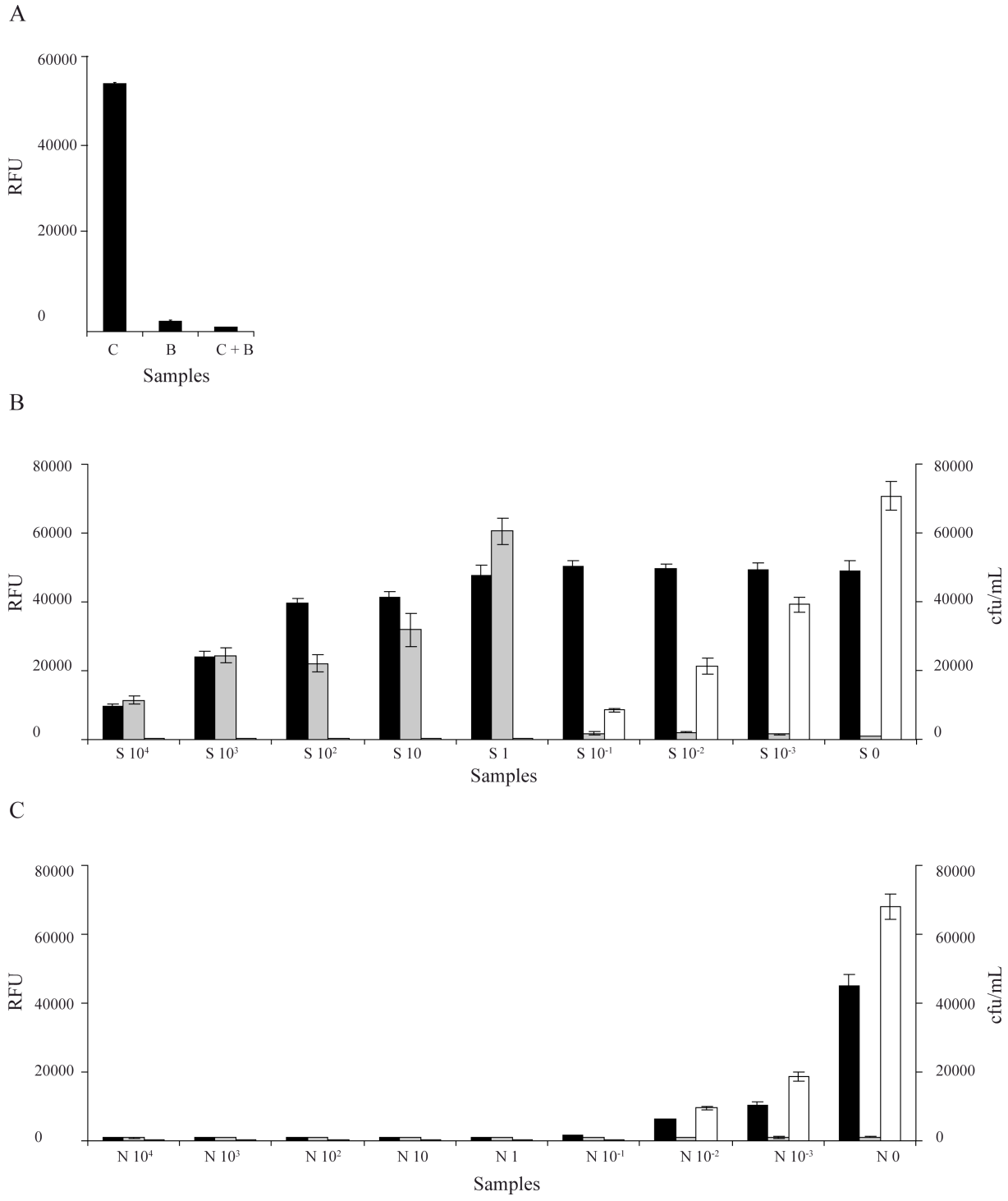

Figure 30. Fluorescence signals of the tPA-based readout system and corresponding bacterial titres. (A) The fluorescence was determined for reporter cells (C), *S. aureus* (B) and co-cultures of both (C+B). (B) and (C) Streptomycin (S) or sodium azide (N) were added at the indicated concentrations (in mg/L). Subsequently, the fluorescence signals (scale according to the Y-axis on the left-hand side) were determined for the co-cultures (grey bars), as well as for the reporter cells alone (black bars). In parallel, the supernatants of the co-cultures were plated on agar and surviving colonies were counted the next day (white bars, scale according to the Y-axis on the right-hand side).

3.4) Correlation between fluorescence signals and growth inhibition of S. aureus

To benchmark our fluorescence readout, we repeated our co-cultivation experiments, and determined the effect of the antibiotic by plating the co-culture supernatants on agar and counting any resulting colonies. In the absence of streptomycin, we determined an increase in the bacterial titer from 105±21 cfu/mL (on addition of the bacterial inoculum to the reporter cells) to 70830±4328 cfu/mL after 3 days. In the presence of streptomycin, however, final bacterial titres were observed to decrease with increasing streptomycin concentrations (Figure 30B). At concentrations of 1 mg/L (the concentration mediating the strongest signal in the fluorescence readout) and above, no surviving colonies were counted. A similar effect was observed when using sodium azide as the antimicrobial agent (Figure 30C). As for streptomycin, increasing concentrations resulted in decreasing bacterial titres. In the absence of the results from the novel fluorescence assay, these results would lead to the false conclusion that sodium azide might be a good antibiotic. Hence, the assay based on the co-cultivation of pathogens with human reporter cells is highly preferable.

3.5) Reliability of the assay

To further characterise the quality of the novel fluorescence assay we determined its Z-factors using the fluorescence values for the co-cultures in the presence (positive control) or absence (negative control) of streptomycin (Table 4). For all concentrations ≥ 1 mg/L, the Z-factor exceeded 0.79 with the best value being 0.95 when using 10 mg/L streptomycin.

Table 4. Z-factors and signal to background ratios for different concentrations of streptomycin.

Concentration of streptomycin (mg/mL)	Z-factor	Signal to background
10^4	0.68	10.25
10^3	0.84	18.76
10^2	0.84	10.10
10	0.95	14.56
1	0.79	25.24
10^{-1}	-3.57	0.93
10^{-2}	-2.00	0.80
10^{-3}	-2.11	0.73

These values mean that the assay clearly fulfils the requirements for being an 'excellent' assay (Zhang et al., 1999). The signal to background values (fluorescence of the positive control divided by the fluorescence of the negative control) for the assayed samples where in the range 0.73–25.24.

As the next step, we determined the reproducibility of the assay by performing two completely independent sets of experiments (Run1 and Run2) on two different days. Each experiment contained triplicates of all samples for which fluorescence was determined (using streptomycin concentrations of 10^{-3}–10^4 mg/L; 54 samples per run). Subsequently, the values obtained for Run1 were plotted against the corresponding values for Run2 (Figure 31). The resulting data points in the dot plot show a linear correlation, demonstrating a high degree of reproducibility for the assay. The fitted trend line has a coefficient of determination (R^2) of 0.881. In parallel, we determined the (mean) relative standard deviation (RSD) between the replicates in one run (intra-comparison) and between the two runs (inter-comparison). The obtained values of 9.41% and 9.91% demonstrate the reliability and robustness of the assay, respectively.

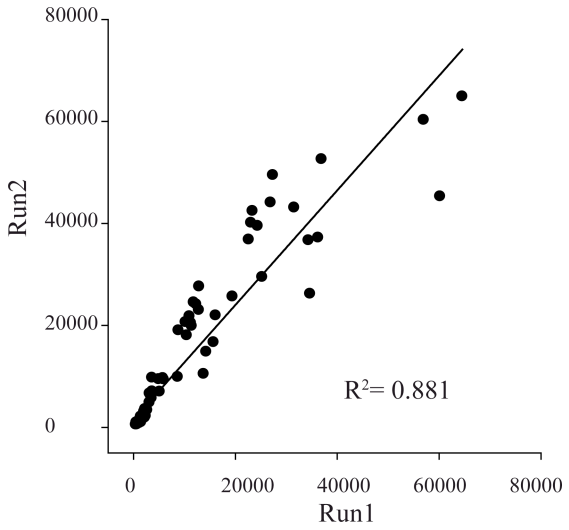

Figure 31. Reproducibility of the co-cultivation assay. Two completely independent sets of experiments were performed on two different days (using the same sample compositions). The fluorescence signals for all samples of Run1 were plotted against the corresponding fluorescence signals of Run2. R^2 = determination coefficient.

We also performed individual experiments using penicillin as a model antibiotic and obtained similar Z-factors (0.81–0.91 when using concentrations of 10–10^3 mg/L). The signal to background values for the assayed samples where in the range 8.89–27.64 (Figure 32 and Table 5).

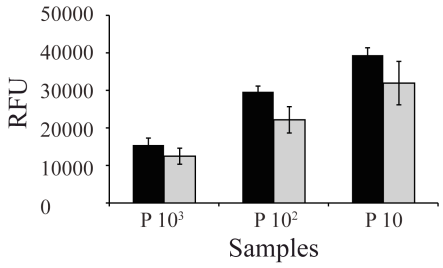

Figure 32. Fluorescence signals of the tPA-based readout system and corresponding bacterial titres. Penicillin (P) was added at the indicated concentrations (in mg/L). Subsequently, the fluorescence signals were determined for the co-cultures (grey bars), as well as for the reporter cells alone (black bars).

Table 5. Z-factors and signal to background ratios for different concentrations of penicillin.

Concentration of penicillin (mg/mL)	Z-factor	Signal to background
10^3	0.89	8.89
10^2	0.81	13.54
10	0.91	27.64

4 Discussion

We have developed a generic fluorescence assay to measure the inhibition of the growth of metabolically-active pathogens. The system is based on the competitive co-cultivation of human reporter cells with the pathogen of interest. Using *S. aureus* as a model organism, we obtained Z-factors of up to 0.95 and a relative standard deviation of 9.41% for all samples within one run and 9.91% when comparing equal samples between two runs. According to our experiments, the minimum concentration of streptomycin required to efficiently inhibit the growth of *S. aureus* is in the range of 0.1 mg/L to 1 mg/L. This is in good agreement with our own plating experiments and other studies that found minimum inhibitory concentrations (MICs) (in liquid medium) of 0.065 mg/L, 0.4 mg/L and 2 mg/L for different strains of *S. aureus* (Zakaria et al., 2007; Zenilman et al., 1986).

Hence, the results obtained with our novel assay are comparable with existing screens that are not based on the co-cultivation of two species. It is noteworthy that we also performed individual experiments using penicillin as a model antibiotic and obtained similar Z-factors (0.81–0.91 when using concentrations of 10–10^3 mg/L). The novel assay is, therefore, both generic and reliable.

The main advantage of the current system is the fact that it allows the identification of specific antibiotics effective against metabolically active pathogens, even if they are not well characterised. It requires neither detailed knowledge about potential drug targets, nor genetic modification of the pathogen (e.g. to establish a reporter system). Using live/dead stains we were able to show that without adding effective antibiotics to the co-cultures, human reporter cells eventually die due to the lack of nutrition and,

to a lesser extent, changes in the pH. This mechanism should, in theory, be adaptable to any metabolically active pathogen.

Even if the pathogen of interest has been well characterised and potential drug targets are known, it seems advantageous to use a reporter system based on human cells. This way, adverse side-effects of the screened compounds are taken into account directly: we have shown here that sodium azide, a toxic compound harming both the pathogen and the human reporter cells, does not yield a positive fluorescence signal. Furthermore, we observed decreasing fluorescence signals for streptomycin concentrations > 1 mg/L. This is likely due to its cytotoxic side effects at high concentrations (as demonstrated in our control experiments). It is well known that exposure to streptomycin affects the viability of human cells and can result in chromosome aberrations and cell death (Kodama et al., 1980; Lemeire et al., 2007).

In summary, the assay system described here allows compounds with non-specific inhibitory properties to be immediately excluded in the primary screen and the determination of the optimal concentration of specific antibiotics. A secondary screen to probe for cytotoxicity against human cells is not required, thus saving time and money. Even though the screening system does not elucidate the mode of action of the screened molecules (e.g. it does not discriminate among compounds which do not penetrate the cell membrane), it might be useful for the identification of novel drug targets. Since the assay is compatible with poorly characterised pathogens, it might also lead to the discovery of compounds that act on previously uncharacterised targets, which could ultimately be identified using labelled or immobilised molecules (Oda et al., 2003).

General Conclusion

This thesis was focused on the development of novel applications of droplet-based microfluidics. Droplet–based microfluidics allow the generation of monodisperse and isolated microvessels at very high rates with great accuracy and control. In a typical experiment, each microvessel corresponds to an aqueous droplet, containing all the reactants for an experiment and is separated from other microdroplets by an immiscible continuous phase. By screening the microdroplets rapidly in microfluidic systems, e.g. by performing a fluorescence readout for each individual drop, it is possible to rapidly analyse very high numbers of reactions. These features constitute a very promising platform for combinatorial chemistry, protein evolution and ultra high–throughput screening for drug discovery.

Using droplets as independent microreactors requires no cross-contamination between them. Therefore, it is interesting to use fluorocarbon oil as the continuous phase. Fluorocarbon oils are both hydrophobic and lipophobic, hence they have very low solubility for the biological contents of the aqueous phase. Nonetheless, droplets are prone to coalescence, thus for droplet-based applications surfactants are essential. The surfactants must meet strict requirements: They must stabilise the droplets to prevent coalescence, they must be biocompatible and finally they must prevent mass transfer between droplets.

Surfactants to stabilise water-in-fluorocarbon emulsions are scarce. Therefore, we synthesised a variety of novel perfluorinated surfactants and analysed the stability of microfluidically-produced droplets, the biocompatibility of the surfactants in biological assays and the leakage of drop contents into neighbouring droplets. All the produced surfactants efficiently stabilised the droplets and all of them were biocompatible. Leaking into the oil phase was observed and was shown to be mostly dependant on the nature of the drop contents. Rhodamine 110 was retained more efficiently than 7-amino-4-methylcoumarine (AMC) because of its hydrophilicity. However, AMC substrates are most sensitive and convenient (in bulk assays) among many synthetic substrates used for fluorescence assays. Due to the low solubility of

the AMC moiety in water, an organic solvent such as dimethyl sulfoxide must be added as a cosolvent, which can affect the fluorescence behaviour. In order to overcome these limitations caused by the hydrophobic nature of AMCs, a water-soluble fluorogenic amine could be used, e.g. a 7-aminocoumarin-4-methane-sulfonic acid based substrate (ACMS) (Sato et al., 1988). In recent studies, it was shown that substituent groups like methyl can increase the transport of droplet contents by diffusion, because it enhances the hydrophobic nature of the molecule (Courtois et al., 2009). The sulfonic acid function linked to the methyl group counterbalances this effect and drastically increases the hydrophilicity of AMC. Hence these modified AMCs could be perfectly suited for droplet-based applications, as our results show that the hydrophilicity of a compound is the key determinant for low mass transfer.

Having synthesised a stabilising and biocompatible surfactant, we developed a novel directed evolution method, based on the microfluidic compartmentalisation of viral particles displaying single protein variants on their membrane. The system allows the monitoring of enzymatic activities of protein variants displayed on the viral particles. Using a mammalian expression system enabled the protein to undergo posttranslational modifications such as disulfide bridging and glycosylation. In contrast to conventional phage display, the compartmentalisation of these viruses into aqueous droplets allowed the use of soluble substrates/products and therefore the selection for multiple turnovers. In particular, we demonstrated the sorting of tissue plasminogen activator (tPA)-displaying and neuraminidase (NA)-displaying viruses according to the enzymatic conversion of a fluorogenic substrate for tPA. For this purpose we generated mixtures of MLV-tPA particles (active) and MLV-NA particles (inactive) in a ratio of 1:100 and 1:1000. We analysed up to 500 samples per second and obtained enrichment factors for the active particles of 84-fold (1:100 mixture) and 260-fold (1:1000 mixture) during a single selection round. Due to the fact that the genotype and phenotype are coupled on viral particles, the system should allow directed evolution of structurally complex mammalian enzymes towards specific catalytic properties. This could, for example, be exploited for the selection of tPA variants with enhanced therapeutic properties.

Since 1982 the FDA approved several genetically engineered tPA variants for use in humans, because of its clinical relevance. tPA is of great commercial interest since it

is one of the most effective drugs for emergency therapy of life threatening pathological thrombi. In 2008, the world wide sales of recombinant tPA comprised about $275 million. A big advantage of tPA in contrast to other fibrinolytic agents is its specific activation by fibrin. Fibrin binds to the finger and kringle 2 domains of tPA and lowers its Michaelis constant (K_M) for plasminogen from 65 µmol/L to 0.16 µmol/L. Therefore thrombi are dissolved locally while systemically circulating plasminogen is much less affected. However, this so called fibrin specificity is not sufficient to completely avoid side effects such as micro bleedings in the brain and the gastrointestinal tract. Furthermore, another limitation of current tPA therapies is the fact that the enzyme is highly sensitive to the endogenous plasminogen activator inhibitor 1 (PAI-1), which unfortunately is present at high concentrations in blood clots (Huber, 2001a, b) (the target site of the drug). Hence relatively high doses must be administered, frequently causing severe side effects such as micro bleedings in the brain or the gastrointestinal tract (Baruah et al., 2006; Wang, 2002). Consequently, further genetic engineering of tPA is required.

The screening system described here could be used for the evolution of PAI-1-resistant tPA variants. Even though less PAI-1-sensitive tPA variants have been described (Werner, 2001), they are still not sufficiently resistant against the endogenous inhibitor. As demonstrated here, assaying tPA activity in presence of PAI-1 should allow the selection of highly resistant variants when starting from a diversified gene library. Furthermore, applying this selection method, it should be possible to screen for tPA activity both in the presence and absence of fibrin, thereby allowing selection for increased fibrin cofactor specificity. The direct result of the selections would be new tPA variants with enhanced therapeutic properties.

In general, our method should be of special interest for the optimisation of mammalian enzymes in clinical use, such as anticoagulants (tPA, Urokinase) (Graham, 2003a; Naff et al., 2000), enzymes in cancer therapy (Pegaspargase, Rasburicase) (Graham, 2003b; Jeha et al., 2005) or enzymes for the treatment of genetic diseases (Pegademase, Alglucerase, Dornase α) (Vellard, 2003).

Another significant advantage of our system over alternative assay formats (e.g. microtiter plates), is the tiny sample volume which gives rise to massively reduced screening costs. When using 12 pL droplets (as demonstrated in Chapter I and II), the assay volumes are decreased approximately 10^6-fold in comparison to microtiter

plates (assuming an assay volume of 10 µL). This means that the consumables costs for screening 10^7 tPA variants is reduced from at least $3,500,000 to only $4.2, a nearly 10^6-fold reduction (Table 6).

Table 6. Comparison of the consumables costs for microtiter plate systems and droplet-based microfluidics, based on the described assay for tPA activity (costs for inhibition experiments are shown in brackets):

	Microtiter plate system	**Droplet-based microfluidics**
Sample volume	10 µL	12 pL
Costs per sample		
Recombinant plasminogen	$0.15	$0.000,000,18
Fluorogenic substrate	$0.30	$0.000,000,36
(PAI-1)	$0.50	$0.000,000,60
Total	$0.95	$0.000,001,12
Costs for 10^7 samples	**$4,500,000 ($8,500,000)**	**$5.20 ($11.20)**

The first step of producing tPA-displaying viruses was the generation of tPA-expressing cells. We observed that the enzymatic activity correlated with the cell viability. In a second project we made use of this effect and developed a competition-based assay for the selection of species-specific antibiotics that do not harm human cells (human cells displaying tPA and bacteria were competitively co-cultivated).

The goal of this project was the development of an assay allowing to monitor cytotoxic effects already during the primary screen. In particular, we wanted to set up a system in which the readout signal correlated with the viability of human cells. Since we observed that the enzymatic activity of tPA-expressing cells correlated with their viability, we decided to exploit this property in a novel assay for the selection of species-specific antibodies.

The system is based on the competitive co-cultivation of human reporter cells displaying tPA with the pathogen of interest. In the absence of an effective antibiotic, the pathogen outgrows the indicator cells, which finally die due to the lack of nutrition and the accumulation of cytotoxic waste products. In contrast, the presence of a specific antibiotic that does not harm human cells results in the death of the pathogen and the proliferation of the reporter cells. Thus, this assay allows

simultaneous monitoring of inhibitory and cytotoxic properties during the primary screen. A further advantage of this system is the fact that it enables the identification of specific antibiotics effective against pathogens, even if they are not well characterised. It requires, neither detailed knowledge about potential drug targets, nor genetic modification of the pathogen (e.g. to establish a reporter system).

In further applications, this method could be used for competitive co-cultivation of human reporter cells displaying tPA with human cancer cells. In the absence of an effective anticancer drug, the cancer cells should outgrow the indicator cells resulting in their death. In contrast, the presence of an effective anticancer drug should result in the death of the cancer cells and the survival of the reporter cells. Hence, this method could lead to the discovery of novel highly specific anticancer drugs.

Résumé de thèse

Technologie des microgouttelettes dans les systèmes microfluidiques et ingénierie de l'activateur plasminogène tissulaire pour des applications biomédicales

Introduction

Depuis 1982 la FDA a approuvé l'utilisation sur des humains, de variants d'activateurs tissulaire du plasminogène (tPA) génétiquement modifiés (http://www.fda.gov/), pour leur importance thérapeutique. Le tPA a un grand intérêt commercial (275 millions de dollars de chiffre d'affaires en 2008) car cette protéase est utilisée comme médicament thrombolytique lors d'infarctus du myocarde ou d'un accident vasculaire cérébral.

Le tPA a un grand avantage, si on le compare à d'autres agents fibrinolytiques, c'est son activation spécifique par la fibrine. La fibrine se lie aux domaines doigt et kringle-2 du tPA et baisse sa constante de Michaelis (K_M) envers le plasminogène de 65 µmol/L à 0.16 µmol/L. Grâce à cette qualité, les caillots de sang sont dissous localement, le plasminogène circulant continuellement dans le sang n'étant pas affecté. Cette spécificité envers la fibrine n'est néanmoins pas suffisante pour éviter certains effets secondaires tels que des microsaignements du cerveau ou du système digestif. En outre, le tPA est très sensible aux inhibiteurs endogènes (PAIs), ceux-ci étant présents dans les thromboses riches en thrombocytes.

C'est la raison pour laquelle des variants de tPA plus performants qui seront moins sensibles aux inhibiteurs endogènes et qui ne causeront plus d'hémorragies doivent être crées. Ces variants de tPA possédant des propriétés optimisées pourront être utilisés pour le traitement de thromboses.

Les différents objectifs de ce travail de thèse étaient de développer un système microfluidique pour la sélection de variants génétiquement modifiés de tPA et de créer un système de criblage à haut débit, basé sur un test fluorogénique du tPA, pour la sélection d'antibiotiques.

1 Une approche microfluidique pour l'évolution dirigée du tPA exprimé sur des rétrovirus

Objectifs: Le développement d'un système microfluidique pour la sélection de variants génétiquement modifiés de tPA présents sur la membrane de particules virales.

1.1) Description du projet

Les principes de l'évolution Darwinienne peuvent être appliqués dans le laboratoire pour créer de nouvelles protéines. Les différents systèmes d'évolution dirigé nécessitent 3 éléments essentiels : Premièrement, une méthode permettant de créer une diversité génétique ; deuxièmement, un moyen efficace permettant de lier le génotype au phénotype ; et troisièmement, une étape de sélection de l'activité biologique.

Les systèmes d'évolution dirigée peuvent être classés en trois sous-classes, la sous-classe dépendant du moyen utilisé pour lier le génotype au phénotype et de la méthode de sélection. Lors de sélections in vivo, le lien entre le génotype et le phénotype et la sélection elle-même ont lieu in vivo, compartimentalisé dans des cellules. Pour les systèmes de sélection partiellement in vivo, le lien entre le génotype et le phénotype est obtenu grâce à une étape in vivo dans les cellules mais l'étape de sélection a lieu in vitro. Le lien entre le génotype et le phénotype et la sélection se passent in vitro dans les systèmes de sélection in vitro. Les méthodes les plus communes pour l'évolution de biomolécules sont : le phage display, le ribosome display, la compartimentation in vitro (IVC) et le SELEX.

Le phage display est une méthode généralement utilisée pour l'évolution dirigée de protéines, elle permet de produire une immense diversité de variants de protéines exprimés sur la membrane de particules virales (diversité de la banque $<10^{12}$) (Smith, 1985). Ces variants de protéines peuvent être sélectionnés soit pour leur affinité de liaison (p.ex. les anticorps) soit pour leur activité catalytique (p.ex. les enzymes). La sélection d'enzymes pour leur activité catalytique requiert néanmoins l'utilisation de substrats et/ou produits immobilisés, ce qui empêche la sélection de protéines sur plusieurs cycles catalytiques.

La compartimentation in vitro (IVC) est une technologie utilisant des émulsions qui miment les compartiments cellulaires in vitro, elle est basée sur l'idée que l'évolution Darwinienne repose sur le lien entre le génotype et le phénotype (Griffiths and Tawfik, 2006; Tawfik and Griffiths, 1998). Chaque compartiment ne contient qu'un seul gène. Lorsque le gène est transcrit et/ou traduit, ses produits (ARNs ou/et protéines) sont emprisonnés avec le gène codant à l'intérieur du compartiment. La conversion non spécifique du substrat en produit par le mélange de traduction et non par l'enzyme peut tout de même se traduire par des bruits de fonds élevés.

En outre, le tPA est une protéine nécessitant des modifications post-traductionnelles (ponts disulfure, glycosylations) pour être active et aucune de ces méthodes ne répond à ces exigences.

Le but de ce projet de thèse était de développer une méthode nous permettant d'outrepasser ces limites : La compartimentation dans des systèmes microfluidiques de particules virales exprimant des variants de protéines uniques sur leur surface (Clausell-Tormos et al., 2008; Whitesides, 2006). L'encapsulation de ces particules dans des gouttes nous a permit d'utiliser des substrats/produits solubles et donc la sélection pour de multiples cycles catalytiques a été possible. L'utilisation d'un système d'expression mammifère a permit aux protéines de subir les modifications post-traductionnelles (ponts disulfure, glycosylations) nécessaires.

1.2) Description des Méthodes utilisées

Le système modèle que nous avons utilisé est basé sur l'utilisation de particules rétrovirales exprimant du tPA (particules actives) et une protéine contrôle non apparentée (neuraminidase, NA, particules inactives). Pour produire ces particules,

nous avons transfecté des cellules HEK293T avec un plasmide codant pour MLV gag/pol et un plasmide codant pour une forme membranaire de tPA ou NA.

Des gouttes monodisperses d'un volume de 12 picolitres contenant un mélange de variants actifs et inactifs, du plasminogène et un substrat fluorescent ont été crées (Figure 1A et B).

Les gouttelettes stabilisées grâce à un tensio-actif (synthétisé préalablement) ont étés collectés dans un réservoir et incubés pendant 24h à 37°C. Après incubation nous avons réinjecté l'émulsion dans une puce microfluidique et nous avons mesuré la fluorescence de chaque goutte avec un tube photomultiplicateur (PMT) lors de son passage à travers une ligne laser de 488 nm (Figure 1C).

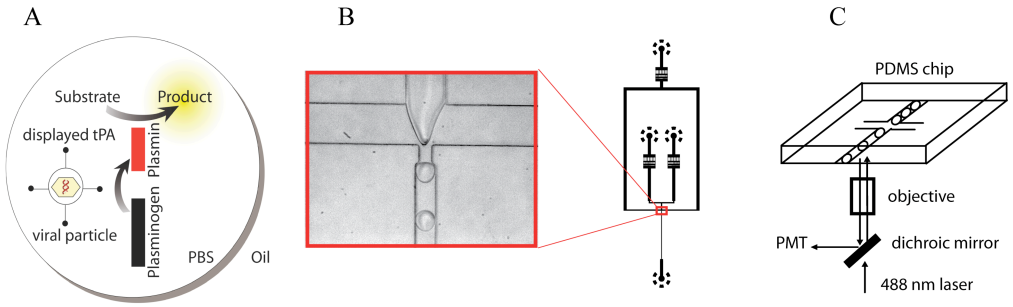

Figure 1. La réaction enzymatique dans une goutte. (A) Le tPA est exprimé sur la membrane de particules virales. Il convertit le plasminogène en plasmine, qui à son tour convertit substrat en produit fluorescent. (B) Une puce microfluidique. Le « Coflow » de deux phases aqueuses et la production de gouttes. (C) Montage optique.

1.3) Résultats et Conclusions

Les virus exprimant le tPA sur leur membrane ont généré un signal fluorescent élevé après addition de plasminogène et le substrat fluorogénique Z-FR-Rhodamine 110 (Z-FR-Rhodamine, Interchim). Lors de cette réaction, le tPA présent à la surface des virus a converti le plasminogène en plasmine, qui à son tour a converti la Z-FR-Rhodamine 110 en Rhodamine 110, résultant en un signal fluorescent.

Les virus exprimant la NA n'ont pas converti le plasminogène en plasmine et donc n'ont pas transformé la Z-FR-Rhodamine 110 en Rhodamine 110. Par conséquent, les gouttes contenant des variants de tPA ont donné un signal fluorescent dix fois

supérieur à celui de gouttes vides ou de gouttes qui contenaient des particules inactives de NA.

Nous avons crée un système permettant de monitorer l'activité enzymatique, de variants de protéines uniques d'une banque, exprimés sur la membrane de particules virales. En plus, nous avons développé uns système nous permettant de trier des virus en utilisant comme critère la présence ou l'absence d'activité enzymatique (Baret et al., 2009b).

2 Sélection d'anticorps spécifiques à une espèce grâce à l'utilisation de la nouvelle forme de tPA exprimée sur la membrane virale.

Objectifs: Le développement d'un système de criblage à haut débit pour la sélection d'antibiotiques spécifiques à une espèce et qui ne nuisent pas aux cellules humaines.

2.1) Description du projet

Pour pouvoir produire des particules virales exprimant du tPA, nous avons d'abord dû créer des cellules mammifères exprimant le tPA. Nous avons observé que nous pouvions corréler la survie cellulaire avec l'activité enzymatique du tPA présent sur la membrane cellulaire. Dans un deuxième projet nous avons utilisé cet effet pour développer un système de sélection d'antibiotiques spécifiques à une espèce et qui ne nuisent pas aux cellules humaines.

Les maladies infectieuses et parasitaires sont la deuxième cause de décès dans le monde après les maladies cardiovasculaires. Les infections respiratoires représentent à elles seules 6,5% de tous les décès dans le monde. Il y a donc une très forte demande pour de nouveaux antibiotiques et des tests permettant le criblage des grandes bibliothèques de composés pour des propriétés antimicrobiennes.

Les tests de criblage pour trouver des antibiotiques peuvent être divisés en deux grandes catégories: les tests biochimiques et les tests sur des cellules entières. Pour les tests biochimiques on utilise généralement des protéines isolées et purifiées de l'agent pathogène. Cependant, cette stratégie nécessite l'utilisation de cibles médicamenteuses bien caractérisées et peut conduire à la sélection de composés qui ne présentent pas d'activité envers l'agent pathogène entier.

Ces limitations peuvent être contournées en utilisant des tests sur des cellules entières. Dans ces systèmes les changements de phénotype du pathogène (p.ex. arrêt de croissance) peuvent être détectés en réponse à un médicament. Dans le cas le plus simple, la croissance bactérienne peut être observée aisément grâce à un signal détectable facilement. Parmi ces signaux on peut compter : des changements dans l'absorption, la fluorescence, bioluminescence (Bio-Siv) ou la libération de CO2 étiqueté radioactivement (Bactec) (Arain et al., 1996; De La Fuente et al., 2006; Srivastava et al., 1998; Tarrand and Groschel, 1985).

Cependant, ces types de tests nécessitent une connaissance détaillée de l'agent pathogène et de ses cibles médicamenteuses potentielles ainsi que les modifications génétiques des micro-organismes correspondants.

Un inconvénient commun des tests biochimiques et cellulaires est la possible sélection de composés qui nuisent aux cellules humaines ainsi qu'aux agents pathogènes. Même en utilisant des cibles médicamenteuses spécifiques pour le pathogène, les éventuels effets secondaires cytotoxiques pour les cellules humaines ne peuvent pas être complètement exclus. Par conséquent, un premier criblage servant à caractériser des molécules aux propriétés nouvelles, biologiquement actives sera habituellement suivi d'un deuxième criblage, qui déterminera le degré de cytotoxicité envers les cellules humaines.

Le but de ce projet était le développement d'un test permettant de contrôler les effets cytotoxiques déjà pendant la première étape de criblage. Nous voulions créer un système dans lequel le signal de lecture pouvait être corrélé avec la viabilité des cellules humaines. Nous avons remarqué que le signal de fluorescence des cellules exprimant le tPA pouvait être corrélé avec la survie des cellules. C'est la raison pour laquelle nous avons décidé d'utiliser la même forme de tPA que nous avons utilisé pour la sélection de variants de tPA (exprimés sur la membrane des particules virales) mais exprimés sur la membrane cellulaire.

2.2) Description des Méthodes utilisées

Nous avons développé un nouveau test basé sur la cocultivation de cellules humaines avec un pathogène métaboliquement actif. *S. aureus* et les cellules générant un signal fluorescent en permanence ont été cocultivées de façon compétitive. Comme le signal de lecture du test était généré par les cellules humaines (au lieu des micro-organismes), aucune modification génétique (pour pouvoir obtenir un signal fluorescent) de l'agent pathogène n'a été nécessaire. Les signaux de fluorescence ont été déterminés en présence et absence d'antibiotiques (pénicilline et streptomycine) et d'un composé toxique pour les deux espèces (de l'azoture de sodium).

L'utilisation d'un système basé sur la détection d'un signal fluorescent généré par des cellules humaines a été avantageux parce que les effets secondaires indésirables (cytotoxicité) des composés criblés ont pu être pris en compte directement. Nous avons choisi des cellules dérivées des HEK293T ce sont de cellules exprimant une forme membranaire et marquée avec l'hémagglutinine de l'activateur tissulaire du plasminogène (HEK293T-tPA). Ces cellules ont été initialement développés pour des tests d'inhibition virale (brevet WO2006082385) et génèrent un signal fluorescent lors de l'addition de plasminogène et du substrat fluorogénique HDVLK-7-amino-4-méthylcoumarine (HDVLK-AMC, Bachem). Au cours de cette réaction, le tPA (exprimé sur la membrane cellulaire) a convertit le plasminogène en plasmine, qui a ensuite libèré le groupement 7-amino-4-méthylcoumarine de HDVLK-AMC et nous avons obtenu un signal fluorescent (Figure 2A).

L'étape suivante consistait à trouver un moyen pour cocultiver de façon compétitive les cellules avec un agent pathogène métaboliquement actif. Nous voulions mettre en place un système dans lequel l'absence d'un antibiotique se traduirait par la mort cellulaire due à la croissance excessive de l'agent pathogène, et en présence d'un antibiotique les cellules resteraient en vie générant un fort signal fluorescent (Figure 2B).

En utilisant *S. aureus* (souche ATCC 52156) comme organisme modèle, nous avons déterminé si les cellules distribuées dans des plaques de 96 puits mourraient à cause de la croissance de l'agent pathogène. Nous avons inoculé des échantillons avec des quantités différentes de *S. aureus* en présence et en absence de la streptomycine (à des concentrations de 10^{-3}-10^{4} mg/L) et nous avons effectué des analyses microscopiques au cours des jours suivants.

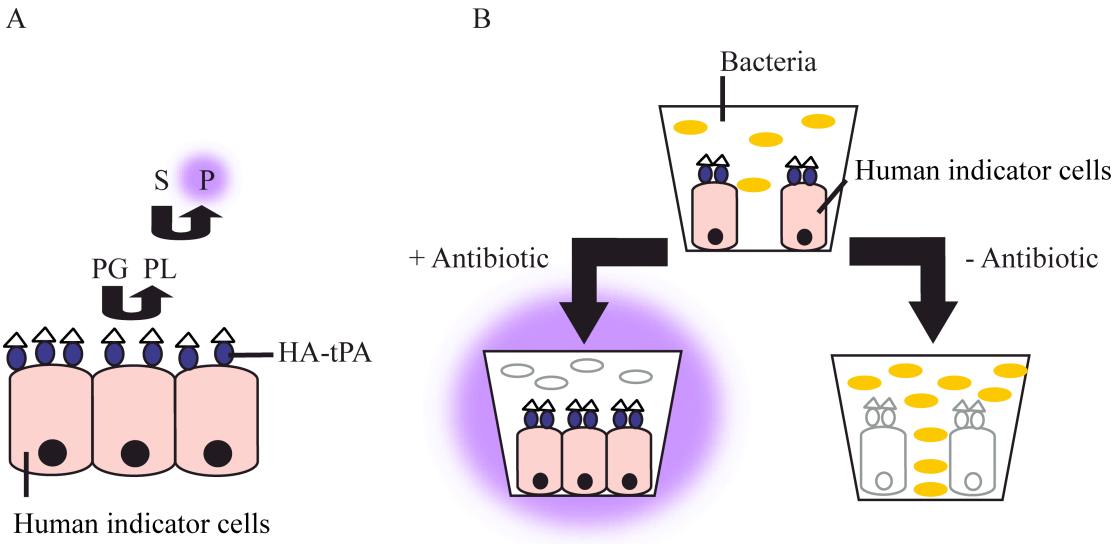

Figure 2. Test pour la sélection d'antibiotiques spécifiques à une espèce. (A) Cellules humaines exprimant une forme membranaire et marquée avec l'hémagglutinine de l'activateur tissulaire du plasminogène (tPA-HA) sur leur surface. Cette enzyme convertit le plasminogène (PG) en plasmine (PL), qui à son tour transforme un substrat (S) en un produit fluorescent (P). (B) Cocultivation de cellules humaines avec un pathogène métaboliquement actif. En l'absence d'un antibiotique efficace (- antibiotique), les cellules meurent à cause de la croissance excessive de l'agent pathogène, du manque de nutriments et de l'accumulation des déchets cytotoxiques. Par conséquent, aucun signal de fluorescence n'est généré. En revanche, la présence d'un antibiotique efficace (+ antibiotique) entraîne la mort de l'agent pathogène et la prolifération cellulaire. En conséquence, l'addition des composants du test produit un fort signal fluorescent.

2.3) Résultats et Conclusions

En l'absence d'un antibiotique efficace nous avons observé la mort cellulaire à cause de la croissance excessive de *S. aureus* et aucun signal fluorescent n'a été généré. Inversement, l'addition de streptomycine a entraîné la croissance des cellules et un signal fluorescent élevé. Lors de l'addition l'azoture de sodium, seul un très faible signal de fond a été obtenu, prouvant sa toxicité. Le test s'est avéré très fiable (facteur Z> 0,9) et nous avons pu corréler des signaux fluorescents élevés avec l'inhibition efficace de *S. aureus*, ces résultats ont aussi étés vérifiés grâce à des tests d'UFC (unité de formation de colonie).

Nous avons développé un test fluorescent nous permettant de mesurer l'inhibition d'agents pathogènes métaboliquement actifs. Le système est basé sur la cocultivation

de cellules humaines exprimant du tPA avec l'agent pathogène d'intérêt. L'avantage principal du système présenté est le fait qu'il permet l'identification d'antibiotiques efficaces contre des agents pathogènes, même s'ils ne sont pas bien caractérisés. Il ne nécessite pas de connaissances précises sur les cibles médicamenteuses, ni la modification génétique de l'agent pathogène (Granieri et al., 2009).

Conclusions et Perspectives

Nous avons développé un nouveau système permettant de monitorer l'activité catalytique de variants individuels d'une enzyme. Le génotype et le phénotype sont liés sur des particules virales, le système devrait donc permettre l'évolution dirigée d'enzymes vers des propriétés catalytiques spécifiques. Contrairement au phage display, le cloisonnement de ces virus dans des gouttelettes aqueuses permet l'utilisation de substrats/produits solubles et donc la sélection sur plusieurs cycles catalytiques.En outre, nous avons développé un système de tri qui permet de trier des variants actifs de tPA à partir d'un mélange de variants actifs et inactifs.

Nous avons créé un test pour la sélection d'antibiotiques spécifiques à une espèce et qui ne nuisent pas aux cellules humaines. Ce test, basé sur un test fluorogénique du tPA, permet de contrôler la cytotoxicité d'un antibiotique déjà pendant la première étape de criblage.

Bibliography

Agresti, J.J., Kelly, B.T., Jaschke, A., and Griffiths, A.D. (2005). Selection of ribozymes that catalyse multiple-turnover Diels-Alder cycloadditions by using in vitro compartmentalization. Proc Natl Acad Sci U S A *102*, 16170-16175.

Aharoni, A., Griffiths, A.D., and Tawfik, D.S. (2005). High-throughput screens and selections of enzyme-encoding genes. Curr Opin Chem Biol *9*, 210-216.

Anna, S.L., Bontoux, N., and Stone, H.A. (2003). Formation of dispersions using "flow focusing" in microchannels. Appl Phys Lett *82*, 364.

Arain, T.M., Resconi, A.E., Hickey, M.J., and Stover, C.K. (1996). Bioluminescence screening in vitro (Bio-Siv) assays for high-volume antimycobacterial drug discovery. Antimicrob Agents Chemother *40*, 1536-1541.

Astrup, T., and Permin, P.M. (1947). Fibrinolysis in the Animal Organism. Nature *159*, 681-682

Bachrach, E., Marin, M., Pelegrin, M., Karavanas, G., and Piechaczyk, M. (2000). Efficient cell infection by Moloney murine leukemia virus-derived particles requires minimal amounts of envelope glycoprotein. J Virol *74*, 8480-8486.

Bancroft, E.A. (2007). Antimicrobial resistance: it's not just for hospitals. JAMA *298*, 1803-1804.

Baret, J.C., Kleinschmidt, F., El Harrak, A., and Griffiths, A.D. (2009a). Kinetic aspects of emulsion stabilization by surfactants: a microfluidic analysis. Langmuir *25*, 6088-6093.

Baret, J.C., Miller, O.J., Taly, V., Ryckelynck, M., El-Harrak, A., Frenz, L., Rick, C., Samuels, M.L., Hutchison, J.B., Agresti, J.J*., et al.* (2009b). Fluorescence-activated droplet sorting (FADS): efficient microfluidic cell sorting based on enzymatic activity. Lab Chip *9*, 1850-1858.

Baruah, D.B., Dash, R.N., Chaudhari, M.R., and Kadam, S.S. (2006). Plasminogen activators: a comparison. Vascul Pharmacol *44*, 1-9.

Beck, Z.Q., Hervio, L., Dawson, P.E., Elder, J.H., and Madison, E.L. (2000). Identification of efficiently cleaved substrates for HIV-1 protease using a phage display library and use in inhibitor development. Virology *274*, 391-401.

Bennett, W.F., Paoni, N.F., Keyt, B.A., Botstein, D., Jones, A.J., Presta, L., Wurm, F.M., and Zoller, M.J. (1991). High resolution analysis of functional determinants on human tissue-type plasminogen activator. J Biol Chem *266*, 5191-5201.

Bernath, K., Magdassi, S., and Tawfik, D.S. (2005). Directed evolution of protein inhibitors of DNA-nucleases by in vitro compartmentalization (IVC) and nano-droplet delivery. J Mol Biol *345*, 1015-1026.

Bertschinger, J., and Neri, D. (2004). Covalent DNA display as a novel tool for directed evolution of proteins in vitro. Protein Eng Des Sel *17*, 699-707.

Bibette, J., Morse, D.C., Witten, T.A., and Weitz, D.A. (1992). Stability criteria for emulsions. Phys Rev Lett *69*, 2439-2442.

Binz, H.K., Stumpp, M.T., Forrer, P., Amstutz, P., and Pluckthun, A. (2003). Designing repeat proteins: well-expressed, soluble and stable proteins from combinatorial libraries of consensus ankyrin repeat proteins. J Mol Biol *332*, 489-503.

Blackburn, M., Data, A., Denham, H., and Wentworth, J.P. (1998). Catalytic antibodies. Adv Phys Org Chem *3*, 249.

Bode, W., and Renatus, M. (1997). Tissue-type plasminogen activator: variants and crystal/solution structures demarcate structural determinants of function. Curr Opin Struct Biol *7*, 865-872.

Boder, E.T., and Wittrup, K.D. (1997). Yeast surface display for screening combinatorial polypeptide libraries. Nat Biotechnol *15*, 553-557.

Brinkmann, U., Chowdhury, P.S., Roscoe, D.M., and Pastan, I. (1995). Phage display of disulfide-stabilized Fv fragments. J Immunol Methods *182*, 41-50.

Brown, E.D., and Wright, G.D. (2005). New targets and screening approaches in antimicrobial drug discovery. Chem Rev *105*, 759-774.

Buchholz, C.J., Duerner, L.J., Funke, S., and Schneider, I.C. (2008). Retroviral display and high throughput screening. Comb Chem High Throughput Screen *11*, 99-110.

Buchholz, C.J., Peng, K.W., Morling, F.J., Zhang, J., Cosset, F.L., and Russell, S.J. (1998). In vivo selection of protease cleavage sites from retrovirus display libraries. Nat Biotechnol *16*, 951-954.

Burbaum, J.J. (1998). Miniaturization technologiesin HTS: how fast, how small,how soon? Drug discovery today *3*, 313-322.

Cantin, R., Methot, S., and Tremblay, M.J. (2005). Plunder and stowaways: incorporation of cellular proteins by enveloped viruses. J Virol *79*, 6577-6587.

Cheng, J., Chen, J.F., Zhao, M., Luo, Q., Wen, L.X., and Papadopoulos, K.D. (2007). Transport of ions through the oil phase of W(1)/O/W(2) double emulsions. J Colloid Interface Sci *305*, 175-182.

Clausell-Tormos, J., Lieber, D., Baret, J.C., El-Harrak, A., Miller, O.J., Frenz, L., Blouwolff, J., Humphry, K.J., Koster, S., Duan, H.*, et al.* (2008). Droplet-based microfluidic platforms for the encapsulation and screening of Mammalian cells and multicellular organisms. Chem Biol *15*, 427-437.

Coffin, J.M., Hughes, S.H., and Varmus, H.E. (1997). Retroviruses, CSHL Press.

Collen, D., and Lijnen, H.R. (1984). New approaches to thrombolytic therapy. Arteriosclerosis *4*, 579-585.

Corey, M.J., and Corey, E. (1996). On the failure of de novo-designed peptides as biocatalysts. Proc Natl Acad Sci U S A *93*, 11428-11434.

Cosset, F.L., Morling, F.J., Takeuchi, Y., Weiss, R.A., Collins, M.K., and Russell, S.J. (1995). Retroviral retargeting by envelopes expressing an N-terminal binding domain. J Virol *69*, 6314-6322.

Cosset, F.L., and Verhoeyen, E. (2007). Target gene transfer with surface-engineered lentiviral vectors. Gene transfer: delivery and expression of DNA and RNA : a laboratory manual *CSHL Press*, 119-127.

Courtois, F., Olguin, L.F., Whyte, G., Bratton, D., Huck, W.T., Abell, C., and Hollfelder, F. (2008). An integrated device for monitoring time-dependent in vitro expression from single genes in picolitre droplets. Chembiochem *9*, 439-446.

Courtois, F., Olguin, L.F., Whyte, G., Theberge, A.B., Huck, W.T., Hollfelder, F., and Abell, C. (2009). Controlling the retention of small molecules in emulsion microdroplets for use in cell-based assays. Anal Chem *81*, 3008-3016.

De La Fuente, R., Sonawane, N.D., Arumainayagam, D., and Verkman, A.S. (2006). Small molecules with antimicrobial activity against E. coli and P. aeruginosa identified by high-throughput screening. Br J Pharmacol *149*, 551-559.

de Vos, A.M., Ultsch, M.H., Kelley, R.F., Padmanabhan, K., Tulinsky, A., Westbrook, M.L., and Kossiakoff, A.A. (1992). Crystal Structure of the Kringle 2 Domain of Tissue Plasminogen Activator at 2.4 Angström Resolution. Biochemistry *31*, 270-279.

Debye, P. (1949). Light scattering in soap solutions. J Phys Colloid Chem *53*, 1-8.

Demartis, S., Huber, A., Viti, F., Lozzi, L., Giovannoni, L., Neri, P., Winter, G., and Neri, D. (1999). A strategy for the isolation of catalytic activities from repertoires of enzymes displayed on phage. J Mol Biol *286*, 617-633.

Dendukuri, D., Tsoi, K., Hatton, T.A., and Doyle, P.S. (2005). Controlled synthesis of nonspherical microparticles using microfluidics. Langmuir *21*, 2113-2116.

Deng, S.J., MacKenzie, C.R., Sadowska, J., Michniewicz, J., Young, N.M., Bundle, D.R., and Narang, S.A. (1994). Selection of antibody single-chain variable fragments with improved carbohydrate binding by phage display. J Biol Chem *269*, 9533-9538.

DeVito, J.A., Mills, J.A., Liu, V.G., Agarwal, A., Sizemore, C.F., Yao, Z., Stoughton, D.M., Cappiello, M.G., Barbosa, M.D., Foster, L.A.*, et al.* (2002). An array of target-specific screening strains for antibacterial discovery. Nat Biotechnol *20*, 478-483.

Dhahbi, J.M., Kim, H.J., Mote, P.L., Beaver, R.J., and Spindler, S.R. (2004). Temporal linkage between the phenotypic and genomic responses to caloric restriction. Proc Natl Acad Sci U S A *101*, 5524-5529.

Dittrich, P.S., and Manz, A. (2006). Lab-on-a-chip: microfluidics in drug discovery. Nat Rev Drug Discov *5*, 210-218.

Doi, N., Kumadaki, S., Oishi, Y., Matsumura, N., and Yanagawa, H. (2004). In vitro selection of restriction endonucleases by in vitro compartmentalization. Nucleic Acids Res *32*, e95.

Dove, A. (1999). Drug screening--beyond the bottleneck. Nat Biotechnol *17*, 859-863.

Edmonds, W.F., Hillmyer, M.A., and Lodge, T.P. (2007). Synthesis and Self-assembly of Highly Incompatible Polybutadiene Poly(hexafluoropropylene oxide) Diblock Copolymers. Macromolecules *40*, 4917-4923.

Fernandez-Gacio, A., Uguen, M., and Fastrez, J. (2003). Phage display as a tool for the directed evolution of enzymes. Trends Biotechnol *21*, 408-414.

Francisco, J.A., Campbell, R., Iverson, B.L., and Georgiou, G. (1993). Production and fluorescence-activated cell sorting of Escherichia coli expressing a functional antibody fragment on the external surface. Proc Natl Acad Sci U S A *90*, 10444-10448.

Frenz, L., Blank, K., Brouzes, E., and Griffiths, A.D. (2009). Reliable microfluidic on-chip incubation of droplets in delay-lines. Lab Chip *9*, 1344-1348.

Frenz, L., Blouwolff, J., Griffiths, A.D., and Baret, J.C. (2008a). Microfluidic production of droplet pairs. Langmuir *24*, 12073-12076.

Frenz, L., El Harrak, A., Pauly, M., Begin-Colin, S., Griffiths, A.D., and Baret, J.C. (2008b). Droplet-based microreactors for the synthesis of magnetic iron oxide nanoparticles. Angew Chem Int Ed Engl *47*, 6817-6820.

Fujii, I., Fukuyama, S., Iwabuchi, Y., and Tanimura, R. (1998). Evolving catalytic antibodies in a phage-displayed combinatorial library. Nat Biotechnol *16*, 463-467.

Gavrilescu, L.C., and Van Etten, R.A. (2007). Production of replication-defective retrovirus by transient transfection of 293T cells. J Vis Exp, 550.

Gerdts, C.J., Sharoyan, D.E., and Ismagilov, R.F. (2004). A synthetic reaction network: chemical amplification using nonequilibrium autocatalytic reactions coupled in time. J Am Chem Soc *126*, 6327-6331.

Ghadessy, F.J., Ong, J.L., and Holliger, P. (2001). Directed evolution of polymerase function by compartmentalized self-replication. Proc Natl Acad Sci U S A *98*, 4552-4557.

Goff, J. (2007). Fields Virology. Lippincott Williams & Wilkins, Philadelphia, 1971-1839.

Graham, G.D. (2003a). Tissue plasminogen activator for acute ischemic stroke in clinical practice: a meta-analysis of safety data. Stroke *34*, 2847-2850.

Graham, M.L. (2003b). Pegaspargase: a review of clinical studies. Adv Drug Deliv Rev *55*, 1293-1302.

Granieri, L., Miller, O.J., Griffiths, A.D., and Merten, C.A. (2009). A competition-based assay for the screening of species-specific antibiotics. J Antimicrob Chemother *64*, 62-68.

Greis, K.D., Zhou, S., Siehnel, R., Klanke, C., Curnow, A., Howard, J., and Layh-Schmitt, G. (2005). Development and validation of a whole-cell inhibition assay for bacterial methionine aminopeptidase by surface-enhanced laser desorption ionization-time of flight mass spectrometry. Antimicrob Agents Chemother *49*, 3428-3434.

Griffin, W.C. (1949). Classification of Surface-Active Agents by 'HLB' Journal of the Society of Cosmetic Chemists *1* 311.

Griffiths, A.D., and Tawfik, D.S. (2006). Miniaturising the laboratory in emulsion droplets. Trends Biotechnol *24*, 395-402.

Hai, M., Bernath, K., Tawfik, D., and Magdassi, S. (2004). Flow cytometry: a new method to investigate the properties of water-in-oil-in-water emulsions. Langmuir *20*, 2081-2085.

Hai, M., and Magdassi, S. (2004). Investigation on the release of fluorescent markers from w/o/w emulsions by fluorescence-activated cell sorter. J Control Release *96*, 393-402.

Hanes, J., and Pluckthun, A. (1997). In vitro selection and evolution of functional proteins by using ribosome display. Proc Natl Acad Sci U S A *94*, 4937-4942.

Hansson, L.O., Widersten, M., and Mannervik, B. (1997). Mechanism-based phage display selection of active-site mutants of human glutathione transferase A1-1 catalyzing SNAr reactions. Biochemistry *36*, 11252-11260.

Hatakeyama, T., Chen, D.L., and Ismagilov, R.F. (2006). Microgram-scale testing of reaction conditions in solution using nanoliter plugs in microfluidics with detection by MALDI-MS. J Am Chem Soc *128*, 2518-2519.

Holtze, C., Rowat, A.C., Agresti, J.J., Hutchison, J.B., Angile, F.E., Schmitz, C.H., Koster, S., Duan, H., Humphry, K.J., Scanga, R.A.*, et al.* (2008). Biocompatible surfactants for water-in-fluorocarbon emulsions. Lab Chip *8*, 1632-1639.

Hong, J., Edel, J.B., and deMello, A.J. (2009). Micro- and nanofluidic systems for high-throughput biological screening. Drug Discov Today *14*, 134-146.

Huber, K. (2001a). Plasminogen activator inhibitor type-1 (part one): basic mechanisms, regulation, and role for thromboembolic disease. J Thromb Thrombolysis *11*, 183-193.

Huber, K. (2001b). Plasminogen activator inhibitor type-1 (part two): role for failure of thrombolytic therapy. PAI-1 resistance as a potential benefit for new fibrinolytic agents. J Thromb Thrombolysis *11*, 195-202.

Huebner, A., Bratton, D., Whyte, G., Yang, M., Demello, A.J., Abell, C., and Hollfelder, F. (2009). Static microdroplet arrays: a microfluidic device for droplet trapping, incubation and release for enzymatic and cell-based assays. Lab Chip *9*, 692-698.

Jeha, S., Kantarjian, H., Irwin, D., Shen, V., Shenoy, S., Blaney, S., Camitta, B., and Pui, C.H. (2005). Efficacy and safety of rasburicase, a recombinant urate oxidase

(Elitek), in the management of malignancy-associated hyperuricemia in pediatric and adult patients: final results of a multicenter compassionate use trial. Leukemia *19*, 34-38.

Johnston, K.P., Randolph, T., Bright, F., and Howdle, S. (1996). Toxicology of a PFPE Surfactant. Science *272*, 1726.

Jung, S., and Pluckthun, A. (1997). Improving in vivo folding and stability of a single-chain Fv antibody fragment by loop grafting. Protein Eng *10*, 959-966.

Kehoe, J.W., and Kay, B.K. (2005). Filamentous phage display in the new millennium. Chem Rev *105*, 4056-4072.

Khandurina, J., and Guttman, A. (2002). Microchip-based high-throughput screening analysis of combinatorial libraries. Curr Opin Chem Biol *6*, 359-366.

Khare, P.D., Russell, S.J., and Federspiel, M.J. (2003). Avian leukosis virus is a versatile eukaryotic platform for polypeptide display. Virology *315*, 303-312.

Kodama, F., Fukushima, K., and Umeda, M. (1980). Chromosome aberrations induced by clinical medicines. J Toxicol Sci *5*, 141-150.

Koroleva, M.Y., and Yurtov, E.V. (2006). Water mass transfer in W/O emulsions. J Colloid Interface Sci *297*, 778-784.

Koster, S., Angile, F.E., Duan, H., Agresti, J.J., Wintner, A., Schmitz, C., Rowat, A.C., Merten, C.A., Pisignano, D., Griffiths, A.D*., et al.* (2008). Drop-based microfluidic devices for encapsulation of single cells. Lab Chip *8*, 1110-1115.

Lamba, D., Bauer, M., Huber, R., Fischer, S., Rudolph, R., Kohnert, U., and Bode, W. (1996). The 2.3 A crystal structure of the catalytic domain of recombinant two-chain human tissue-type plasminogen activator. J Mol Biol *258*, 117-135.

Lee, J.N., Park, C., and Whitesides, G.M. (2003). Solvent compatibility of poly(dimethylsiloxane)-based microfluidic devices. Anal Chem *75*, 6544-6554.

Lemeire, K., Van Merris, V., and Cortvrindt, R. (2007). The antibiotic streptomycin assessed in a battery of in vitro tests for reproductive toxicology. Toxicol In Vitro *21*, 1348-1353.

Levin, A.M., and Weiss, G.A. (2006). Optimizing the affinity and specificity of proteins with molecular display. Mol Biosyst *2*, 49-57.

Link, D.R., Anna, S.L., Weitz, D.A., and Stone, H.A. (2004). Geometrically mediated breakup of drops in microfluidic devices. Phys Rev Lett *92*, 054503.

Link, D.R., Grasland-Mongrain, E., Duri, A., Sarrazin, F., Cheng, Z., Cristobal, G., Marquez, M., and Weitz, D.A. (2006). Electric control of droplets in microfluidic devices. Angew Chem Int Ed Engl *45*, 2556-2560.

Llevadot, J., Giugliano, R.P., and Antman, E.M. (2001). Bolus fibrinolytic therapy in acute myocardial infarction. JAMA *286*, 442-449.

Madison, E.L., Kobe, A., Gething, M.J., Sambrook, J.F., and Goldsmith, E.J. (1993). Converting tissue plasminogen activator to a zymogen: a regulatory triad of Asp-His-Ser. Science *262*, 419-421.

Maffia, A.M., 3rd, Kariv, I.I., and Oldenburg, K.R. (1999). Miniaturization of a Mammalian Cell-Based Assay: Luciferase Reporter Gene Readout in a 3 Microliter 1536-Well Plate. J Biomol Screen *4*, 137-142.

Mary, P., Studer, V., and Tabeling, P. (2008). Microfluidic droplet-based liquid-liquid extraction. Anal Chem *80*, 2680-2687.

Mastrobattista, E., Taly, V., Chanudet, E., Treacy, P., Kelly, B.T., and Griffiths, A.D. (2005). High-throughput screening of enzyme libraries: in vitro evolution of a beta-galactosidase by fluorescence-activated sorting of double emulsions. Chem Biol *12*, 1291-1300.

Mazutis, L., Baret, J.C., and Griffiths, A.D. (2009). A fast and efficient microfluidic system for highly selective one-to-one droplet fusion. Lab Chip *9*, 2665-2672.

Mere, L., Bennett, T., Coassin, P., England, P., Hamman, B., Rink, T., Zimmerman, S., and Negulescu, P. (1999). Miniaturized FRET assays and microfluidics: key components for ultra-high-throughput screening. Drug Discov Today *4*, 363-369.

Miller, O.J., Bernath, K., Agresti, J.J., Amitai, G., Kelly, B.T., Mastrobattista, E., Taly, V., Magdassi, S., Tawfik, D.S., and Griffiths, A.D. (2006). Directed evolution by in vitro compartmentalization. Nat Methods *3*, 561-570.

Naff, N.J., Carhuapoma, J.R., Williams, M.A., Bhardwaj, A., Ulatowski, J.A., Bederson, J., Bullock, R., Schmutzhard, E., Pfausler, B., Keyl, P.M.*, et al.* (2000). Treatment of intraventricular hemorrhage with urokinase : effects on 30-Day survival. Stroke *31*, 841-847.

Nikles, D., Bach, P., Boller, K., Merten, C.A., Montrasio, F., Heppner, F.L., Aguzzi, A., Cichutek, K., Kalinke, U., and Buchholz, C.J. (2005). Circumventing tolerance to the prion protein (PrP): vaccination with PrP-displaying retrovirus particles induces humoral immune responses against the native form of cellular PrP. J Virol *79*, 4033-4042.

Oda, Y., Owa, T., Sato, T., Boucher, B., Daniels, S., Yamanaka, H., Shinohara, Y., Yokoi, A., Kuromitsu, J., and Nagasu, T. (2003). Quantitative chemical proteomics for identifying candidate drug targets. Anal Chem *75*, 2159-2165.

Ott, D.E. (2008). Cellular proteins detected in HIV-1. Rev Med Virol *18*, 159-175.

Parekh, R.B., Dwek, R.A., Rudd, P.M., Thomas, J.R., Rademacher, T.W., Warren, T., Wun, T.C., Hebert, B., Reitz, B., Palmier, M.*, et al.* (1989). N-glycosylation and in vitro enzymatic activity of human recombinant tissue plasminogen activator expressed in Chinese hamster ovary cells and a murine cell line. Biochemistry *28*, 7670-7679.

Parker, J.A., Markis, J.E., Palla, A., Goldhaber, S.Z., Royal, H.D., Tumeh, S., Kim, D., Rustgi, A.K., Holman, B.L., Kolodny, G.M.*, et al.* (1988). Pulmonary perfusion after rt-PA therapy for acute embolism: early improvement assessed with segmental perfusion scanning. Radiology *166*, 441-445.

Pays, K., Giermanska-Kahn, J., Pouligny, B., Bibette, J., and Leal-Calderon, F. (2002). Double emulsions: how does release occur? J Control Release *79*, 193-205.

Peng, K.W., Vile, R., Cosset, F.L., and Russell, S. (1999). Selective transduction of protease-rich tumors by matrix-metalloproteinase-targeted retroviral vectors. Gene Ther *6*, 1552-1557.

Pennica, D., Holmes, W.E., Kohr, W.J., Harkins, R.N., Vehar, G.A., Ward, C.A., Bennett, W.F., Yelverton, E., Seeburg, P.H., Heyneker, H.L*., et al.* (1983). Cloning and expression of human tissue-type plasminogen activator cDNA in E. coli. Nature *301*, 214-221.

Pereira, D.A., and Williams, J.A. (2007). Origin and evolution of high throughput screening. Br J Pharmacol *152*, 53-61.

Piirma, I. (1992). Polymeric Surfactants. CRC Press, Marcel Dekker.

Qureshi, N. (1996). Tissue plasminogen activator for acute ischemic stroke. N Engl J Med *334*, 1406.

Randow, F., and Sale, J.E. (2006). Retroviral transduction of DT40. Subcell Biochem *40*, 383-386.

Renatus, M., Engh, R.A., Stubbs, M.T., Huber, R., Fischer, S., Kohnert, U., and Bode, W. (1997). Lysine 156 promotes the anomalous proenzyme activity of tPA: X-ray crystal structure of single-chain human tPA. EMBO J *16*, 4797-4805.

Roach, L.S., Song, H., and Ismagilov, R.F. (2005). Controlling nonspecific protein adsorption in a plug-based microfluidic system by controlling interfacial chemistry using fluorous-phase surfactants. Anal Chem *77*, 785-796.

Roberts, R.W., and Szostak, J.W. (1997). RNA-peptide fusions for the in vitro selection of peptides and proteins. Proc Natl Acad Sci U S A *94*, 12297-12302.

Russell, S.J., Hawkins, R.E., and Winter, G. (1993). Retroviral vectors displaying functional antibody fragments. Nucleic Acids Res *21*, 1081-1085.

Sato, E., Matsuhisa, A., Sakashita, M., and Kanaoka, Y. (1988). New water-soluble fluorogenic amine. 7-Aminocoumarin-4-methanesulfonic acid (ACMS) and related substrates for proteinases. Chem Pharm Bull (Tokyo) *36*, 3496-3502.

Schultz, P.G., and Lerner, R.A. (1995). From molecular diversity to catalysis: lessons from the immune system. Science *269*, 1835-1842.

Sepp, A., and Choo, Y. (2005). Cell-free selection of zinc finger DNA-binding proteins using in vitro compartmentalization. J Mol Biol *354*, 212-219.

Sheehan, J.J., and Tsirka, S.E. (2005). Fibrin-modifying serine proteases thrombin, tPA, and plasmin in ischemic stroke: a review. Glia *50*, 340-350.

Shestopalov, I., Tice, J.D., and Ismagilov, R.F. (2004). Multi-step synthesis of nanoparticles performed on millisecond time scale in a microfluidic droplet-based system. Lab Chip *4*, 316-321.

Shi, W., Qin, J., Ye, N., and Lin, B. (2008). Droplet-based microfluidic system for individual Caenorhabditis elegans assay. Lab Chip *8*, 1432-1435.

Shusta, E.V., Kieke, M.C., Parke, E., Kranz, D.M., and Wittrup, K.D. (1999). Yeast polypeptide fusion surface display levels predict thermal stability and soluble secretion efficiency. J Mol Biol *292*, 949-956.

Siegel, A., Bruzewicz, D., Weibel, D., and Whitesides, G. (2007.). Microsolidics: Fabrication of three-dimensional metallic microstructures in poly(dimethylsiloxane). Advanced Materials *19* 727–733.

Smith, B.O., Downing, A.K., Driscoll, P.C., Dudgeon, T.J., and Campbell, I.D. (1995). The solution structure and backbone dynamics of the fibronectin type I and epidermal growth factor-like pair of modules of tissue-type plasminogen activator. Structure *3*, 823-833.

Smith, G.P. (1985). Filamentous fusion phage: novel expression vectors that display cloned antigens on the virion surface. Science *228*, 1315-1317.

Smith, G.P., and Petrenko, V.A. (1997). Phage Display. Chem Rev *97*, 391-410.

Song, H., Chen, D.L., and Ismagilov, R.F. (2006). Reactions in droplets in microfluidic channels. Angew Chem Int Ed Engl *45*, 7336-7356.

Song, H., and Ismagilov, R.F. (2003). Millisecond kinetics on a microfluidic chip using nanoliters of reagents. J Am Chem Soc *125*, 14613-14619.

Song, H., Tice, J.D., and Ismagilov, R.F. (2003). A microfluidic system for controlling reaction networks in time. Angew Chem Int Ed Engl *42*, 768-772.

Soumillion, P., Jespers, L., Bouchet, M., Marchand-Brynaert, J., Winter, G., and Fastrez, J. (1994). Selection of beta-lactamase on filamentous bacteriophage by catalytic activity. J Mol Biol *237*, 415-422.

Squires, v.M., and Quake, S.R. (2005.). Microfluidics: Fluid physics at the nanoliter scale. Reviews Of Modern Physics *77*, 977–1026.

Srisa-Art, M., Kang, D.K., Hong, J., Park, H., Leatherbarrow, R.J., Edel, J.B., Chang, S.I., and deMello, A.J. (2009). Analysis of protein-protein interactions by using droplet-based microfluidics. Chembiochem *10*, 1605-1611.

Srivastava, R., Deb, D.K., Srivastava, K.K., Locht, C., and Srivastava, B.S. (1998). Green fluorescent protein as a reporter in rapid screening of antituberculosis compounds in vitro and in macrophages. Biochem Biophys Res Commun *253*, 431-436.

Studer, A., Hadida, S., Ferritto, R., Kim, S.Y., Jeger, P., Wipf, P., and Curran, D.P. (1997). Fluorous synthesis: a fluorous-phase strategy for improving separation efficiency in organic synthesis. Science *275*, 823-826.

Sundberg, S.A. (2000). High-throughput and ultra-high-throughput screening: solution- and cell-based approaches. Curr Opin Biotechnol *11*, 47-53.

Tadros, T.F. (2005). Applied Surfactants-Principles and Applications. Wiley-VCH Verlag GMBH& Co, Weinheim.

Tarrand, J.J., and Groschel, D.H. (1985). Evaluation of the BACTEC radiometric method for detection of 1% resistant populations of Mycobacterium tuberculosis. J Clin Microbiol *21*, 941-946.

Tawfik, D.S., and Griffiths, A.D. (1998). Man-made cell-like compartments for molecular evolution. Nat Biotechnol *16*, 652-656.

Teh, S.Y., Lin, R., Hung, L.H., and Lee, A.P. (2008). Droplet microfluidics. Lab Chip *8*, 198-220.

The World Health Organisation, W. (2004). The world health report 2004 - changing history. The world health report 2004 120-125.

Thorsen, T., Roberts, R.W., Arnold, F.H., and Quake, S.R. (2001). Dynamic pattern formation in a vesicle-generating microfluidic device. Phys Rev Lett *86*, 4163-4166.

Tramantano, A., Janda, K.D., and Lerner, R.A. (1986). Catalytic antibodies. Science ***234***, 1566.

Vanapalli, S.A., Banpurkar, A.G., van den Ende, D., Duits, M.H., and Mugele, F. (2009). Hydrodynamic resistance of single confined moving drops in rectangular microchannels. Lab Chip *9*, 982-990.

Vanwetswinkel, S., Avalle, B., and Fastrez, J. (2000). Selection of beta-lactamases and penicillin binding mutants from a library of phage displayed TEM-1 beta-lactamase randomly mutated in the active site omega-loop. J Mol Biol *295*, 527-540.

Varmus, H.E. (1982). Form and function of retroviral proviruses. Science *216*, 812-820.

Vellard, M. (2003). The enzyme as drug: application of enzymes as pharmaceuticals. Curr Opin Biotechnol *14*, 444-450.

Walsh, G., and Jefferis, R. (2006). Post-translational modifications in the context of therapeutic proteins. Nat Biotechnol *24*, 1241-1252.

Walters, W.P., and Namchuk, M. (2003). Designing screens: how to make your hits a hit. Nat Rev Drug Discov *2*, 259-266.

Wang, J. (2002). On-chip enzymatic assays. Electrophoresis *23*, 713-718.

Wang, Y., Rubtsov, A., Heiser, R., White, J., Crawford, F., Marrack, P., and Kappler, J.W. (2005). Using a baculovirus display library to identify MHC class I mimotopes. Proc Natl Acad Sci U S A *102*, 2476-2481.

Waters, D.L., Holton, T.A., Ablett, E.M., Lee, L.S., and Henry, R.J. (2005). cDNA microarray analysis of developing grape (Vitis vinifera cv. Shiraz) berry skin. Funct Integr Genomics *5*, 40-58.

Werner, R.G. (2001). Improving natural principles with genetic engineering: TNK-tissue plasminogen activator. Arzneimittelforschung *51*, 516-520.

Whitesides, G.M. (2006). The origins and the future of microfluidics. Nature *442*, 368-373.

Wittwer, A.J., and Howard, S.C. (1990). Glycosylation at Asn-184 inhibits the conversion of single-chain to two-chain tissue-type plasminogen activator by plasmin. Biochemistry *29*, 4175-4180.

Wolff, A., Perch-Nielsen, I.R., Larsen, U.D., Friis, P., Goranovic, G., Poulsen, C.R., Kutter, J.P., and Telleman, P. (2003). Integrating advanced functionality in a microfabricated high-throughput fluorescent-activated cell sorter. Lab Chip *3*, 22-27.

Ye, N., Qin, J., Shi, W., Liu, X., and Lin, B. (2007). Cell-based high content screening using an integrated microfluidic device. Lab Chip *7*, 1696-1704.

Yonezawa, M., Doi, N., Kawahashi, Y., Higashinakagawa, T., and Yanagawa, H. (2003). DNA display for in vitro selection of diverse peptide libraries. Nucleic Acids Res *31*, e118.

Yu, Y., and Wong, P.K. (1992). Studies on compartmentation and turnover of murine retrovirus envelope proteins. Virology *188*, 477-485.

Zhang, J.H., Chung, T.D., and Oldenburg, K.R. (1999). A Simple Statistical Parameter for Use in Evaluation and Validation of High Throughput Screening Assays. J Biomol Screen *4*, 67-73.

Zheng, B., and Ismagilov, R.F. (2005). A microfluidic approach for screening submicroliter volumes against multiple reagents by using preformed arrays of nanoliter plugs in a three-phase liquid/liquid/gas flow. Angew Chem Int Ed Engl *44*, 2520-2523.

Zheng, B., Tice, J.D., Roach, L.S., and Ismagilov, R.F. (2004). A droplet-based, composite PDMS/glass capillary microfluidic system for evaluating protein crystallization conditions by microbatch and vapor-diffusion methods with on-chip X-ray diffraction. Angew Chem Int Ed Engl *43*, 2508-2511.

Zhong, G., Lerner, R.A., and Barbas, I.C. (1999). Broadening the Aldolase Catalytic Antibody Repertoire by Combining Reactive Immunization and Transition State Theory: New Enantio- and Diastereoselectivities. Angew Chem Int Ed Engl *38*, 3738-3741.